Electrochemical characterisation of the redox behaviour of quinoide components in membrane models

I n a u g u r a l d i s s e r t a t i o n

zur

Erlangung des akademischen Grades eines

Doktors der Naturwissenschaften (Dr. rer. nat.)

der

Mathematisch-Naturwissenschaftlichen Fakultät

der

Universität Greifswald

vorgelegt von

Karuppasamy Dharmaraj

geboren am 22.05.1996

in Sivakasi, India

Greifswald, 30.11.2020

Dekan: Prof. Dr. Gerald Kerth

1. Gutachter : Prof. Dr. Fritz Scholz (University of Greifswald)

2. Gutachter : Prof. Dr. Richard G. Compton (University of Oxford)

Tag der Promotion: 25.02.2021

Contents

Abbreviations and symbols

Acetyl CoA   –   acetyl coenzyme A

ADP   –   adenosine diphosphate

ATP   –   adenosine triphosphate

CL's   –   cardiolipins

DMPC   –   1,2-dimyristoyl-sn-glycero-3-phosphocholine

DPPH   –   2,2-diphenyl-1-picrylhydrazyl

$FADH_2$ –   flavin adenine dinucleotide

ITIES   –   interface between two immiscible electrolyte solutions

pK_a –   acidity constant

MK-n –   menaquinone with 'n' isoprenoid units

MK's   –   menaquinones

MK/MKH_2 –   menaquinone/menahydroquinone redox couple

nCL   –   natural cardiolipin (heart, bovine)

NADH   –   nicotinamide adenine dinucleotide

NADPH   –   nicotinamide adenine dinucleotide phosphate

Q/QH_2 –   quinone/hydroquinone redox couple

TMCL   –   1,1',2,2' tetramyristoyl cardiolipin

UQ's   –   ubiquinones

E' –   biochemical standard potential

ΔG –   free energy change

$\Delta G^{\ominus}_{aq \to org}$ –   standard free energy of ion transfer from aqueous to organic phase

H_3O^+ –   hydronium ion

$K_{\text{ion pair}}$ –   ion pair equilibrium constant

ΔS –   entropy change

1   Introduction

1.1   Outline

The leading idea of this thesis is to study the effects of (i) membrane composition and (ii) membrane environment (aqueous phases) on the redox properties of membrane-confined redox active compounds. For solutions, it is known since long, how strong solvents affect the redox properties of dissolved redox active species. However, for membranes this question has not yet been addressed, although it can be supposed that such effects may be important to understand the role of membrane-confined redox active compounds in biological systems. To interrogate this problem, a monolayer model was chosen. It consists of a lipid monolayer with embedded menaquinones on mercury electrodes. Since ion transfer across membranes is also a crucial question, in the first part of this project, DPPH was studied as a new redox probe for transferring anions and cation between an organic and an aqueous phase.

1.2   Physicochemical properties of biological membranes

Biological membranes are dynamic structures, which separate two aqueous regions and sustain the structural integrity and organisation of life. The membranes compartmentalise living entities, confine living processes, and most importantly, control the exchange of matter and energy with the environment and/or other cellular and subcellular elements. The interpretation of the physical characteristics of membranes can be traced back to I. Langmuir's experiments with oil films on water, and their interpretation [1], followed by the models of E. Gorter and F. Grendel [2], J. F. Danielli and H. Davson [3], and several others [4]. A much more detailed model of the membrane structure has been published by S. J. Singer and G. L. Nicholson, who have viewed the membrane as a two-dimensional lipid fluid bilayer with embedded globular molecules [5]. Later, a new view of the membrane structure was given by K. Simons and E. Ikonen [6]. It was based on the dynamic clustering of sphingolipids and cholesterol to form detergent insoluble complex structures called rafts or domains. In 2014, special importance was given to the mosaic nature of membrane structures, notably to the interactions of membrane elements and a revised S. J. Singer and G. L. Nicholson model was provided by G. L. Nicolson [7]. Technological advancements allowed to interpret the membranes and their component structures in a very detailed way [8-10]. Membranes are essentially built up by amphiphilic molecules, i.e., molecules possessing both hydrophilic and lipophilic units. The amphiphiles of membranes are the lipids. The self-organisation

phenomenon of amphiphilic molecules operates as follows: the hydrophobic tails of the lipids arrange in a layer with all tails attached to each other and exposing all polar groups to one side of the layer. Then, two such layers form a bilayer in which the hydrophobic sides face each other and expose the polar surfaces to either side of the bilayer (the membrane), i.e., towards the aqueous environment. The resulting membrane is a barrier for ions and molecules, and thus also for energy fluxes. Though lipids are the main components and vital for the membrane functions, other constituents, like proteins and carbohydrates, play also most important roles for the flow of matter, energy, and information. Membrane components diverge greatly between the cell types and cell organelles. For instance, the weight ratio of lipid to protein in plasma membranes is close to 1 and for mitochondrial membranes [11] it is near to 2 or 3. Also, the permeability of ionic solutes varies between the membranes [12]. These variations are vital for the membrane functions of certain types of cells and organelles. Because of the fluid nature, the lipid membranes can deform in several ways, generally with elastic stresses and strains to match the hydrophobic thickness of the transmembrane proteins and save the hydrophobic edge curvature forces. The membrane proteins are structurally adapted to the membranes by their hydrophobicity, van der Waals forces, hydrogen bonds, and electrostatic interactions [13-15]. Lipids generally possess diverse structural phases depending on the phase transition temperatures. In addition, the membrane components and the lipids are not distributed evenly, but may form domains [16-19], which have distinguished properties and functions [20, 21]. The polar head groups of the lipids and ions in the aqueous region are typically solvated by the water molecules. The structure and orientation of water molecules on the membrane surface are primarily determined by the net charge of the lipid head groups [22]. This provides a unique environment for interfacial chemical reactions. Our life evolved from the aqueous environment, and Nature has chosen the hydrophobic effect for holding the hydrocarbon chains together without causing crystallisation (due to presence of unsaturated lipids and cholesterol). This drives the membranes to the supra-molecular organisation and it can squeeze and deform the membranes without any disruptions [23]. Lipid head groups, water molecules, and ionic solutes determine the electrostatic environment of the membrane for interfacial reactions. Some of the membrane elements act as pores and channels of the membranes. The dynamic processes of life are taking place in a well-structured network.

1.3   Water – an essential component of biological membranes

Water is a natural solvent interacting with all living matter on the 'Planet Earth' [24-27]. An adult human body consists of 68% water [28] and a loss of 15% would be fatal. Water acts as a life matrix and currently living organisms on earth cannot sustain, without this elementary molecule [29]. Water serves largely as the source of protons and the proton transfer across the membranes is a fundamental process of respiration [30, 31] and important for the cellular energetics. The series of physical properties [32], like high melting point (0 °C at 1 atm), high boiling point (100 °C at 1 atm), large surface tension coefficient (73 mN m^{-1} at 20 °C), low dynamic viscosity coefficient (1.00cP at 20°C), high specific heat capacity (4.2 kJ kg^{-1} K^{-1} at 20 °C), high specific latent heat of melting/freezing (2.3 MJ kg^{-1} at 1 atm), high specific latent heat of vaporisation/condensation (334 kJ kg^{-1} at 1 atm), and high dipole moment (1.85 D) and dielectric constant (78.4 at 25 °C) are best suited for the life on earth. Of course, one should formulated it the other way round: life has been best adapted to these properties of water. This ubiquitous solvent accounts for the hydrophobic effect, the one that causes the structural stabilisation of the membranes, source for protons in biochemical reactions, transport of solutes, hydration of cell components, and additional boundless functions [33]. The presence of various ions alters the activity and ionic strength of the water. In mammalian cells, concentration of Na^+, K^+, Mg^{2+}, Ca^{2+}, and Cl^- ions are up to 145, 155, 2, 2, and 120 mM respectively [34]. The functional groups (choline, serine, ethanolamine, phosphate) of the lipid heads in the membrane interact with hydrated ions. They change the surface charge density and the ions interaction can be characterised by ion binding or ion association constant [35]. The association constants are required to understand the membrane-membrane interactions, signal transmission, and energisation of mitochondrial membranes [36]. The perturbations of the water structure at the lipid-water interface extend to several hydration layers [37]. Lipid head groups and different lipid phases modulate the lipid-water interactions. The water molecules bonded to the membrane determine the structural stability of the bilayer, membrane fusion, and mobility of membrane proteins and lipids [38]. The water transport rate through the channels increases with decreasing number of hydrogen bonds in the walls of water channels [39]. There is no doubt that the water is crucial for the thermodynamics and kinetics of biological processes in and at biological membranes.

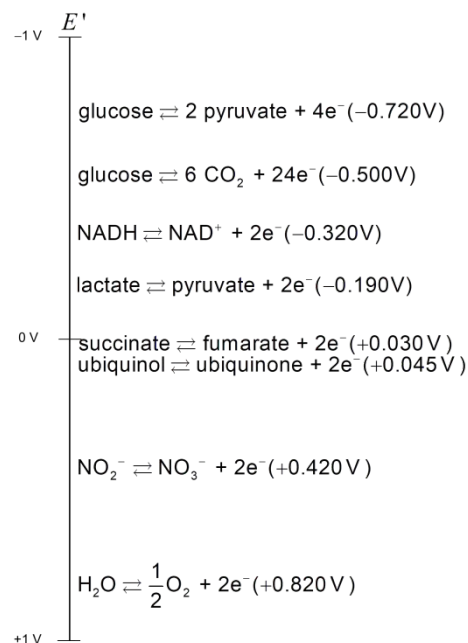1.4   Thermodynamics of biological membranes

The hydration of lipids affects the formation of polymorphic phases. Lamellar (gel, liquid crystalline), micellar aggregates (spherical, cylindrical, disk, inverted, liposome), and non-

lamellar liquid crystalline (hexagonal, inverted hexagonal, inverted micellar cubic, bilayer cubic) aggregates are the common lipid polymorphic phases [40, 41]. The formed phases depend also on the type of lipids and the degree of unsaturation in tails, temperature, pH, and ionic strength of the aqueous electrolyte. The degree of unsaturation of the lipid tails affects the phase transition temperature. An unsaturated carbon bond produces a kink in the tail, disrupt the periodic structure and creates a free space. Lipids that fit into cylindrical, conical, and truncated conical shapes are best for planer bilayers, spherical micelles, and vesicles or inverted micelles structures respectively that maintain the stability of corresponding membrane organisation [42]. The optimal area per head for the stability of a micelle is 60 to 70 $Å^2$ [43]. The origin of antipathy between hydrocarbon and water roots in the strong self-attraction of water [44], the dynamic hydrogen bond network. The hydrophobic tails of the lipid move away from water and form the different structures (micelle, vesicles, bicelles) via self-assembly process, a mostly entropy driven process. The free energy of solvation of an amphiphile in water can be assessed from the free energy contributions by the hydrophilic head and hydrophobic tail separately [45]. The free energy of formation of micelles (and vesicles) from the amphiphiles involve the following contributions [46]: the free energy change caused by the attraction among the hydrophobic tails, that caused by the repulsion of the polar head groups, and that caused by the hydrophobic effect, which is mainly an entropic effect. The overall process leads to non-rigid deformable structures that are essential for membranes to function. The bilayers of vesicles and membranes contain thick hydrophobic inside, which is a barrier for the transport of hydrophilic metabolites and ions. So, the presence of additional structural components in the membrane, e.g., proteins, which provide control of ion transport in response to ion gradients [47]. The transmembrane proteins are folded into the membranes via hydrophobic interactions with the lipids [48]. The internal lateral pressure of the membranes is $30 - 35$ mN m^{-1} and the hydrophobic free energy density at the polar|apolar interface is $36 - 40$ mN m^{-1} [49]. This evidently shows that the internal lateral pressure of the membranes is balanced by the hydrophobic effect that opposes the membrane extension. The hydrophobic effect stabilises the bilayer organisation for the energetic processes by holding together the lipids and other membrane elements (enzymes, ion transporters, redox species).

1.5   Energetics of biochemical reaction

The driving force of a redox reaction is measured in standard reduction potentials or Gibbs free energies. The redox tower of some biological reactions is shown in Fig. 1. The energy

for the cells and the cell organelles comes mainly from the mitochondrial respiratory chain.

E'

−1 V

glucose $\rightleftharpoons$ 2 pyruvate + 4e$^-$ (−0.720V)

glucose $\rightleftharpoons$ 6 CO$_2$ + 24e$^-$ (−0.500V)

NADH $\rightleftharpoons$ NAD$^+$ + 2e$^-$ (−0.320V)

lactate $\rightleftharpoons$ pyruvate + 2e$^-$ (−0.190V)

0 V

succinate $\rightleftharpoons$ fumarate + 2e$^-$ (+0.030 V)
ubiquinol $\rightleftharpoons$ ubiquinone + 2e$^-$ (+0.045 V)

NO$_2^-$ $\rightleftharpoons$ NO$_3^-$ + 2e$^-$ (+0.420 V)

H$_2$O $\rightleftharpoons$ $\frac{1}{2}$O$_2$ + 2e$^-$ (+0.820 V)

+1 V

Fig. 1 The Redox tower shows the biochemical standard potential (E') for some biological reactions [50]

The respiratory electron chain consists of five different complexes in the inner mitochondrial membrane. Each complexes is built up of enzymes, peptides, and other molecules. Since many molecules are relatively stable, the reactions will not proceed immediately because there are small energy barriers, called activation energies. This energetic barriers need to be overcome by the reactants for conversion into the products. Enzymes are catalysts, which lower the activation energies. From thermodynamic point of view, a chemical reaction can proceed spontaneously only if it is accompanied by a decrease in free energy. The oxidation of food releases the energy and temporarily stores it in activated carrier molecules (eg., adenosine triphosphate (ATP)) [51]. Later, the carrier molecules give up their energy through hydrolysis which produces adenosine diphosphate (ADP). Nicotinamide adenine dinucleotide (NADH), nicotinamide adenine dinucleotide phosphate (NADPH), flavin adenine dinucleotide (FADH$_2$), and acetyl coenzyme A (acetyl CoA) are other activated carrier molecules involved in the metabolism. NADH possesses a very negative biochemical redox potential ($E' = -0.320$V , higher energy level) has strong tendency to donate electrons to oxygen ($E' = +0.820$V , high electron affinity) through the complex respiratory chain. The respiratory chain is energetically favourable with a free energy change of $\Delta G = -109$kJ mol^{-1} ($E' = +1.140$V) [52]. The electrons and protons are shuttled between the

enzyme complexes by carriers like ubiquinone and cytochrome c. The proton translocation and electron shuttling in the respiratory chain induce the mitochondrial membrane potential.

1.6   Membrane potential

The membrane potential describes the difference in electric potentials across the membrane, i.e., inside and outside of a cell organelle (like mitochondria). It arises from the difference in surface charges due to the asymmetric distribution of zwitter ionic lipids, presence of charged lipids, and proton diffusion and ionic solutes from the aqueous environment [53]. The membrane potential regulates the channel conductance, binding of drugs, structure of the membrane proteins, and interfacial reactions [54]. There are adsorbed hydrated ions and the diffused ion distribution over the membrane surface. This interfacial region is called Gouy-Chapman-Stern double layer [55]. The stern layer is also influenced by hydrophobic interactions [56]. Beyond the diffuse ion region, there is an isotropic bulk phase. Each membrane organelles possess diverse lipids and ion distribution at the interface, which results in distinct membrane potentials. For example, the rest membrane potentials of some organelles are: −150 to −180 mV for mitochondria, +20 to +30 mV for Golgi apparatus and lysosomes, and around 0 mV for endoplasmic reticulum and nucleus [57]. The proton pumps in the inner mitochondrial membrane also contribute to the mitochondrial membrane potential [58]. Studying the membrane potential and other interfacial biochemical reactions are challenging in case of real membranes. This is due to the presence of various membrane elements and their composition. Therefore, the model biomimetic membranes are helpful to understand the thermodynamics and kinetics of membranes.

1.7   Biomimetic membranes

The specific functions of proteins and lipids and their interactions can be interrogated by using biomimetic membranes. Model membranes act as simple platforms. They can be tailored to mimic real membranes and in order to perform experiments which yield important information [59, 60]. Langmuir monolayers, supported monolayers, bilayers, and tethered layers, micelles, bicelles, liposomes, lipid rafts, and nanodiscs are common membrane model systems. Software simulations can also be applied to study the complex functionality of the biological membranes [61, 62]. Each membrane models has its own advantages and disadvantages that limit the understanding of complete membrane systems. Therefore, using the diverse membrane models combined with various experimental and instrumental techniques, offer an extensive way for better and deeper insights into biological membranes.

Lipid phases, redox elements, dielectrics, ion transport, membrane heterogeneity, and membrane composition properties are accessible using membrane models [63-71]. Lipid monolayers on mercury and solid supported lipid monolayers and bilayers are simple membrane models for the detailed studies of the thermodynamics and kinetics of biological membranes. These two systems are commonly employed for extensive electrochemical studies as models of biological membranes. To characterise these two membrane models, a plethora of electrochemical techniques, such as voltammetry, coulometry, potentiometry, and impedance spectroscopy, has been used. These techniques are operated to obtain thermodynamic and kinetic information of the reactants, intermediates, and products. Together with spectroscopic techniques, the above electrochemical methods can be tuned to monitor in situ intermediate reactions and the orientation and conformation of membrane constituents. Several biochemical reactions take place at the membrane water interface. For example, the protein folding in the lipid matrix creates microenvironments at the interface for many specific biochemical reactions. To study this kind of interfacial reactions, monolayer membrane models are more simple and convenient than bilayers. The monolayer models can provide very useful information regarding the protein interaction [72]. The interfacial reactions depend on the membrane composition and the environment. Therefore, one should not ignore the effect of membrane composition and the surrounding environment to understand the function of membranes.

1.8   Membrane composition affects the thermodynamics and kinetics

Each cellular organelles possess their own unique membrane composition. The membrane composition modulates the protein functions and redox potential of electron transfer carriers. Any change in composition disturbs the membrane elements environment and the associated functions will change. For instance, the lipid type and the environment determine the redox potential of the cytochrome P450 reductase [73]. Also, the protein binding is sensitive to the specific membrane domains [74]. Domains in the membranes act as an ON and OFF switch for the interfacial reactions. Several enzyme-substrates, proteins, and membrane element interactions are specific for the domains rather than occurring in the cell matrix at low concentrations [75]. The electron transfer rate in the redox processes is affected by the membrane composition and membrane environment [76, 77]. The presence of cholesterol has an effect on membrane transport processes, including ion channels, transporters, and receptors [78].

1.9   Membrane transport processes

The liquid-liquid (water|amphiphilic fluid) interface plays a fundamental role in enzymatic reactions and various cell signaling pathways. Membrane transport processes occur by active or passive mechanisms. The fluid lipid membranes are impermeable to the ions due to the presence of the internal hydrophobic layer. The presence of carriers and ion channels provides pathways (energetically and mechanistically) to transfer organic and inorganic ions and protons. Mitochondrial ATP energetics involves the transport of protons as an intermediate [79, 80]. The proton transport is taking place either by diffusion of hydronium (H_3O^+) ions or via the Grotthuss mechanism (proton hopping between the hydrogen-bonded water molecules). The Grotthuss 'structure diffusion' along the surface of membranes, has been shown to operate over distances in the range of 10 nm to 100 µm using physiological and diluted buffers respectively [81]. The ion transport mechanisms via carriers, channels, and pumps can be accessed by lipid membrane models [82, 83]. The interface between two immiscible electrolyte solutions (ITIES) can be used in electrochemistry to access the Gibbs free energy of ion transfer between the two phases [84, 85]. A simple experimental approach to determine the standard Gibbs free energy of ion transfer is to use the three-phase electrochemistry setup. The four-electrode method needing a bipotentiostat is a less convenient alternative. The Gibbs free energy of ion transfer of common organic and inorganic cations and anions, peptides, drugs, amino acids, and neurotransmitters (dopamine, adrealone, acetylcholine, tryptamine, and serotonin) have been previously determined [86-91]. Anion exchange membrane modified liquid-liquid interfaces provide a platform to study hydrophilic anions [92]. In publication No. 1 (Dharmaraj K, Nasri Z, Kahlert H, Scholz F (2018) The electrochemistry of DPPH in three-phase electrode systems for ion transfer and ion association studies. J Electroanal Chem 823:765-772. https://doi.org/10.1016/j.jelechem.2018.06.012) a membrane model for the transfer of anions and cations from aqueous to organic phase (nitrobenzene) using the redox probe 2,2-diphenyl-1-picrylhydrazyl (DPPH) has been studied. The standard free energies of ion transfer ($\Delta G_{aq \to org}^{\ominus}$) of anions like nitrate, perchlorate, trichloroacetate, and hexafluorophosphate and cation like tetrabutylammonium have been determined. The DPPH suffers from strong ion pairing with anions and weakly ion pairing with tetrabutylammonium cation.

1.10 Membrane lipids

The major membrane lipids in mammalian cells are phospholipids (phosphatidylcholine, phosphatidylethanolamine, phosphatidylinositol, phosphatidylserine, and sphingomyelin) and glycolipids. The presence of various lipids is signifying various functions [93]: (i) anionic phospholipids interact with sequences of mitochondrial precursor proteins; (ii) zwitterionic lipids like phosphatidylethanolamine, phosphatidylcholines are for solute transport and membrane protein assembly. Cardiolipins (CL's), the signature lipid of mitochondria, play a role in various mitochondrial processes such as protein transport, cellular signalling, and membrane dynamics [94-97]. Under physiological conditions, CL's prefer to be negatively charged (second acidity constant $pK_{a2} > 8.0$), which conditions CL's to act as proton traps [98] and tightly bond to the ADP/ATP carrier [99]. The lipid composition of membranes is specific for specific cells and organelles. The primary reason for composition changes are diseases and aging, causing gene modifications. The cationic lipids are generally used for drug delivery systems. The endoplasmic reticulum is the major lipid-synthesising organelle in a cell. Mitochondria are also capable of synthesising phospholipids, mainly cardiolipins, phosphatidylglycerols, and phosphatidylethanolamines [100]. These lipids are essential for the electron transport together with isoprenoid quinones and other enzyme complexes for the respiratory chain.

1.11 Isoprenoid quinones

Quinones are the class of natural and synthetic compounds, mainly known as constituents of dyes. Quinones are electrophilic Michael acceptors stabilised by conjugation. The common structural patterns of the quinones are ortho or para-substituted dione conjugated to the aromatic ring (benzoquinone) or a condensed polycyclic aromatic system (naphthoquinone, anthraquinone, anthracyclinone) [101]. Quinones are essential for biological and chemical processes, and common quinones are well-studied compounds. In biological systems, quinones play the major role in blood coagulation (vitamin K), as antioxidants (vitamin E, Coenzyme Q), anti-inflammatory (vitamin E), antibiotics (phaeosphenone), antimicrobials (anthraquinones), and as anti-cancer drugs (thymoquinone) [101]. Ubiquinones (UQ's), i.e., isoprenoid quinones, act as cofactors in the respiratory chain by being present in the membranes. Isoprenoid quinones are compounds composed of quinone head groups and hydrophobic isoprenoid side chains. The latter give the molecule a lipid solubility. Most of the naturally occurring isoprenoid quinones are naphthoquinones (Vitamin K, thermoplasmaquinone, methionaquinone, chlorobiumquinone) and benzoquinones

(ubiquinones, plastoquinones). The ability of the isoprenoid quinones to undergo reversible reduction-oxidation (redox) reaction makes them a special candidate for the hydrogen (proton) shuttling between different protein complexes in biological membranes. Due to their very hydrophobic character, natural UQ's dissolved in lipid bilayers, and bound to proteins in the living cell. Studies have shown that 11 to 33 % of the UQ's in mammalian species is bond to proteins [102]. Previously it has been assumed that the UQ structure is linear. However, theoretical studies have indicated that the ubiquinone molecules are mostly located in the hydrophobic bilayer midplane, with the polar head group oscillating across the membrane [103] and catalysing many reactions besides inhibiting lipid peroxidation [104, 105]. The lowering of UQ levels is related to aging, degenerative diseases, cardiovascular diseases, diabetes, cancer, etc. [106-108]. Although much of the biological details of UQ's are known, yet there is a serious lack of understanding of the role of membrane environment with respect to thermodynamics and kinetics. Thus it is unclear how the nature of lipids affects protein interactions, ion transport, catalysis, and so on. The same applies to another group of isoprenoid quinones, called menaquinone compounds or vitamin K_2 family. Generally, vitamin K is known for anticoagulant properties and it plays a prominent role in human health [109, 110]. Vitamin K is distributed as phylloquinone (vitamin K_1, 2-methyl-1,4-naphthoquinone with a 3-phytyl substituent) and menaquinone (MK - n) with 'n' isoprenoid residues. Vitamin K_2 has a longer half-life than K_1 and its dependent proteins are present in both hard and soft tissues [111, 112]. Phylloquinones are major vitamin K dietary sources and they can be converted to MK-4 [113]. The main function of vitamin K is proton coupled electron transfer (Quinone/Hydroquinone (Q/QH_2)) with the help of other enzymes. Menaquinones (MK's) accounts for 75 - 97 mol % in which MK-7 to -10 are in larger proportion in hepatic vitamin K [114]. Vitamin K dependent proteins are mainly involved in blood coagulation, bone mineralisation, vascular repair, prevention of vascular calcification, inhibiting bone weakening, regulation of cell proliferation, and signal transduction [115-120]. The concentrations of MK-4 and MK-7 in serum samples are 0.050 - 1.598 and 0.074 - 0.759 ng mL^{-1}, respectively [121]. All these concentrations of menaquinones vary between adults and children depending on the type of food intake. The human intestinal tract can absorb the menaquinones in the form of oral drugs and from the fermented food products [122, 123]. MK's are used as a medication for osteoporosis as it protects the osteoblasts from apoptosis and inhibits osteoclast formation [124, 125], inhibiting the growth of cancer cells [126], and has a more beneficial effect on type 2 diabetes mellitus than K_1 [127]. A recent study has shown that in mammalian cells, vitamin K_2 cannot

substitute UQ-10 function in the respiratory chain complex [128]. Several biological benefits of menaquinones are known, but the thermodynamics and kinetics of the MK's are poorly studied. Earlier studies with thin layer voltammetry on carbon electrodes have been performed to analyse the redox properties of vitamin K in absence of lipids [129, 130]. A recent study has shown that the lateral chains of MK-4 and vitamin K_1 are oriented almost in parallel to the myristoyl chains of the 1,2-dimyristoyl-sn-glycero-3-phosphocholine (DMPC) lipid [131]. The electrochemical properties of many vitamins are insufficiently known [132], as well as their thermodynamics and kinetics in membranes. Therefore, it is essential to study the electrochemical properties of MK's in membrane environments. The electrochemical characterisation of MK's in membrane models has been studied with respect to acid-base and redox properties in publication No. 2 (Dharmaraj K, Silva JIR, Kahlert H, Lendeckel U, Scholz F (2020) The acid–base and redox properties of menaquinone MK-4, MK-7, and MK-9 (vitamin K_2) in DMPC monolayers on mercury. Eur Biophys J 49:279–288. https://doi.org/10.1007/s00249-020-01433-0) and the effect of membrane composition and the aqueous environment on MK's in publication No. 3 (Dharmaraj K, Dattler D, Kahlert H, Lendeckel U, Nagel F, Delcea M, Scholz F (2020) The effects of the chemical environment of menaquinones in lipid monolayers on mercury electrodes on the thermodynamics and kinetics of their electrochemistry. Submitted to European Biophysics Journal. Submitted for publication on November 4, 2020. Submission ID: EBJO-D-20-00209).

2   Summary

The main objective of this project was the electrochemical characterisation of MK's in membrane models. This is crucial to understand the thermodynamic and kinetic behaviour of the MK's in the membranes. The important findings of this thesis are:

(i)   accessing the ion pair equilibrium constant of anions and cations with DPPH redox probe as a model study using the three-phase electrochemistry,

(ii)   the redox potentials of menaquinone-4, -7, and -9 in DMPC monolayers and the acidity constants of MK's in membranes monolayer model, and

(iii)   the effects of membrane composition and the aqueous environment on the thermodynamics and kinetics of MK's in membrane models.

The electrochemical study of ion transfer between two immiscible (organic|aqueous) phases (three-phase electrochemistry) has provided the standard free energies of ion transfer. Further, the ion pair equilibrium constants of the studied ions with DPPH have been determined, see **publication No. 1** (Dharmaraj K, Nasri Z, Kahlert H, Scholz F (2018) The electrochemistry of DPPH in three-phase electrode systems for ion transfer and ion association studies. J Electroanal Chem 823:765-772. https://doi.org/10.1016/j.jelechem.2018.06.012). There are several redox compounds (decamethylferrocene, iodine, tetraphenylporphyrin, UQ-10) available, which can be used to transfer either anions or cations, and only very few allow to study both anion and cation transfer. DPPH is one of them because it can be reduced to DPPH$^-$ and oxidised to DPPH$^+$. Since DPPH can transfer both anions and cations, the tetrabutylammonium perchlorate is used to transfer perchlorate anion and tetrabutylammonium cation. The standard free energies of anions like nitrate, perchlorate, trichloroacetate, and hexafluorophosphate and the cation tetrabutylammonium have been measured. The measured standard free energies of ion transfer of anions and cation have been found to deviate from previously reported data. This discrepancy is caused by ion pairing. The DPPH suffers strong ion pair formation with the anions and weak ion pairing with tetrabutylammonium cation. The ion pairing equilibrium constants ($\log K_{\text{ion pair}}$) for each anion at different concentrations are identical and characteristic for each anion. Cations like tetramethylammonium and tetraethylammonium are not enough hydrophilic to support the ion transfer with DPPH. The DPPH-tetrabutylammonium tetrafluoroborate-graphite-paraffin composite electrode exhibits a stable

electrochemical system DPPH/DPPH⁻ by using the tetrabutylammonium cation as charge compensation from the aqueous electrolyte. Since this model study provides valuable thermodynamic information of ion transfer across the aqueous|organic interface, this system can be tuned for other experiments to determine ion transfer energies and ion pairing energies.

After the model ion transfer study to access the $\Delta G^{\ominus}_{\text{aq}\to\text{org}}$ and $\log K_{\text{ion pair}}$, we were interested in the electrochemical characterisation of quinoide compounds particularly the MK's in membrane monolayer models. The acid-base and redox properties of menaquinone-4, -7, and -9 in DMPC lipid monolayers on mercury have been studied and described in **publication No. 2** (Dharmaraj K, Silva JIR, Kahlert H, Lendeckel U, Scholz F (2020) The acid–base and redox properties of menaquinone MK-4, MK-7, and MK-9 (vitamin K$_2$) in DMPC monolayers on mercury. Eur Biophys J 49:279–288. https://doi.org/10.1007/s00249-020-01433-0). The DMPC monolayers spiked with MK's have been prepared by adhesion-spreading of DMPC liposomes containing MK's. Using buffers from pH 4.0 to 14.0, the redox potentials have been calculated. The MK's exhibit electrochemically reversible systems and thin film behaviour. The formal potentials have been determined for MK-4, -7, and -9 and it has been found that MK-7 and -9 exhibit identical potentials. Only the formal potential of MK-4 is slightly more positive than that of the other MK's. The acidity constants are identical for the three MK's, and all higher than 12.0. Therefore under physiological conditions i.e., pH 7.4, the MK's are present in the completely protonated form (MK/MKH$_2$). The reason for the identical and larger acidity constants can be explained as follows: generally, these diprotic acids (QH$_2$) have two acidity constants. When dissolved in solution, they have two well separated $\text{p}K_{\text{a}}$'s, but in the case of surface immobilised system (as also in monolayers), they have identical $\text{p}K_{\text{a}}$'s, which are also higher than those of the dissolved species. This is because these immobilised molecules do not behave like individual molecules, but rather act as a separate phase together with the lipids. The protolysis of the dissolved acids is mainly driven by the entropy by structuring the water molecules around the ions. Therefore, the entropy of the dissolved species is larger than that of the surface immobilised molecules ($\Delta S_{\text{dissolved}} > \Delta S_{\text{surface confined}}$). The decrease in entropy of the surface immobilised molecules (monolayer) causes the higher stability of the protonated form, which ultimately results in larger acidity constants. The number of electrons transferred between oxidised and reduced forms of MK-4 at pH 7.4 is found to be 2. These measurements were

performed by chronocoulometry. The overall electrode process involves two protons and two electrons ($2e^-$ / $2H^+$). From this study, we can understand that these MK molecules are highly efficient to transfer two electrons and two protons for redox reaction in the DMPC lipid environment.

With this primary understanding of the electrochemical behaviour of MK's, we have further extended the study to see the effects of membrane composition and of the aqueous environment of the MK's (cf. **publication No. 3** (Dharmaraj K, Dattler D, Kahlert H, Lendeckel U, Nagel F, Delcea M, Scholz F (2020) The effects of the chemical environment of menaquinones in lipid monolayers on mercury electrodes on the thermodynamics and kinetics of their electrochemistry. Submitted to European Biophysics Journal. Submitted for publication on November 4, 2020. Submission ID: EBJO-D-20-00209)). The effects of cholesterol, water activity, and cardiolipins on MK's have been elucidated. The DMPC-cholesterol system shows five different phases, i.e., gel, liquid disordered, liquid ordered, gel-liquid ordered, and liquid ordered-liquid disordered phases. The thermodynamics and kinetics of MK-7 has been interrogated in all these phases and it could be shown that the thermodynamics are not affected by the presence of cholesterol, however, the kinetics are affected. At low cholesterol content, the separation between anodic and cathodic peaks in cyclic voltammetry is small and increases only at high cholesterol content. The electron transfer rates of MK-7 depend on the nature of DPMC phases and pH of the aqueous electrolyte. Therefore, it could be concluded that the presence of cholesterol affects the kinetics of menaquinones in the used membrane model. The formal potentials increase with decreasing water activity (i.e., increasing the ionic strength), although only slightly (1-29 mV). The water activity does not affect the kinetics of MK-7. The impact of synthetic cardiolipin 1,1',2,2'-tetramyristoyl cardiolipins (TMCL) and natural heart cardiolipin (bovine heart) (nCL) on the electrochemistry of MK-7 has also been studied. The addition of MK-4 to the TMCL does not change the phase transition temperature of TMCL. nCL does not exhibit any phase transition in the temperature range 7 °C to 90 °C. Hence, the MK-4 addition does not affect the phases of the cardiolipins. The formal potential of MK-4 in nCL monolayers has been found to be larger than in TMCL monolayers. Thus the nature of the lipids clearly affects the formal potentials of MK-4. The apparent electron transfer rate constants of MK-4 depend on the type of cardiolipins, TMCL phases, temperature, amount of MK-4 in the membrane, and pH of the aqueous phase. The thermodynamic parameters such as change in free energy, entropy, and enthalpy and activation energy have been also determined for MK-

4. These data also depend on the nature of the membranes. In this regard, it is clear that the membrane composition and the aqueous environment have serious effects on the MK redox system. Thus, the effects of membrane composition and aqueous environment always have to be taken into account when the biological function of membranes are discussed.

The results from this project demonstrate the possibility to determine ion transfer and ion pairing free energies with DPPH, which expands the electrochemical tools for studying ion partition equilibria.

Further, the thermodynamics and kinetics of menaquinones have been accessed in a monolayer membrane model. The results clearly point to the effects of (i) other membrane constituents and (ii) the aqueous inner-cellular (or inner-organelle) phases on the thermodynamics and kinetics of membrane-bond redox active compounds. Although the effects on thermodynamics are obviously small, they may considerably affect the redox equilibria involved in the respiration chain, especially because the redox potentials of the involved systems are rather close to each other. The results of this project show that the kinetics of the redox reactions strongly depend on the composition of membrane and aqueous phase. This may be explained by the faint effects on thermodynamics resulting from its function as driving force, but it may have also other reasons, which need to be studied in future.

3   References

1.   Langmuir I (1917) The constitution and fundamental properties of solids and liquids. II. Liquids. J Am Chem Soc 39:1848-1906. https://doi.org/10.1021/ja02254a006

2.   Gorter E, Grendel F (1925) On bimolecular layers of lipoids on the chromocytes of the blood. J Exp Med 41:439-443. https://doi.org/10.1084/jem.41.4.439

3.   Danielli JF, Davson H (1935) A contribution to the theory of permeability of thin films. J Cell Comp Physiol 5: 495-508. https://doi.org/10.1002/jcp.1030050409

4.   Lombard J (2014) Once upon a time the cell membranes: 175 years of cell boundary research. Biol Direct 9:1-35. https://doi.org/10.1186/s13062-014-0032-7

5.   Singer SJ, Nicolson GL (1972) The fluid mosaic model of the structure of cell membranes. Science 175:720-731. https://doi.org/10.1126/science.175.4023.720

6.   Simons K, Ikonen E (1997) Functional rafts in cell membranes. Nature 387:569-572. https://doi.org/10.1038/42408

7.   Nicolson GL (2014) The Fluid—Mosaic Model of Membrane Structure: Still relevant to understanding the structure, function and dynamics of biological membranes after more than 40 years. Biochim Biophys Acta Biomembr 1838:1451-1466. https://doi.org/10.1016/j.bbamem.2013.10.019

8.   Wang H, Guohui L (2018) Membrane Biophysics New Insights and Methods. Springer, Singapore. https://doi.org/10.1007/978-981-10-6823-2

9.   Gerle C (2019) Essay on Biomembrane Structure. J Membr Biol 252:115-130. https://doi.org/10.1007/s00232-019-00061-w

10.   Mio K, Sato C (2018) Lipid environment of membrane proteins in cryo-EM based structural analysis. Biophys Rev 10:307-316. https://doi.org/10.1007/s12551-017-0371-6

11.   Guidotti G (1972) The composition of biological membranes. Arch Intern Med 129:194-201. https://doi.org/10.1001/archinte.1972.00320020038003

12.   Deamer DW, John B (1986) Permeability of lipid bilayers to water and ionic solutes. Chem Phys Lipids 40:167-188. https://doi.org/10.1016/0009-3084(86)90069-1

13.   Fiedler S, Broecker J, Keller S (2010) Protein folding in membranes. Cell Mol Life Sci 67:1779-1798. https://doi.org/10.1007/s00018-010-0259-0.

14.   White SH, Ladokhin AS, Jayasinghe S, Hristova K (2001) How membranes shape protein structure. J Biol Chem 276:32395-32398. https://doi.org/10.1074/jbc.R100008200

15.   Killian JA, von Heijne G (2000) How proteins adapt to a membrane–water interface. Trends Biochem Sci 25:429-434. https://doi.org/10.1016/S0968-0004(00)01626-1

16.   Owen DM, Gaus K (2013) Imaging lipid domains in cell membranes: the advent of super-resolution fluorescence microscopy. Front Plant Sci 4:503. https://doi.org/10.3389/fpls.2013.00503

17.   Armstrong CL, Marquardt D, Dies H, Kučerka N, Yamani Z, Harroun TA, Katsaras J, Shi AC, Rheinstädteret MC (2013) The observation of highly ordered domains in membranes with cholesterol. PLoS One 8:e66162. https://doi.org/10.1371/journal.pone.0066162

18.   Schroeder F, Woodford JK, Kavecansky J, Wood WG, Joiner C (1995) Cholesterol domains in biological membranes. Mol Membr Biol 12:113-119. https://doi.org/10.3109/09687689509038505

19.   Mukherjee S, Maxfield FR (2004) Membrane domains. Annu Rev Cell Dev Biol 20:839-866. https://doi.org/10.1146/annurev.cellbio.20.010403.095451

20.   Sharpe HJ, Stevens TJ, Munro S (2010) A comprehensive comparison of transmembrane domains reveals organelle-specific properties. Cell 142:158-169. https://doi.org/10.1016/j.cell.2010.05.037

21.   Lemmon MA (2008) Membrane recognition by phospholipid-binding domains. Nat Rev Mol Cell Biol 9:99-111. https://doi.org/10.1038/nrm2328

22.   Mondal JA, Nihonyanagi S, Yamaguchi S, Tahara T (2010) Structure and orientation of water at charged lipid monolayer/water interfaces probed by heterodyne-detected vibrational sum frequency generation spectroscopy. J Am Chem Soc 132:10656-10657. https://doi.org/10.1021/ja104327t

23.   Tanford C (1987) Organizational consequences of the hydrophobic interaction. Proc Indian Acad Sci (Chem Sci) 98:343-356. https://doi.org/10.1007/BF02861533

24.   Israelachvili J, Wennerström H (1996) Role of hydration and water structure in biological and colloidal interactions. Nature 379:219-225. https://doi.org/10.1038/379219a0

25.   Beall PT (1983) States of water in biological systems. Cryobiology 20:324-334. https://doi.org/10.1016/0011-2240(83)90021-4

26.   Grant WD (2004) Life at low water activity. Phil Trans R Soc Lond B 359:1249-1267. https://doi.org/10.1098/rstb.2004.1502

27.   Cooke R, Kuntz ID (1974) The properties of water in biological systems. Annu Rev Biophys Bioeng 3:95-126. https://doi.org/10.1146/annurev.bb.03.060174.000523

28.   Mitchell HH, Hamilton TS, Steggerda FR, Bean HW (1945) The chemical composition of the adult human body and its bearing on the biochemistry of growth. J Biol Chem 158:625-637.

29.   Ball P (2017) Water is an active matrix of life for cell and molecular biology. Proc Natl Acad Sci U S A 114:13327-13335. https://doi.org/10.1073/pnas.1703781114

30.   Amdursky N, Lin Y, Aho N, Groenhof G (2019) Exploring fast proton transfer events associated with lateral proton diffusion on the surface of membranes. Proc Natl Acad Sci U S A 116:2443-2451. https://doi.org/10.1073/pnas.1812351116

31.   Ruitenberg M, Kannt A, Bamberg E, Fendler K, Michel H (2002) Reduction of cytochrome c oxidase by a second electron leads to proton translocation. Nature 417:99-102. https://doi.org/10.1038/417099a

32.   Raicu V, Aurel P (2008) The Molecular Basis of Life. In: Integrated molecular and cellular biophysics, Springer, Netherlands, pp 7-38. https://doi.org/10.1007/978-1-4020-8268-9

33.   Ball P (2008) Water as an active constituent in cell biology. Chem Rev 108:74-108. https://doi.org/10.1021/cr068037a

34.   Boal, D (2012) Signals and switches. In: Mechanics of the Cell, 2nd edn. Cambridge University Press, pp 496-524. https://doi.org/10.1017/CBO9781139022217

35.   Dobrzyńska I (2019) Association equilibria of divalent ions on the surface of liposomes formed from phosphatidylcholine. Eur Phys J E 42:3. https://doi.org/10.1140/epje/i2019-11762-6

36.   Hauser H, Levine BA, Williams RJP (1976) Interactions of ions with membranes. Trends Biochem Sci 1: 278-281. https://doi.org/10.1016/0968-0004(76)90352-2

37.   Arsov Z (2015) Long-range lipid-water interaction as observed by ATR-FTIR spectroscopy. In: Anibal Disalvo E (ed) Membrane Hydration The Role of Water in the Structure and Function of Biological Membranes. In: Robin Harris J (series ed) Subcellular Biochemistry, Vol 71, Springer International Publishing, Switzerland, pp 127-159. https://doi.org/10.1007/978-3-319-19060-0

38.   Schneider AS, Middaugh CR, Oldewurtel MD (1979) Role of bound water in biological membrane structure: fluorescence and infrared studies. J Supramol Struct 10:265-275. https://doi.org/10.1002/jss.400100215

39.   Horner A, Pohl P (2018) Single-file transport of water through membrane channels. Faraday Discuss 209:9-33. https://doi.org/10.1039/C8FD00122G

40.   Luzzati V, Husson F (1962) The structure of the liquid-crystalline phases of lipid-water systems. J Cell Biol 12:207-219. https://doi.org/10.1083/jcb.12.2.207

41. Koynova R, Tenchov B (2013) Transitions between lamellar and non-lamellar phases in membrane lipids and their physiological roles. OA Biochemistry, 1:1-9. http://www.oapublishinglondon.com/article/602#

42. Silver BL (1985) Micelles, Vesicles, and Bilayers—Steric Factors. In: The Physical Chemistry of MEMBRANES An Introduction to the Structure and Dynamics of Biological Membranes Springer, Dordrecht, pp 57-74. https://doi.org/10.1007/978-94-010-9628-7

43. Tanford C (1980) Micelles: Introduction. In: THE HYDROPHOBIC EFFECT: FORMATION OF MICELLES AND BIOLOGICAL MEMBRANES, 2nd edn. John Wiley & Sons, USA, pp 36-44

44. Tanford C (1979) Interfacial free energy and the hydrophobic effect. Proc Natl Acad Sci U S A 76:4175-4176. https://doi.org/10.1073/pnas.76.9.4175

45. Chandler D (2005) Interfaces and the driving force of hydrophobic assembly. Nature 437:640-647. https://doi.org/10.1038/nature04162

46. Tanford C (1974) Theory of micelle formation in aqueous solutions. J Phys Chem 78:2469-2479. https://doi.org/10.1021/j100617a012

47. Tanford C (1978) The hydrophobic effect and the organization of living matter. Science 200:1012-1018. https://doi.org/10.1126/science.653353

48. Dyson HJ, Wright PE, Scheraga HA (2006) The role of hydrophobic interactions in initiation and propagation of protein folding. Proc Natl Acad Sci U S A 103:13057-13061. https://doi.org/10.1073/pnas.0605504103

49. Marsh D (1996) Lateral pressure in membranes. Biochim Biophys Acta Rev Biomembr 1286:183-223. https://doi.org/10.1016/S0304-4157(96)00009-3

50. Milo R, Phillips R (2015) Energies and Forces. In: Cell biology by the numbers, 1st edn. Garland Science, New York, pp 153-207. https://doi.org/10.1201/9780429258770

51. Bruce A, Alexander J, Julian L, David M, Martin R, Keith R, Peter W (2014) Cell Chemistry and Bioenergetics. In: Molecular biology of the cell, 6th edn. Garland Science, New York, pp 43-108

52. Bruce A, Alexander J, Julian L, David M, Martin R, Keith R, Peter W (2014) Energy conversion: mitochondria and chloroplasts. In: Molecular biology of the cell, 6th edn. Garland Science, New York, pp 753-812

53. Gurtovenko AA, Vattulainen I (2008) Membrane potential and electrostatics of phospholipid bilayers with asymmetric transmembrane distribution of anionic lipids. J Phys Chem B 112:4629-4634. https://doi.org/10.1021/jp8001993

54.   McLaughlin S (1989) The electrostatic properties of membranes. Annu Rev Biophys Biophys Chem 18:113-136. https://doi.org/10.1146/annurev.bb.18.060189.000553

55.   Bedzyk MJ, Bommarito GM, Caffrey M, Penner TL (1990) Diffuse-double layer at a membrane-aqueous interface measured with x-ray standing waves. Science 248:52-56. https://doi.org/10.1126/science.2321026

56.   Scheu R, Chen Y, Subinya M, Roke S (2013) Stern layer formation induced by hydrophobic interactions: a molecular level study. J Am Chem Soc 135:19330-19335. https://doi.org/10.1021/ja4102858

57.   Xu H, Martinoia E, Szabo I (2015) Organellar channels and transporters. Cell calcium 58:1-10. https://doi.org/10.1016/j.ceca.2015.02.006

58.   Zorova LD, Popkov VA, Plotnikov EY, Silachev DN, Pevzner IB, Jankauskas SS, Babenko VA, Zorov SD, Balakireva AV, Juhaszova M, Sollott SJ (2018) Mitochondrial membrane potential. Anal Biochem 552:50-59. https://doi.org/10.1016/j.ab.2017.07.009

59.   Sebaaly C, Greige-Gerges H, Charcosset C (2019) Lipid Membrane Models for Biomembrane Properties' Investigation. In: Angelo B, Catherine C (eds.) Current Trends and Future Developments on (Bio-) Membranes Membrane Processes in the Pharmaceutical and Biotechnological Field, Elsevier pp 311-340. https://doi.org/10.1016/C2016-0-04295-X

60.   Simons K, Vaz WL (2004) Model systems, lipid rafts, and cell membranes. Annu Rev Biophys Biomol Struct 33:269-295. https://doi.org/10.1146/annurev.biophys.32.110601.141803

61.   Enkavi G, Javanainen M, Kulig W, Róg T, Vattulainen I (2019) Multiscale simulations of biological membranes: the challenge to understand biological phenomena in a living substance. Chem Rev 119:5607-5774. https://doi.org/10.1021/acs.chemrev.8b00538

62.   Brasseur R (2019) Molecular Description of Biological Membranes by Computer Aided Conformational Analysis. Vol 1, CRC Press, USA

63.   Heise N, Scholz F (2017) Assessing the effect of the lipid environment on the redox potentials of the coenzymes Q_{10} and Q_4 using lipid monolayers made of DOPC, DMPC, TMCL, TOCL, and natural cardiolipin (nCL) on mercury. Electrochem Commun 81:141-144. https://doi.org/10.1016/j.elecom.2017.07.002

64.   Stottrup BL, Keller SL (2006) Phase behavior of lipid monolayers containing DPPC and cholesterol analogs. Biophys J 90:3176-3183. https://doi.org/10.1529/biophysj.105.072959

65.   Gordillo GJ, Schiffrin DJ (1994) Redox properties of ubiquinon (UQ_{10}) adsorbed on a mercury electrode. J Chem Soc Faraday Trans 90:1913-1922. https://doi.org/10.1039/FT9949001913

66.   Vogel V, Möbius D (1988) Hydrated polar groups in lipid monolayers: Effective local dipole moments and dielectric properties. Thin Solid Films 159:73-81. https://doi.org/10.1016/0040-6090(88)90618-9

67.   Kenaan A, El Zein R, Kilinc V, Lamant S, Raimundo JM, Charrier AM (2018) Ultrathin supported lipid monolayer with unprecedented mechanical and dielectric properties. Adv Funct Mater 28:1801024. https://doi.org/10.1002/adfm.201801024

68.   Alobeedallah H, Cornell B, Coster H (2018) The effect of cholesterol on the dielectric structure of lipid bilayers. J Membrane Biol 251:153-161. https://doi.org/10.1007/s00232-017-0007-6

69.   Morigaki K, Tanimoto Y (2018) Evolution and development of model membranes for physicochemical and functional studies of the membrane lateral heterogeneity. Biochim Biophys Acta Biomembr 1860:2012-2017. https://doi.org/10.1016/j.bbamem.2018.03.010

70.   Peetla C, Rao KS, Labhasetwar V (2009) Relevance of biophysical interactions of nanoparticles with a model membrane in predicting cellular uptake: study with TAT peptide-conjugated nanoparticles. Mol Pharmaceutics 6:1311-1320. https://doi.org/10.1021/mp900011h

71.   Ramakrishnan M, Anbazhagan V, Pratap TV, Marsh D, Swamy MJ (2001) Membrane insertion and lipid-protein interactions of bovine seminal plasma protein PDC-109 investigated by spin-label electron spin resonance spectroscopy. Biophys J 81:2215-2225. https://doi.org/10.1016/S0006-3495(01)75869-9

72.   Brockman H (1999) Lipid monolayers: why use half a membrane to characterize protein-membrane interactions?. Curr Opin Struct Biol 9:438-443. https://doi.org/10.1016/S0959-440X(99)80061-X

73.   Das A, Sligar SG (2009) Modulation of the cytochrome P450 reductase redox potential by the phospholipid bilayer. Biochemistry 48:12104-12112. https://doi.org/10.1021/bi9011435

74.   Escribá PV, Busquets X, Inokuchi JI, Balogh G, Török Z, Horváth I, Harwood JL, Vígh L (2015) Membrane lipid therapy: Modulation of the cell membrane composition and structure as a molecular base for drug discovery and new disease treatment. Prog Lipid Res 59:38-53. https://doi.org/10.1016/j.plipres.2015.04.003

75.   Almeida PF, Pokorny A, Hinderliter A (2005) Thermodynamics of membrane domains. Biochim Biophys Acta Biomembr 1720:1-13. https://doi.org/10.1016/j.bbamem.2005.12.004

76.   Büge U, kadenbach B (1986) Influence of buffer composition, membrane lipids and proteases on the kinetics of reconstituted cytochrome-c oxidase from bovine liver and heart.   Eur   J   Biochem   161:383-390.   https://doi.org/10.1111/j.1432-1033.1986.tb10457.x

77.   Cheddar G, Tollin G (1991) Electrostatic effects on the kinetics of electron transfer reactions of cytochrome c caused by binding to negatively charged lipid bilayer vesicles.   Arch   Biochem   Biophys   286:201-206.   https://doi.org/10.1016/0003-9861(91)90028-H

78.   Bastiaanse EL, Höld KM, Van der Laarse A (1997) The effect of membrane cholesterol content on ion transport processes in plasma membranes. Cardiovasc Res 33:272-283. https://doi.org/10.1016/s0008-6363(96)00193-9

79.   Jeuken LJ, Bushby RJ, Evans SD (2007) Proton transport into a tethered bilayer lipid membrane.   Electrochem   Commun   9:610-614.   https://doi.org/10.1016/j.elecom.2006.10.045

80.   Agmon N, Gutman M (2011) Proton fronts on membranes. Nat   Chem   3:840-842. https://doi.org/10.1038/nchem.1184

81.   Serowy S, Saparov SM, Antonenko YN, Kozlovsky W, Hagen V, Pohl P (2003) Structural   proton   diffusion   along   lipid   bilayers.   Biophys   J   84:1031-1037. https://doi.org/10.1016/S0006-3495(03)74919-4

82.   Läuger P (1985) Mechanisms of biological ion transport—carriers, channels, and pumps in artificial lipid membranes. Angew Chem Int Ed Engl 24:905-923. https://doi.org/10.1002/anie.198509051

83.   Bordi F, Cametti C, Motta A (2000) Ion permeation across model lipid membranes: A kinetic approach. J Phys Chem B 104:5318-5323. https://doi.org/10.1021/jp000005i

84.   Volkov AG, Deamer DW (1996) Liquid-Liquid Interfaces Theory and Methods. CRC press, USA

85.   Volkov AG (2001) Liquid interfaces in chemical, biological and pharmaceutical applications. In: Hubbard AT (ed) SURFACTANT SCIENCE SERIES, Vol 95, Marcel Dekker, USA

86.   Gulaboski R, Mirceski V, Komorsky-Lovric S, Lovric M (2020) Three-phase electrodes: simple and efficient tool for analysis of ion transfer processes across liquid-liquid interface—twenty years on. J Solid State Electrochem 24:1-9. https://doi.org/10.1007/s10008-020-04629-8

87.   Scholz F, Schröder U, Gulaboski R, Doménech-Carbó A (2015) Electrochemistry of immobilized particles and droplets: Experiments with three-phase electrodes. 2nd edn. Springer   International   Publishing,   Switzerland.   https://doi.org/10.1007/978-3-319-10843-8

88. Santos HA (2007) Improving the biomimetic properties of liquid/liquid interfaces: electrochemical and physicochemical characterisation. Dissertation, Helsinki University of Technology

89. Santos HA, García-Morales V, Pereira CM (2010) Electrochemical properties of phospholipid monolayers at liquid–liquid interfaces. ChemPhysChem 11:28-41. https://doi.org/10.1002/cphc.200900609

90. ZHONG LJ, Li-Fang GAO, Feng-Hua LI, Shi-Yu GAN, Li NIU (2019) Neurotransmitter Biomolecule Transfers Across Liquid/Liquid Interface Through A Thick Organic Membrane-Modified Electrode. Chinese J Anal Chem 47:e19001-e19008. https://doi.org/10.1016/S1872-2040(18)61137-5

91. Colombo ML, Sweedler JV, Shen M (2015) Nanopipet-based liquid–liquid interface probes for the electrochemical detection of acetylcholine, tryptamine, and serotonin via ionic transfer. Anal Chem 87:5095-5100. https://doi.org/10.1021/ac504151e

92. Hu D, Wang H, Gao K, Jiang X, Wang M, Long Y, Chen Y (2014) Anion transfer across "anion channels" at the liquid/liquid interface modified by anion-exchange membrane. RSC Adv 4:57035-57040. https://doi.org/10.1039/C4RA09985K

93. Dowhan W (1997) Molecular basis for membrane phospholipid diversity: why are there so many lipids? Annu Rev Biochem 66:199-232. https://doi.org/10.1146/annurev.biochem.66.1.199

94. Dudek J (2017) Role of cardiolipin in mitochondrial signaling pathways. Front Cell Dev Biol 5:90. https://doi.org/10.3389/fcell.2017.00090

95. Paradies G, Paradies V, Ruggiero FM, Petrosillo G (2019) Role of cardiolipin in mitochondrial function and dynamics in health and disease: Molecular and pharmacological aspects. Cells 8:728. https://doi.org/10.3390/cells8070728

96. Osman C, Voelker DR, Langer T (2011) Making heads or tails of phospholipids in mitochondria. J Cell Biol 192:7-16. https://doi.org/10.1083/jcb.201006159

97. Gohil VM, Greenberg ML (2009) Mitochondrial membrane biogenesis: phospholipids and proteins go hand in hand. J Cell Biol 184:469-472. https://doi.org/10.1083/jcb.200901127

98. Haines TH, Dencher NA (2002) Cardiolipin: a proton trap for oxidative phosphorylation. FEBS Lett 528:35-39. https://doi.org/10.1016/S0014-5793(02)03292-1

99. Beyer K, Klingenberg M (1985) ADP/ATP carrier protein from beef heart mitochondria has high amounts of tightly bound cardiolipin, as revealed by phosphorus-31 nuclear magnetic resonance. Biochemistry 24:3821-3826. https://doi.org/10.1021/bi00336a001

100.   Horvath SE, Daum G (2013) Lipids of mitochondria. Prog Lipid Res 52:590-614. https://doi.org/10.1016/j.plipres.2013.07.002

101.   El-Najjar N, Gali-Muhtasib H, Ketola RA, Vuorela P, Urtti A, Vuorela H (2011) The chemical and biological activities of quinones: overview and implications in analytical detection. Phytochem Rev 10:353-370. https://doi.org/10.1007/s11101-011-9209-1

102.   Lass A, Sohal RS (1999) Comparisons of coenzyme Q bound to mitochondrial membrane proteins among different mammalian species. Free Radical Biol Med 27:220-226. https://doi.org/10.1016/S0891-5849(99)00085-4

103.   Lenaz G (1988) Role of mobility of redox components in the inner mitochondrial membrane. J Membrain Biol 104:193-209. https://doi.org/10.1007/BF01872322

104.   Shi H, Noguchi N, Niki E (1999) Comparative study on dynamics of antioxidative action of α-tocopheryl hydroquinone, ubiquinol, and α-tocopherol against lipid peroxidation. Free Radic Biol Med 27:334-346. https://doi.org/10.1016/S0891-5849(99)00053-2

105.   Bentinger M, Brismar K, Dallner G (2007) The antioxidant role of coenzyme Q. Mitochondrion 7:S41-S50. https://doi.org/10.1016/j.mito.2007.02.006

106.   Dhanasekaran M, Ren J (2005) The emerging role of coenzyme Q-10 in aging, neurodegeneration, cardiovascular disease, cancer and diabetes mellitus. Curr Neurovasc Res 2:447-459. https://doi.org/10.2174/156720205774962656

107.   Hyun DH, Hernandez JO, Mattson MP, de Cabo R (2006) The plasma membrane redox system in aging. Ageing Res Rev 5:209-220. https://doi.org/10.1016/j.arr.2006.03.005

108.   Kumar A, Kaur H, Devi P, Mohan V (2009) Role of coenzyme Q10 (CoQ10) in cardiac disease, hypertension and Meniere-like syndrome. Pharmacol Ther 124:259-268. https://doi.org/10.1016/j.pharmthera.2009.07.003

109.   Simes DC, Viegas CS, Araújo N, Marreiros C (2020) Vitamin K as a Diet Supplement with Impact in Human Health: Current Evidence in Age-Related Diseases. Nutrients 12:138. https://doi.org/10.3390/nu12010138

110.   Fusaro M, Gallieni M, Porta, C, Nickolas TL, Khairallah P (2020) Vitamin K effects in human health: new insights beyond bone and cardiovascular health. J Nephrol 33:239-249. https://doi.org/10.1007/s40620-019-00685-0

111.   Halder M, Petsophonsakul P, Akbulut AC, Pavlic A, Bohan F, Anderson E, Maresz K, Kramann R, Schurgers L (2019) Vitamin K: double bonds beyond coagulation insights into differences between vitamin K1 and K2 in health and disease. Int J Mol Sci 20:896. https://doi.org/10.3390/ijms20040896

112.   Beulens JW, Booth SL, van den Heuvel EG, Stoecklin E, Baka A, Vermeer C (2013) The role of menaquinones (vitamin K_2) in human health. Br J Nutr 110:1357-1368. https://doi.org/10.1017/S0007114513001013

113.   Okano T, Shimomura Y, Yamane M, Suhara Y, Kamao M, Sugiura M, Nakagawa K (2008) Conversion of Phylloquinone (Vitamin K_1) into Menaquinone-4 (Vitamin K_2) in Mice two possible routes for menaquinone-4 accumulation in cerebra of mice. J Biol Chem 283:11270-11279. https://doi.org/10.1074/jbc.M702971200

114.   McCarthy PT, Shearer MJ, Gau G, Crampton OE, Barkhan P (1986) Vitamin K content of human liver at different ages. Haemostasis 16:84-85 (Abstract)

115.   Suttie JW, Nelsestuen GL (1980) Mechanism Of Action Of Vitamin K: Synthesis Of Y-Carboxyglutamic Aci. Crit Rev Biochem 8:191-223. https://doi.org/10.3109/10409238009105469

116.   Price PA (1988) Role of vitamin-K-dependent proteins in bone metabolism. Annu Rev Nutr 8:565-583. https://doi.org/10.1146/annurev.nu.08.070188.003025

117.   Benzakour O, Kanthou C (2000) The anticoagulant factor, protein S, is produced by cultured human vascular smooth muscle cells and its expression is up-regulated by thrombin. Blood 95:2008-2014. https://doi.org/10.1182/blood.V95.6.2008

118.   Tsaioun KI (1999) Vitamin K–dependent Proteins in the Developing and Aging Nervous System. Nutr Rev 57:231-240. https://doi.org/10.1111/j.1753-4887.1999.tb06950.x

119.   Wen L, Chen J, Duan L, Li S (2018) Vitamin K-dependent proteins involved in bone and cardiovascular health. Mol Med Rep 18:3-15. https://doi.org/10.3892/mmr.2018.8940

120.   Shanahan CM, Proudfoot D, Farzaneh-Far A, Weissberg PL (1998) The role of Gla proteins in vascular calcification. Crit Rev Eukar Gene Expr 8:357-375. https://doi.org/10.1615/CritRevEukarGeneExpr.v8.i3-4.60

121.   Dunovska K, Klapkova E, Sopko B, Cepova J, Prusa R (2019) LC–MS/MS quantitative analysis of phylloquinone, menaquinone-4 and menaquinone-7 in the human serum of a healthy population. PeerJ 7:e7695. https://doi.org/10.7717/peerj.7695

122.   Shearer MJ (1992) Vitamin K metabolism and nurtiure. Blood Rev 6:92-104. https://doi.org/10.1016/0268-960X(92)90011-E

123.   Shino M (1988) Determination of endogenous vitamin K (phylloquinone and menaquinone-n) in plasma by high-performance liquid chromatography using platinum oxide catalyst reduction and fluorescence detection. Analyst 113:393-397. https://doi.org/10.1039/AN9881300393

124.   Urayama S, Kawakami A, Nakashima T, Tsuboi M, Yamasaki S, Hida A, Ichinose Y, Nakamura H, Ejima E, Aoyagi T, Nakamura T (2000) Effect of vitamin K_2 on osteoblast apoptosis: vitamin K_2 inhibits apoptotic cell death of human osteoblasts induced by Fas, proteasome inhibitor, etoposide, and staurosporine. J Lab Clin Med 136:181-193. https://doi.org/10.1067/mlc.2000.108754

125.   Kameda T, Miyazawa K, Mori Y, Yuasa T, Shiokawa M, Nakamaru Y, Mano H, Hakeda Y, Kameda A, Kumegawa M (1996) Vitamin K_2 inhibits osteoclastic bone resorption by inducing osteoclast apoptosis. Biochem Biophys Res Commun 220:515-519. https://doi.org/10.1006/bbrc.1996.0436

126.   Xv F, Chen J, Duan L, Li S (2018) Research progress on the anticancer effects of vitamin K2 (Review). Oncol Lett 15:8926-8934. https://doi.org/10.3892/ol.2018.8502

127.   Li Y, peng Chen J, Duan L, Li S (2018) Effect of vitamin K2 on type 2 diabetes mellitus: A review. Diabetes Res Clin Pract 136:39-51. https://doi.org/10.1016/j.diabres.2017.11.020

128.   Cerqua C, Casarin A, Pierrel F, Fonseca LV, Viola G, Salviati L, Trevisson E (2019) Vitamin K2 cannot substitute Coenzyme Q_{10} as electron carrier in the mitochondrial respiratory chain of mammalian cells. Sci Rep 9:1-7. https://doi.org/10.1038/s41598-019-43014-y

129.   Petrova SA, Ksenzhek OS, Kolodyazhnyi MV (2000) Redox properties of naturally occurring naphthoquinones: vitamin $K_{2(20)}$ and lapachol. Russ J Electrochem 36:767–772. https://doi.org/10.1007/BF02757678

130.   Ksenzhek OS, Petrova SA, Kolodyazhny MV, Oleinik SV (1977) Redox properties of K-group vitamins. Bioelectrochem Bioenerg 4:335–345. https://doi.org/10.1016/0302-4598(77)80035-4

131.   Ausili A, Clemente J, Pons-Belda ÓD, de Godos A, Corbalán-García S, Torrecillas A, Teruel JA, Gomez-Fernández JC (2020) Interaction of Vitamin K_1 and Vitamin K_2 with Dimyristoylphosphatidylcholine and Their Location in the Membrane. Langmuir 36:1062-1073. https://doi.org/10.1021/acs.langmuir.9b03552

132.   Lovander MD, Lyon JD, Parr IV DL, Wang J, Parke B, Leddy J (2018) Critical review—electrochemical properties of 13 vitamins: a critical review and assessment. J Electrochem Soc 165:G18-G49. https://doi.org/10.1149/2.1471714jes

4   List of publications

Publications accepted in peer reviewed journals

1. <u>Dharmaraj K</u>, Nasri Z, Kahlert H, Scholz F (2018) The electrochemistry of DPPH in three-phase electrode systems for ion transfer and ion association studies. J Electroanal Chem 823:765-772. https://doi.org/10.1016/j.jelechem.2018.06.012

2. <u>Dharmaraj K</u>, Silva JIR, Kahlert H, Lendeckel U, Scholz F (2020) The acid–base and redox properties of menaquinone MK-4, MK-7, and MK-9 (vitamin K_2) in DMPC monolayers on mercury. Eur Biophys J 49:279–288. https://doi.org/10.1007/s00249-020-01433-0

Manuscript submitted

1. <u>Dharmaraj K</u>, Dattler D, Kahlert H, Lendeckel U, Nagel F, Delcea M, Scholz F (2020) The effects of the chemical environment of menaquinones in lipid monolayers on mercury electrodes on the thermodynamics and kinetics of their electrochemistry. Submitted to European Biophysics Journal. Submitted for publication on November 4, 2020. Submission ID: EBJO-D-20-00209.

5   Author contributions

1. <u>Dharmaraj K</u>, Nasri Z, Kahlert H, Scholz F (2018) The electrochemistry of DPPH in three-phase electrode systems for ion transfer and ion association studies. J Electroanal Chem 823:765-772. https://doi.org/10.1016/j.jelechem.2018.06.012
    KD, ZN, and FS were responsible for the study design. KD performed and analysed the ion transfer experiments with the immobilised droplets (about 90% of the experimental work). ZN performed the experiments with the composite electrodes (about 10% of the experimental work). All authors discussed and interpreted the results. FS and KD wrote the manuscript and all authors revised the manuscript.

2. <u>Dharmaraj K</u>, Silva JIR, Kahlert H, Lendeckel U, Scholz F (2020) The acid–base and redox properties of menaquinone MK-4, MK-7, and MK-9 (vitamin K_2) in DMPC monolayers on mercury. Eur Biophys J 49:279–288. https://doi.org/10.1007/s00249-020-01433-0
    KD and FS were responsible for the study design. KD performed the experiments and analysed the data. KD, JIRS, HK, UL, and FS discussed and interpreted the results. FS and KD wrote the manuscript and all authors revised the manuscript.

3. <u>Dharmaraj K</u>, Dattler D, Kahlert H, Lendeckel U, Nagel F, Delcea M, Scholz F (2020) The effects of the chemical environment of menaquinones in lipid monolayers on mercury electrodes on the thermodynamics and kinetics of their electrochemistry. Submitted to European Biophysics Journal. Submitted for publication on November 4, 2020. Submission ID: EBJO-D-20-00209
    KD and FS were responsible for the study design. KD performed the experiments relating to the effects of cholesterol and water activity experiments. DD made the cardiolipins experiments supervised by KD. FN did the calorimetric measurements. KD analysed the data. KD, DD, HK, UL, FN, MD, and FS discussed and interpreted the results. KD and FS wrote the manuscript and all authors revised the content.

Prof. Dr. Fritz Scholz	Karuppasamy Dharmaraj

6   Publications

6.1   Publication No. 1

The electrochemistry of DPPH in three-phase electrode systems for ion transfer and ion association studies

Karuppasamy Dharmaraj, Zahra Nasri, Heike Kahlert, Fritz Scholz,

The electrochemistry of DPPH in three-phase electrode systems for ion transfer and ion association studies

Karuppasamy Dharmaraj, Zahra Nasri, Heike Kahlert, Fritz Scholz*

Institut für Biochemie, Universität Greifswald, Felix-Hausdorff-Straße 4, D-17487 Greifswald, Germany

ARTICLE INFO

ABSTRACT

The three-phase electrochemistry of 2,2-diphenyl-1-picrylhydrazyl (DPPH) has been studied by attaching a droplet of nitrobenzene (NB) containing DPPH to a graphite electrode in an aqueous electrolyte solution. Since DPPH can be reduced to DPPH$^-$ and oxidized to DPPH$^+$, the accompanying ion transfer to NB and ion pair formation in NB are accessible. The anion transfer from water to nitrobenzene is accompanied by the formation of ion pairs [DPPH$^+$An$^-$] with nitrate, hexafluorophosphate, perchlorate and trichloroacetate. The ion pair formation of DPPH$^-$ with tetrabutylammonium cations is very weak. When the DPPH is dissolved in molten paraffin together with the salt tetrabutylammonium tetrafluoroborate (TBATFB), and composite electrodes are produced by mixing the paraffin with graphite powder, DPPH exhibits a typically surface electrochemical response providing a rather stable system DPPH/DPPH$^-$.

1. Introduction

Three-phase electrochemistry is typically realised with electroactive solids undergoing insertion electrochemical reaction (e.g. in battery materials). Using organic solvent droplets containing dissolved redox active compounds, allows to expand three-phase electrochemistry in order to study the thermodynamics ruling insertion electrochemistry [1–5]. In that arrangement, the electrochemical reaction commences at the three-phase boundary. Studies of the thermodynamics of insertion electrochemical reactions are of general importance as they provide the key to distinguish between the contributions of electron and ion transfer to the overall electrochemical reaction [6, 7]. Decamethylferrocene (DMFC) has been used extensively for the transfer of anions. For cations, iodine [8] and iron(III) tetraphenyl porphyrin chloride [9] are applicable. Only one compound (lutetium bis(tetra-*tert*-butylphthalocyaninato) has been reported so far [10, 11] to be able to transfer both anions and cations; however, that complex is not commercially available. Instead of using droplets of organic solvents, also solid phases capable of insertion electrochemical reactions can be used to determine free energies of ion transfer between different solvents, even between miscible solvents [6, 7]. The electrochemistry of DPPH dissolved in organic solvents [12, 13] and also as solid material [14] is well documented. Here we show that the stable radical 2,2-diphenyl-1-picrylhydrazyl (DPPH) can be also used for ion transfer studies, although ion pair formation complicates the system. The DPPH study has been performed also to better understand the behavior of DPPH in lipid

monolayers, which will be reported in due course.

Experiments with DPPH-TBATFB-graphite-paraffin composite electrode indicate a possible use for detecting radical scavengers.

2. Experimental

2.1. Chemicals

The following chemicals were used: tetramethylammonium bromide (TMAB) (99%), KNO$_3$ ($\geq$99%), nitrobenzene (GC Assay) and paraffin in pastille form were from Merck, Germany. Tetraethylammonium bromide (TEAB) (99%), tetrabutylammonium bromide (TBAB), tetrabutylammonium hydroxide (TBAOH) and potassium hexafluorophosphate (PHFP) ($\geq$98%) were from Fluka, Switzerland. Tetrabutylammonium perchlorate (TBAP) ($\geq$98%), TBATFB (99%) and DPPH from Sigma Aldrich, Germany, and sodium perchlorate from VEB Laborchemie Jena, Germany. Sodium trichloroacetate (CCl$_3$COONa) and graphite powder (99.99%) were from Alfa Aesar, Germany. Potassium chloride (99.5%), disodium hydrogen phosphate (98%) and sodium dihydrogen phosphate (98%) were from Roth, Germany. Paraffin impregnated graphite electrodes (PIGE's) have been prepared as previously reported [15].

2.2. Instrumentation

CV's were recorded using the AUTOLAB PGSTAT 12 (Metrohm,

Switzerland) in conjunction with a conventional three-electrode cell in all experiments. The working electrode was a PIGE with diameter of 5 mm, the reference electrode was Ag/AgCl (sat. KCl) and a platinum rod served as counter electrode.

Electrode preparation

    (a) Graphite electrodes with attached nitrobenzene droplets containing DPPH

One microliter droplets of nitrobenzene containing, if not otherwise stated, $10^{-3}\,mol\,L^{-1}$ DPPH, where dispensed with a μL-pipette to the polished circular surface of paraffin impregnated graphite electrodes.

    (b) Composite electrodes consisting of graphite, DPPH, and TBATFB

DPPH and TBATFB were dissolved in melted paraffin (m.p.: 56–58 °C) and mixed with graphite powder to prepare composite electrodes. Three different electrodes were made:

    (El-1) 2.26 mass-% DPPH, 37.59 mass-% paraffin, 60.15 mass-% graphite (0.015 g DPPH, 0.25 g paraffin, 0.4 g graphite),

    (El-2) 2.03 mass-% DPPH, 10.14 mass-% TBATFB, 33.78 mass-% paraffin, 54.05 mass-% graphite (0.015 g DPPH, 0.075 g TBATFB, 0.25 g paraffin, 0.4 g graphite), and,

    (El-3) 2.22 weight-% DPPH, 40.00 weight-% TBATFB, 22.22 mass-% paraffin, 35.56 mass-% graphite (0.025 g DPPH, 0.45 g TBATFB, 0.25 g paraffin, 0.4 g graphite).

A portion of each composite mixture was pressed into 5 mm diameter plastic rods and used as working electrode. The electrode surface was polished on a piece of weighing paper.

All the measurements were performed in 50 mM phosphate buffer (pH 7.0).

3. Results and discussion

3.1. Electrochemistry of DPPH in an immobilized nitrobenzene droplet coupled to the transfer of counter ions from water to nitrobenzene

DPPH exhibits in nitrobenzene (NB) solutions two reversible redox systems:

$$DPPH + e^- \rightleftharpoons DPPH^- \qquad \text{(Equilibrium I)}$$

(mid-peak potential $E^{mp}_{D/D^-} = 0.225\,V$ vs SCE), and

$$DPPH \rightleftharpoons DPPH^+ + e^- \qquad \text{(Equilibrium II)}$$

(mid-peak potential $E^{mp}_{D^+/D} = 0.790\,V$ vs SCE) [13]. The nitro groups of DPPH are irreversibly reduced when the potential is decreased below about $-0.5\,V$, but this has been avoided in all experiments reported here. Fig. 1 shows consecutive cyclic voltammograms (CV's) recorded with a graphite electrode to the surface of which was attached a 1 μL droplet of NB with $10^{-3}\,mol\,L^{-1}$ DPPH. The surrounding aqueous solution contained 4 mmol L^{-1} tetrabutylammonium perchlorate (TBAP). Unfortunately, a larger salt concentration could not be used because of the poor solubility of TBAP in water. Two main voltammetric systems are present, one with a mid-peak potential of around 0.35 V and the other around 0.87 V, indicating that the first is caused by the system DPPH/DPPH$^-$ and the second by DPPH/DPPH$^+$. The very small system at around 0.75 V could not been yet elucidated. Although the CV's show slight changes in the course of cycles, the mid-peak potentials are relative constant. The CV's exhibit a third system which precedes the DPPH/DPPH$^+$ couple, but only when the CV's are recorded in the full potential range.

(a) Cation transfer caused by DPPH reduction
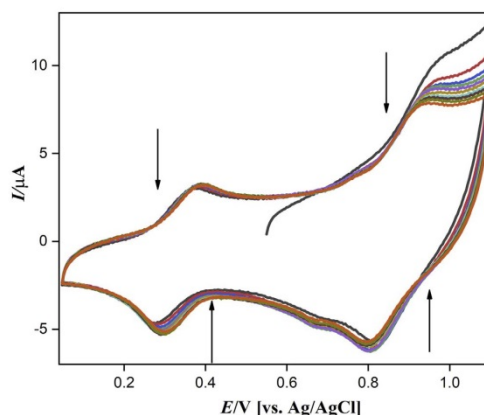
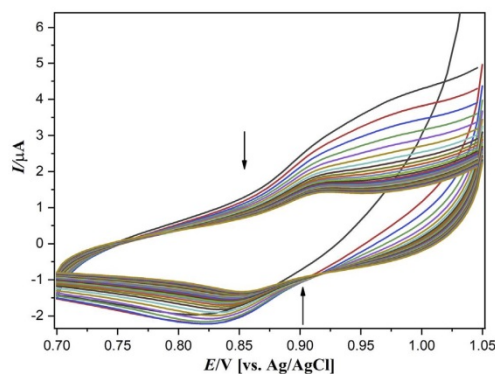**Fig. 1.** Cyclic voltammograms of 1 μL nitrobenzene droplet containing $10^{-3}\,mol\,L^{-1}$ DPPH attached to a PIGE and surrounded by an aqueous electrolyte containing 4 mmol L^{-1} TBAP. Scan rate: 10 mV s^{-1}, starting potential: 0.5 V. The arrows mark the changes of voltammograms during cycling.
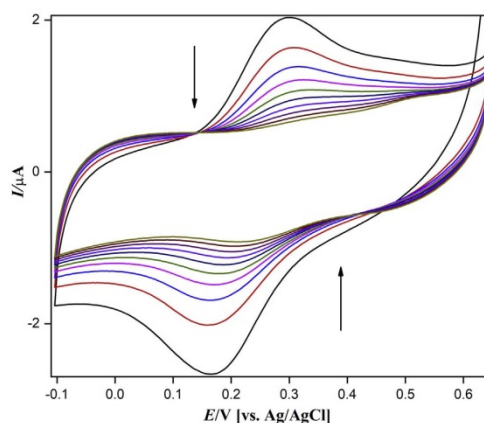
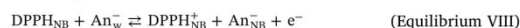**Fig. 2.** Cyclic voltammograms of 1 μL nitrobenzene droplet containing $10^{-3}\,mol\,L^{-1}$ DPPH attached to a PIGE and surrounded by an aqueous electrolyte containing 0.1 mol L^{-1} TMAB. Scan rate: 10 mV s^{-1}, starting potential: 0.65 V. The arrows mark the changes of voltammograms during cycling.

Following this experiment, separate studies have been performed with the two main redox couples: Fig. 2 shows the couple DPPH/DPPH$^-$ with an aqueous electrolyte containing 0.1 mol L^{-1} tetramethylammonium bromide (TMAB). The peak currents rapidly decreased in consecutive cycles, and the droplet completely lost its pink colour. This is indicative of a transfer of DPPH$^-$ from NB to water, where it disappears due to diffusion into the bulk. Obviously, tetramethylammonium cations are not hydrophobic enough to support the electrode reaction.

$$DPPH_{NB} + e^- + TMA^+_w \rightleftharpoons DPPH^-_{NB} + TMA^+_{NB} \qquad \text{(Equilibrium III)}$$
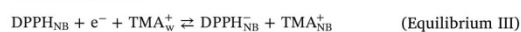
with a cation transfer from water to NB. The proceeding electrode reaction is instead:

$$DPPH_{NB} + e^- \rightleftharpoons DPPH^-_w \qquad \text{(Equilibrium IV)}$$

Essentially the same observations were made when using
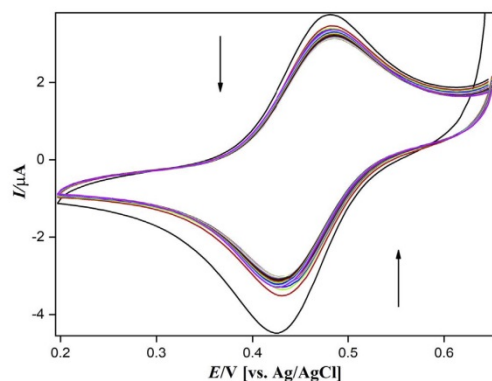
Fig. 3. Cyclic voltammograms of a 1 μL nitrobenzene droplet containing 10^{-3} mol L^{-1} DPPH attached to a PIGE and surrounded by an aqueous electrolyte containing 0.05 mol L^{-1} TBAB. Scan rate: 10 mV s^{-1}, starting potential: 0.65 V. The arrows mark the changes of voltammograms during cycling.

Fig. 4. Cyclic voltammograms of a 1 μL nitrobenzene droplet containing 10^{-3} mol L^{-1} DPPH attached to a PIGE and surrounded by an aqueous electrolyte containing 0.1 mol L^{-1} KNO$_3$. Scan rate: 10 mV s^{-1}, starting potential: 1.05 V. The arrows mark the changes of voltammograms during cycling.

tetraethylammonium cations. When tetrabutylammonium cations are provided in the aqueous phase, the voltammetric system is rather stable, i.e. only minor changes of peak currents are observed (cf. Fig. 3). The electrode reaction could be:

$$\text{DPPH}_{\text{NB}} + e^- + \text{TBA}^+_{\text{w}} \rightleftharpoons \text{DPPH}^-_{\text{NB}} + \text{TBA}^+_{\text{NB}} \qquad \text{(Equilibrium V)}$$
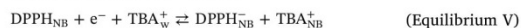
If that reaction is operative, for the condition $c_{\text{DPPH}_{\text{w}}} \ll c_{\text{TBA}^+_{\text{w}}}$, the slope of the mid-peak potential vs. $\log c_{\text{TBA}^+_{\text{w}}}$ should be $+59$ mV at 25 °C [2]. Experimentally we found a strong dependence of the formal potential on TBAB concentration (Fig. 7): in the lower concentration region the slope is around 95 mV and in the higher concentration region the slope is 23 mV. Since TBAB can partition between NB and water, a mixed mechanism with involvement of partitioned Br$^-$ is also possible:

$$\text{DPPH}_{\text{NB}} + e^- + \text{Br}^-_{\text{NB}} \rightleftharpoons \text{DPPH}^-_{\text{NB}} + \text{Br}^-_{\text{w}} \qquad \text{(Equilibrium VI)}$$
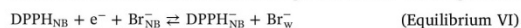
If the reactions V and VI proceed simultaneously, the slope may vary with TBAB concentration in the aqueous phase. The peak separation in CV is 54 and 58 mV for $c_{\text{TBA}^+_{\text{w}}} = 0.1$ mol L^{-1} and $c_{\text{TBA}^+_{\text{w}}} = 0.05$ mol L^{-1}, respectively, which is in agreement assuming a one-electron reaction. For $c_{\text{TBA}^+_{\text{w}}} = 0.01$ mol L^{-1} the peak separation increased to 99 mV, and for $c_{\text{TBA}^+_{\text{w}}} = 0.005$ mol L^{-1} the peak separation was even 123 mV, indicating increasing irreversibility. Because of the described problems using TBAB, we performed experiments using tetrabutylammonium hydroxide (TBAOH), as the hydroxide ions are much more hydrophilic than bromide, and a simultaneous transfer of OH$^-$ with TBA$^+$ is excluded. Using TBAOH the slope of formal potentials versus logarithm of TBA$^+$ concentration was 70 mV (in the range of TBAOH concentrations 0.1 mol L^{-1} to 5 mmol L^{-1}). Since in that system now the Equilibrium V is obviously operative, the following equation can be applied:

$$\Delta\varphi^\ominus_{\text{w}\rightarrow\text{NB, TBA}^+} = E^{\ominus'}_{\text{c, DPPH}^{0/+1}_{\text{NB}}, \text{TBA}^+_{\text{w}\rightarrow\text{NB}}} - E^\ominus_{\text{DPPH}^{0/-1}_{\text{NB}}} - \frac{RT}{F}\ln c_{\text{TBA}^+_{\text{w}}} - \frac{RT}{F}\ln\frac{2}{C^0_{\text{DPPH}_{\text{NB}}}} \qquad (1)$$

when the condition $C^0_{\text{DPPH}_{\text{NB}}} \ll c_{\text{TBA}^+_{\text{w}}}$ is kept [2]. Using this equation, $\Delta G^\ominus_{\text{w}\rightarrow\text{NB, TBA}^+}$ is found to be -10.61 KJ mol^{-1} ($\Delta\varphi^\ominus_{\text{w}\rightarrow\text{NB, TBA}^+} = 0.11$ V). Previously, using DMFC as redox probe, we have determined $\Delta G^\ominus_{\text{w}\rightarrow\text{NB, TBA}^+} = -8.2$ KJ mol^{-1} ($\Delta\varphi^\ominus_{\text{w}\rightarrow\text{NB, TBA}^+} = 0.085$ V). As we show in the paragraph on ion pair formation, the more negative value calculated here is most probably the result of the additional driving force due to that ion pair formation in NB.

(b) Anion transfer caused by DPPH oxidation

The system

$$\text{DPPH}_{\text{NB}} \rightleftharpoons \text{DPPH}^+_{\text{NB}} + e^- \qquad \text{(Equilibrium VII)}$$

should be capable to transfer anions from the aqueous phase to NB, according to the electrode reaction:

$$\text{DPPH}_{\text{NB}} + \text{An}^-_{\text{w}} \rightleftharpoons \text{DPPH}^+_{\text{NB}} + \text{An}^-_{\text{NB}} + e^- \qquad \text{(Equilibrium VIII)}$$

Therefore, experiments have been performed providing different anions in the aqueous phase. With nitrate ions in the concentration range from 10^{-1} mol L^{-1} to $5\cdot10^{-3}$ mol L^{-1} the voltammetric peak currents quickly decreased (cf. Fig.4). With perchlorate anions, the voltammetric system was stable (Fig. 5), and the formal potential shifted by -61 mV with $\log c_{\text{An}^-_{\text{w}}}$. The peak separation was 86 mV for nitrate (NO$_3^-$), 83 mV for perchlorate (ClO$_4^-$), 151 mV for hexafluorophosphate (HFP$^-$), and 88 mV for trichloroacetate (TCA$^-$). With the exception of hexafluorophosphate, the values are not too different from the 60 mV of a one-electron process. The calculation of the $\Delta\varphi^\ominus_{\text{w}\rightarrow\text{NB, An}^-}$ values was performed with the equation:

$$\Delta\varphi^\ominus_{\text{w}\rightarrow\text{NB, An}^-} = E^{\ominus'}_{\text{c, DPPH}^{0/+1}_{\text{NB}}, \text{An}^-_{\text{w}\rightarrow\text{NB}}} - E^\ominus_{\text{DPPH}^{0/+1}_{\text{NB}}} + \frac{RT}{F}\ln c_{\text{An}^-_{\text{w}}} - \frac{RT}{F}\ln\frac{C^0_{\text{DPPH}_{\text{NB}}}}{2} \qquad (2)$$

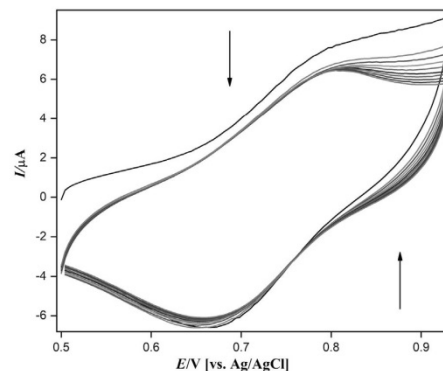**Fig. 5.** Cyclic voltammograms of a 1 μL nitrobenzene droplet containing 10^{-3} mol L^{-1} DPPH and surrounded by an electrolyte containing 0.1 mol L^{-1} NaClO$_4$. Scan rate: 10 mV s^{-1}, starting potential: 0.5 V. The arrows mark the changes of voltammograms during cycling.

Table 1
Standard free energies of anion transfer $\Delta G^{\ominus}_{w \to NB, An^-}$ in kJ mol^{-1} as determined with the help of DPPH oxidation, and literature values.

Anion	This work	[1]	[16]	[17]	[18]	[19]	[20]
NO_3^-	17.92	26.05	26.05	24	24.4	26.1	24.4
ClO_4^-	3.31	8.01	8.78	10	8	7.7	8.7
TCA^-	16.36	18.8 [21]					
HFP^-	−4.95		−1.16				

and using the relation $\Delta G^{\ominus}_{w \to NB, An^-} = -nF\Delta\varphi^{\ominus}_{w \to NB, An^-}$ the standard free energies of anion transfer $\Delta G^{\ominus}_{w \to NB, An^-}$ were found (see Table 1).

In view of the rather consistent values provided in literature and in our previous measurements, we assume that the significantly smaller values calculated in this study are the result of an additional driving force for the transfer of anions from water to NB. This additional driving force can be explained by ion pair formation of the kind $[DPPH^+ anion^-]$ (see next paragraph).

Quantitative treatment of a possible ion pair formation of DPPH$^-$ and DPPH$^+$ with the transferred counter ions in nitrobenzene

(a) Ion pair formation of DPPH$^+$ with transferred anions

When the electrochemically generated DPPH$^+$ cations form ion pairs with the transferred anions, the following equilibria have to be considered:
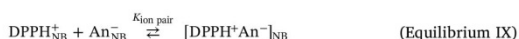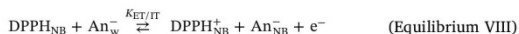
$$DPPH_{NB} + An_w^- \overset{K_{ET/IT}}{\rightleftarrows} DPPH_{NB}^+ + An_{NB}^- + e^- \qquad \text{(Equilibrium VIII)}$$

$$DPPH_{NB}^+ + An_{NB}^- \overset{K_{ion\ pair}}{\rightleftarrows} [DPPH^+An^-]_{NB} \qquad \text{(Equilibrium IX)}$$

Neglecting the deviations between activities and concentrations, the ion pair formation has the following equilibrium constant $K_{ion\ pair}$:

$$K_{ion\ pair} = \frac{c_{([DPPH^+An^-])_{NB}}}{c_{An_{NB}^-} c_{DPPH_{NB}^+}} \qquad (3)$$

because of the electroneutrality condition ($c_{DPPH_{NB}^+} = c_{An_{NB}^-}$) it follows from Eq. (3) that

$$c_{DPPH_{NB}^+}^2 = \frac{c_{([DPPH^+An^-])_{NB}}}{K_{ion\ pair}} \qquad (4)$$

The formal potential of the Equilibrium VIII is:

$$E^{\ominus'}_{c, DPPH_{NB}^{0/+1}, An_{-w \to NB}^-} = E^{\ominus}_{DPPH_{NB}^{0/+1}} + \Delta\varphi^{\ominus}_{w \to NB, An^-} + \frac{RT}{F}\ln\frac{c_{DPPH_{NB}}c_{An_{NB}^-}}{c_{DPPH_{NB}^+}c_{An_w^-}} \qquad (5)$$

with $c_{DPPH_{NB}^+} = c_{An_{NB}^-}$ follows for the case of ion pair formation:

$$E^{\ominus'}_{c, DPPH_{NB}^{0/+1}, An_{-w \to NB}^-, ion\ pair} = E^{\ominus}_{DPPH_{NB}^{0/+1}} + \Delta\varphi^{\ominus}_{w \to NB, An^-} + \frac{RT}{F}\ln\frac{c_{DPPH_{NB}^+}^2}{c_{DPPH_{NB}}c_{An_w^-}} \qquad (6)$$

Substituting $c_{DPPH_{NB}^+}^2$ from Eq. (6), yields:

$$E^{\ominus'}_{c, DPPH_{NB}^{0/+1}, An_{-w \to NB}^-, ion\ pair} = E^{\ominus}_{DPPH_{NB}^{0/+1}} + \Delta\varphi^{\ominus}_{w \to NB, An^-} - \frac{RT}{F}\ln c_{An_w^-} + \frac{RT}{F}\ln\frac{c_{([DPPH^+An^-])_{NB}}}{c_{DPPH_{NB}}K_{ion\ pair}} \qquad (7)$$

Mass conservation (no transfer of DPPH species to water) can be expressed as follows

$$c_{DPPH_{NB}} + c_{DPPH_{NB}^+} + c_{([DPPH^+An^-])_{NB}} = C^0_{DPPH_{NB}}, \qquad (8)$$

where $C^0_{DPPH_{NB}}$ denotes the overall concentration of DPPH (all species). At the formal potential, the concentrations of oxidized and reduced DPPH are equal:

$$c_{([DPPH^+An^-])_{NB}} + c_{DPPH_{NB}^+} = c_{DPPH_{NB}} = \frac{C^0_{DPPH_{NB}}}{2} \qquad (9)$$

Assuming that in this balance equation the relation $c_{([DPPH^+An^-])_{NB}} \gg c_{DPPH_{NB}^+}$ holds, i.e.,

Table 2
Logarithm of equilibrium constants of ion pair formation using Eq. (12), and the average of literature values of $\Delta\varphi^{\ominus}_{w \to NB, An^-}$ (0.256 V for nitrate, 0.089 V for perchlorate, and 0.195 V for trichloroacetate, −0.012 V for hexafluorophosphate), the literature value of $E^{\ominus}_{DPPH_{NB}^{0/+1}}$ [13], and the experimentally measured formal potentials $E^{\ominus'}_{c, DPPH_{NB}^{0/+1}, An_{-w \to NB}^-, ion\ pair}$.

Anions	Concentration [mol L^{-1}]	log $K_{ion\ pair}$
NO_3^-	0.1	4.44
	0.05	4.56
	0.01	4.49
	0.005	4.51
ClO_4^-	0.1	4.26
	0.05	4.25
	0.01	4.15
	0.005	4.28
TCA^-	0.1	3.74
	0.05	3.74
	0.01	3.74
	0.005	3.74
HFP^-	0.1	3.91
	0.05	3.93
	0.01	4.18
	0.005	3.89

$c_{([DPPH^+An^-])_{NB}} \approx c_{DPPH_{NB}} \approx \frac{C^0_{DPPH_{NB}}}{2}$ is a good approximation, one gets:

$$E^{\ominus'}_{c, DPPH_{NB}^{0/+1}, An_{-w \to NB}^-, ion\ pair} = E^{\ominus}_{DPPH_{NB}^{0/+1}} + \Delta\varphi^{\ominus}_{w \to NB, An^-} - \frac{RT}{F}\ln c_{An_w^-} + \frac{RT}{F}\ln\frac{c_{[[DPPH^+An^-]]_{NB}}}{c_{[[DPPH^+An^-]]_{NB}}K_{ion\ pair}} \qquad (10)$$

$$E^{\ominus'}_{c, DPPH_{NB}^{0/+1}, An_{-w \to NB}^-, ion\ pair} = E^{\ominus}_{DPPH_{NB}^{0/+1}} + \Delta\varphi^{\ominus}_{w \to NB, An^-} - \frac{RT}{F}\ln c_{An_w^-} - \frac{RT}{F}\ln K_{ion\ pair} \qquad (11)$$

and for $T = 25\,°C$ the equilibrium constant of ion pair formation can be calculated with equation:

$$\log K_{ion\ pair} = \frac{E^{\ominus}_{DPPH_{NB}^{0/+1}} - E^{\ominus'}_{c, DPPH_{NB}^{0/+1}, An_{-w \to NB}^-, ion\ pair} + \Delta\varphi^{\ominus}_{w \to NB, An^-} - 0.059[V]\log c_{An_w^-}}{0.059[V]} \qquad (12)$$

The standard potential $E^{\ominus}_{DPPH_{NB}^{0/+1}}$ was taken from reference [13], where it has been provided from cyclic voltammetry as the mid-peak potential measured versus an aqueous saturated calomel (SCE) electrode using a two-part salt bridge, where one part (connecting the SCE) was filled with saturated KCl solution, and the other part (connecting with the NB solution) was filled with the same electrolyte as the voltammetric cell (0.1 mol L^{-1} tetraethylammonium perchlorate). We are aware that the salt bridge may introduce a small deviation of the potential referred to an aqueous electrolyte. Of course, we have converted the SCE related data to Ag/AgCl data of our experiments.

Table 2 lists the logarithms of equilibrium constants of ion pair formation for 4 different anions, each at 4 different concentrations in the aqueous phase. For these data we have used the literature values of standard potentials of ion transfer, because they are very consistent, and our data in Table 1 are significantly deviating towards smaller Gibbs energies of transfer. It is very remarkable that the calculated equilibrium constants are independent of the anion concentration in the aqueous phase, which is mandatory when the relation $c_{([DPPH^+An^-])_{NB}} \gg c_{DPPH_{NB}^+}$ really holds. Therefore, the data in Table 2 are strongly supporting validity of the approximation $c_{([DPPH^+An^-])_{NB}} \approx c_{DPPH_{NB}} \approx \frac{C^0_{DPPH_{NB}}}{2}$. Further, the magnitude of the calculated equilibrium constants is typical for this kind of constants for rather small anions and larger organic cations in nitrobenzene [22, 23]. Fig. 6 gives a plot of the $\log K_{ion\ pair}$ data versus the ion potential (charge/radius) of the anions. This plot shows that the ion pair equilibrium constants grow with decreasing ion potential, as it has to be expected. Since the ion pair equilibrium constants are rather high, we
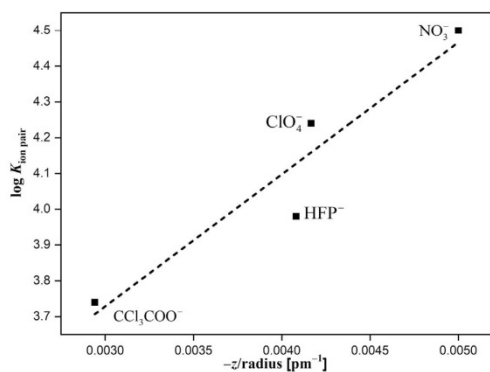
Fig. 6. Plot of the $\log K_{\text{ion pair}}$ data versus the ion potential (charge/radius) of the anions.
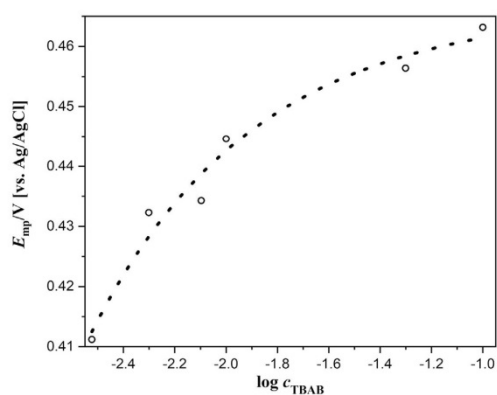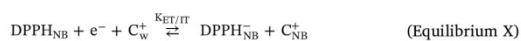

Fig. 7. Plot of the mid-peak potential E_{mp} of DPPH reduction versus logarithm of TBAB concentration in the aqueous phase.

hope that future studies can decide about the correctness of our approach.

(b) Ion pair formation of DPPH⁻ with transferred cations

In the case of reduction of DPPH to DPPH⁻ accompanied by the transfer of charge compensating cations, the following two equilibria will be established:

$$\text{DPPH}_{\text{NB}} + e^- + C_w^+ \overset{K_{\text{ET/IT}}}{\rightleftharpoons} \text{DPPH}_{\text{NB}}^- + C_{\text{NB}}^+ \qquad \text{(Equilibrium X)}$$

$$\text{DPPH}_{\text{NB}}^- + C_{\text{NB}}^+ \overset{K_{\text{ion pair}}}{\rightleftharpoons} [\text{DPPH}^-C^+]_{\text{NB}} \qquad \text{(Equilibrium XI)}$$

Neglecting the deviations between activities and concentrations, the ion pair formation has the following equilibrium constant $K_{\text{ion pair}}$:

$$K_{\text{ion pair}} = \frac{c_{([\text{DPPH}^-C^+])_{\text{NB}}}}{c_{C_{\text{NB}}^+} c_{\text{DPPH}_{\text{NB}}^-}} \qquad (13)$$

Because of the electroneutrality condition ($c_{\text{DPPH}_{\text{NB}}^-} = c_{C_{\text{NB}}^+}$) it follows from Eq. (14) that

$$c_{\text{DPPH}_{\text{NB}}^-}^2 = \frac{c_{([\text{DPPH}^-C^+])_{\text{NB}}}}{K_{\text{ion pair}}} \qquad (14)$$
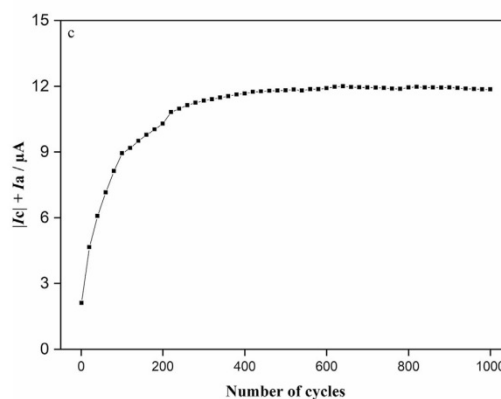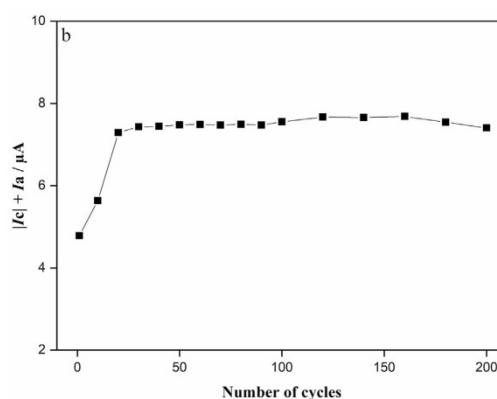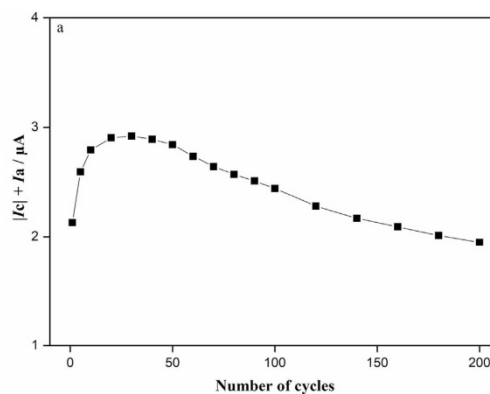
Fig. 8. Changes of the sums of cathodic and anodic peak currents of the DPPH/DPPH⁻ system in successive cyclic voltammograms for **(a)** Electrode El-1, **(b)** Electrode El-2 and **(c)** Electrode El-3 in phosphate buffer (pH 7.0).
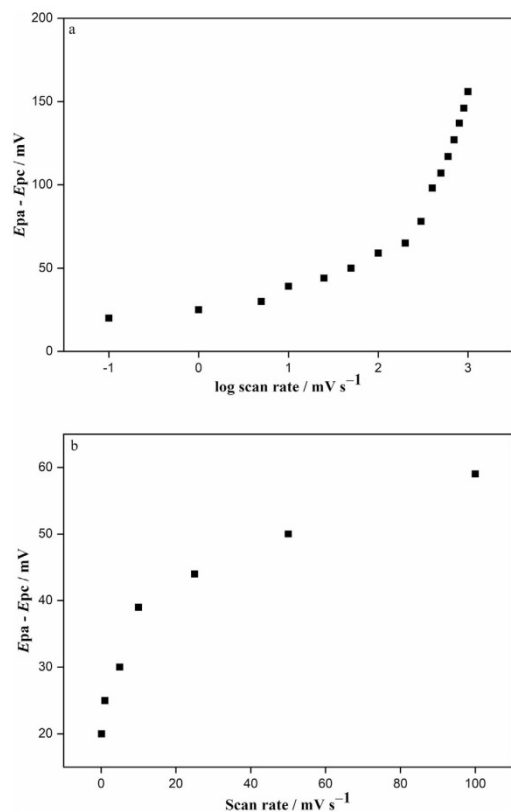
Fig. 9. (a) Peak separation of the DPPH/DPPH⁻ system versus logarithm of scan rate. (b) Peak separation of the DPPH/DPPH⁻ system versus scan rate in the smallest scan rate range.
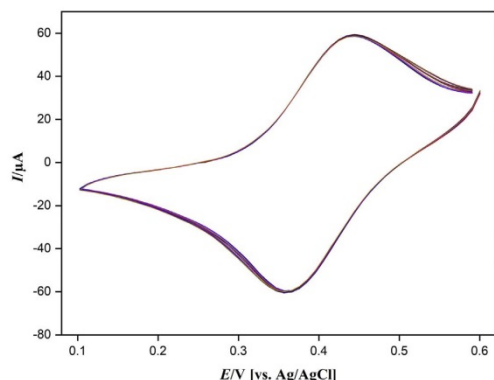
Fig. 10. Plot of every 20th scan between the 800th and 1.000th cyclic voltammograms of electrode El-3 in phosphate buffer (pH 7.0). Scan rate: 100 mV s⁻¹, starting potential: 0.6 V.

The formal potential of the Equilibrium X is:

$$E^{\ominus'}_{c,\,DPPH^{0/-1}_{NB},\,C^+_{w\to NB}} = E^{\ominus}_{DPPH^{0/-1}_{NB}} + \Delta\varphi^{\ominus}_{w\to NB,\,C^+} + \frac{RT}{F}\ln\frac{c_{DPPH_{NB}}\,c_{C^+_w}}{c_{DPPH^-_{NB}}\,c_{C^+_{NB}}} \quad (15)$$

With $c_{DPPH^-_{NB}} = c_{C^+_{NB}}$ follows for the case of ion pair formation:

$$E^{\ominus'}_{c,\,DPPH^{0/-1}_{NB},\,C^+_{w\to NB},\,ion\,pair} = E^{\ominus}_{DPPH^{0/-1}_{NB}} + \Delta\varphi^{\ominus}_{w\to NB,\,C^+} + \frac{RT}{F}\ln\frac{c_{DPPH_{NB}}\,c_{C^+_w}}{c^2_{DPPH^-_{NB}}} \quad (16)$$

Substituting $c^2_{DPPH^-_{NB}}$ from Eq. (16), yields:

$$E^{\ominus'}_{c,\,DPPH^{0/-1}_{NB},\,C^+_{w\to NB},\,ion\,pair} = E^{\ominus}_{DPPH^{0/-1}_{NB}} + \Delta\varphi^{\ominus}_{w\to NB,\,C^+} + \frac{RT}{F}\ln c_{C^+_w} + \frac{RT}{F}\ln\frac{c_{DPPH_{NB}}\,K_{ion\,pair}}{c_{([DPPH^-\,C^+])_{NB}}} \quad (17)$$

Mass conservation (no transfer of DPPH species to water) can be expressed as follows:

$$c_{DPPH^-_{NB}} + c_{DPPH_{NB}} + c_{([DPPH^-C^+])_{NB}} = C^0_{DPPH_{NB}} \quad (18)$$

where $C^0_{DPPH_{NB}}$ denotes the overall concentration of DPPH (all species). At the formal potential, the concentrations of oxidized and reduced DPPH are equal:

$$c_{([DPPH^-C^+])_{NB}} + c_{DPPH^-_{NB}} = c_{DPPH_{NB}} = \frac{C^0_{DPPH_{NB}}}{2} \quad (19)$$

Assuming, that in this balance equation the relation $c_{([DPPH^-C^+])_{NB}} \gg c_{DPPH^-_{NB}}$ holds, the last equation gives the approximation $c_{([DPPH^-C^+])_{NB}} \approx c_{DPPH_{NB}} \approx \frac{C^0_{DPPH_{NB}}}{2}$, from which

follows:

$$E^{\ominus'}_{c,\,DPPH^{0/-1}_{NB},\,C^+_{w\to NB},\,ion\,pair} = E^{\ominus}_{DPPH^{0/-1}_{NB}} + \Delta\varphi^{\ominus}_{w\to NB,\,C^+} + \frac{RT}{F}\ln c_{C^+_w} + \frac{RT}{F}\ln\frac{c_{[DPPH^-\,C^+]_{NB}}\,K_{ion\,pair}}{c_{[DPPH^-\,C^+]_{NB}}} \quad (20)$$

$$E^{\ominus'}_{c,\,DPPH^{0/-1}_{NB},\,C^+_{w\to NB},\,ion\,pair} = E^{\ominus}_{DPPH^{0/-1}_{NB}} + \Delta\varphi^{\ominus}_{w\to NB,\,C^+} + \frac{RT}{F}\ln c_{C^+_w} + \frac{RT}{F}\ln K_{ion\,pair} \quad (21)$$

and for $T = 25\,°C$ the equilibrium constant of ion pair formation can be calculated with equation:

$$\log K_{ion\,pair} = \frac{E^{\ominus'}_{c,\,DPPH^{0/-1}_{NB},\,C^+_{w\to NB},\,ion\,pair} - E^{\ominus}_{DPPH^{0/-1}_{NB}} - \Delta\varphi^{\ominus}_{w\to NB,\,C^+} - 0.059[V]\log c_{C^+_w}}{0.059[V]} \quad (22)$$

Using the average literature value of $\Delta\varphi^{\ominus}_{w\to NB,\,TBA^+} = 0.28\,V$ [17, 24, 25], Table 3 gives the calculated data of the logarithm of equilibrium constants for the formation of ion pairs of DPPH⁻ and TBA⁺. The data vary slightly with TBA⁺ bulk concentration in water, and the average value $K_{ion\,pair} = 2.5$ indicates that the approximation $c_{([DPPH^-C^+])_{NB}} \approx c_{DPPH_{NB}} \approx \frac{C^0_{DPPH_{NB}}}{2}$ is certainly not very good. Nevertheless, the results indicate that the equilibrium constant of ion pair formation of DPPH⁻ with TBA⁺ is small, which is understandable, bearing in mind the large radii of both ions and their considerable lipophilicity. Nevertheless, it may be responsible for the deviation of the Gibbs energy of transfer (−10.61 KJ mol⁻¹) calculated when using the DPPH/DPPH⁻ system.

3.2. Electrochemistry of DPPH in solid paraffin (containing an organic salt) in a graphite-paraffin composite electrode

Electrode El-1 (see experimental part) gave a rather small

Table 3
Logarithm of equilibrium constants of ion pair formation using Eq. (22), and the average of literature value of $\Delta\varphi^{\ominus}_{w\to NB,\,TBA^+}$ (0.28 V for tetrabutylammonium cations), the literature value of $E^{\ominus}_{DPPH^{0/-1}_{NB}}$, and the experimentally measured formal potentials $E^{\ominus'}_{c,\,DPPH^{0/-1}_{NB},\,C^+_{w\to NB},\,ion\,pair}$ for aqueous solutions of TBAOH.

Cation	Concentration [mol L⁻¹]	log $K_{ion\,pair}$
TBA⁺	0.1	0.59
	0.05	0.42
	0.01	0.40
	0.005	0.28

voltammetric system with peak currents that increased during the first 20 cycles, and then continuously decreased (Fig. 8a). Electrode El-2 gave a larger voltammetric signal with increasing peak currents during the first 20 cycles. In the following cycles, the system was rather constant, although slightly fluctuating (Fig. 8b). Electrode El-3 showed a superior behaviour: the peak current reached after the first 500 cycles constant values, which were about four times that of electrode El-1, and they stayed constant until 1000 cycles, without showing any diminishing (Fig. 8c). Fig. 9a shows a plot of peak separation versus logarithm of scan rate and Fig. 9b versus the scan rate in the smallest scan rate range. Fig. 10 depicts every 20th scan between the 800th and 1.000th cyclic voltammogram of electrode El-3. It is not easy to understand, how the DPPH response of the electrodes is working: Unlike in case of nitrobenzene, the DPPH is here dissolved in the *solid paraffin* and a transfer of the TBA^+ cations in to the paraffin is impossible. However, clearly the TBATFB content affects the DPPH response and with increasing salt content, the currents grow. The peak separation approaches 30 mV at the slowest scan rates. Although the peak separation does not reach zero mV, this indicates a surface confined process. The stability of the voltammetric system proves that DPPH is not lost to the solution and, if TBA^+ cations are the charge compensators of $DPPH^-$, also the TFB^- anions are obviously not transferred to the aqueous solution, as there they would diffuse in to the bulk and their surface concentration would decrease. Possibly, they adsorb anions from the aqueous phase, so that charge neutrality is maintained at the surface. Since electrode El-3 provided the properties which are desirable for a sensor, experiments have been performed to use this electrode for the detection and quantification of radical scavengers. DPPH is one of the classical reagents for quantifying radical scavengers [26, 27] and electrochemical sensors containing DPPH have been described previously [e.g 28]. The composite electrodes described here offer the possibility of complete regain of the voltammetric response after exposure of the electrode to radical scavengers and the voltammetric measurement of the diminished DPPH response.

4. Conclusions

2,2-diphenyl-1-picrylhydrazyl (DPPH) can be reduced to $DPPH^-$ and oxidized to $DPPH^+$ in a nitrobenzene droplet immobilized on a graphite electrode and in contact with an aqueous electrolyte solution. In this three-phase arrangement, it offers the possibility to study the charge compensation transfer of cations in case of $DPPH^-$ formation, and that of anions in case of $DPPH^+$ formation. In contrast to the decamethylferrocene/decamethylferrocenium system, which allows studies of anion transfer, DPPH suffers from rather strong ion pair formation ($[DPPH^+An^-]$) and a weak, but not negligible ion pair formation in case of $[DPPH^-TBA^+]$. The systems $DPPH/DPPH^-$ and $DPPH/DPPH^+$ can certainly be suggested for further ion transfer studies in three-phase arrangements; however, data have to be carefully evaluated with respect to a possible ion pair formation of $DPPH^-$ and $DPPH^+$ with transferred cations and anions respectively, and also with respect to a possible transfer of $DPPH^-$ and $DPPH^+$ from the non-aqueous to the aqueous phase. This study will also complemented by future studies of the DPPH electrochemistry in lipid monolayers, similar to our previous publication on ubiquinones [29].

The DPPH-TBATFB-graphite-paraffin composite electrode is an interesting candidate for sensing radical scavengers. Its analytical potential will be evaluated in upcoming studies.

Acknowledgement

References

[1] F. Scholz, Š. Komorsky-Lovrić, M. Lovrić, A new access to Gibbs energies of transfer of ions across liquid | liquid interfaces and a new method to study electrochemical processes at well-defined three-phase junctions, Electrochem. Commun. 2 (2000) 112–118, http://dx.doi.org/10.1016/S1388-2481(99)00156-3.

[2] F. Scholz, R. Gulaboski, Determining the Gibbs energy of ion transfer across water-organic liquid interfaces with three-phase electrodes, ChemPhysChem 6 (2005) 16–28, http://dx.doi.org/10.1002/cphc.200400248.

[3] R.T. Kachoosangi, L. Xiao, G.G. Wildgoose, F. Marken, P.C. Bulmanpage, R.G. Compton, A new method of studying ion transfer at liquid|liquid phase boundaries using a carbon nanotube paste electrode with a redox active binder, J. Phys. Chem. C 111 (2007) 18353–18360, http://dx.doi.org/10.1021/jp0763275.

[4] H. Zhang, L. Sepunaru, S.V. Sokolov, E. Laborda, C. Batchelor-McAuley, R.G. Compton, Electrochemistry of single droplets of inverse (water-in-oil) emulsions, Phys. Chem. Chem. Phys. 19 (2017) 15662–15666, http://dx.doi.org/10.1039/C7CP03300A.

[5] D. Kaluza, W. Adamiak, M. Opallo, M. Jonsson-Niedziolka, Comparison of ion transfer thermodynamics at microfluidic and droplet-based three phase electrodes, Electrochim. Acta 132 (2014) 158–164, http://dx.doi.org/10.1016/j.electacta.2014.03.105.

[6] A. Doménech, I.O. Koshevoy, N. Montoya, A.J. Karttunen, T.A. Pakkanen, Determination of individual Gibbs energies of anion transfer and excess Gibbs energies using an electrochemical method based on insertion electrochemistry of solid compounds, J. Chem. Eng. Data 56 (2011) 4577–4586, http://dx.doi.org/10.1021/je200514c.

[7] A. Doménech, N. Montoya, F. Scholz, Estimation of individual Gibbs energies of cation transfer employing the insertion electrochemistry of solid Prussian blue, J. Electroanal. Chem. 657 (2011) 117–122, http://dx.doi.org/10.1016/j.jelechem.2011.03.033.

[8] V. Mirčeski, R. Gulaboski, F. Scholz, Determination of the standard Gibbs energies of transfer of cations across the nitrobenzene/water interface utilizing the reduction of iodine in an immobilized nitrobenzene droplet, Electrochem. 4 (2002) 814–819, http://dx.doi.org/10.1016/S1388-2481(02)00456-3.

[9] F. Scholz, R. Gulaboski, K. Caban, The determination of standard Gibbs energies of transfer of cations across the nitrobenzene/water interface using a three-phase electrode, Electrochem. Commun. 5 (2003) 929–934, http://dx.doi.org/10.1016/j.elecom.2003.09.005.

[10] F. Quentel, V. Mirčeski, M. L'Her, Lutetium bis(tetra-*tert*-butylphthalocyaninato): a superior redox probe to study the transfer of anions and cations across the water|nitrobenzene interface by means of square-wave voltammetry at the three-phase electrode, J. Phys. Chem. B 109 (2005) 1262–1267, http://dx.doi.org/10.1021/jp045914c.

[11] F. Quentel, C. Elleouet, V. Mirčeski, V. Agmo Hernández, M. L'Her, M. Lovrić, Š. Komorsky-Lovrić, F. Scholz, Studying ion transfers across a room temperature ionic liquid{divides}aqueous electrolyte interface driven by redox reactions of lutetium bis(tetra-*tert*-butylphthalocyaninato), J. Electroanal. Chem. 611 (2007) 192–200, http://dx.doi.org/10.1016/j.jelechem.2007.08.011.

[12] E. Solon, A.J. Bard, The electrochemistry of diphenylpicrylhydrazyl, J. Am. Chem. Soc. 86 (1964) 1926–1928, http://dx.doi.org/10.1021/ja01064a005.

[13] M.K. Kalinowski, J. Klimkiewicz, Solvation effects in the electrochemistry of diphenylpicrylhydrazyl, Monatsh. Chem. 114 (1983) 1035–1043, http://dx.doi.org/10.1007/BF00799027.

[14] Q.K. Zhuang, F. Scholz, F. Pragst, The voltammetric behaviour of solid 2,2-diphenyl-1-picrylhydrazyl (DPPH) microparticles, Electrochem. Commun. 1 (1999) 406–410, http://dx.doi.org/10.1016/S1388-2481(99)00086-7.

[15] F. Scholz, B. Meyer, Voltammetry of solid microparticles immobilized on electrode surfaces, in: A.J. Bard, I. Rubinstein (Eds.), Electroanalytical Chemistry, Vol. 20 Marcel Dekker, New York, 1996, pp. 1–82.

[16] T. Kakiuchi, Partition equilibrium of ionic components in two immiscible electrolyte solutions, in: A.G. Volkov, D.W. Deamer (Eds.), Liquid-liquid Interfaces. Theory and Methods, CRC Press, Boca Raton, 1996, pp. 1–18.

[17] Y. Marcus, Ions in Solution and their Solvation, J. Wiley & Sons Inc., Hoboken, 2015.

[18] P. Vanýsek, Electrochemistry on liquid/liquid interfaces, in: G. Berthier, M.J.S. Dewar, H. Fischer, K. Fukui, G.G. Hall, J. Hinze, H.H. Jaffé, J. Jortner, W. Kutzelnigg, K. Ruedenberg, J. Tomasi (Eds.), Lecture Notes in Chemistry, Vol. 39 Springer-Verlag, Berlin, 1985.

[19] S. Wilke, A modified galvanostatic iR compensation method for electrochemical measurements at liquid-liquid interfaces, J. Electroanal. Chem. 301 (1991) 67–75, http://dx.doi.org/10.1016/0022-0728(91)85459-3.

[20] B. Hundhammer, T. Solomon, H. Alemu, Investigation of the ion transfer across the water-nitrobenzene interface by ac cyclic voltammetry, J. Electroanal. Chem. Interfacial Electrochem. 149 (1983) 179–183, http://dx.doi.org/10.1016/S0022-0728(83)80567-1.

[21] R. Gulaboski, K. Riedl, F. Scholz, Standard Gibbs energies of transfer of halogenate and pseudohalogenate ions, halogen substituted acetates, and cycloalkyl carboxylate anions at the water|nitrobenzene interface, Phys. Chem. Chem. Phys. 5 (2003) 1284–1289, http://dx.doi.org/10.1039/b210356g.

[22] M. Yamane, T. Iwachido, K. Tôei, Studies of the interaction between the picrate ion and alkali metal ions, Bull. Chem. Soc. Jpn. 44 (1971) 745–748, http://dx.doi.org/10.1246/bcsj.44.745.

[23] B.G. Chauhan, W.R. Fawcett, A. Lasia, The influence of ion pairing on the electroreduction of nitromesitylene in aprotic solvents. 1. Thermodynamic aspects, J. Phys. Chem. 81 (1977) 1476–1481, http://dx.doi.org/10.1021/j100530a009.

K. Dharmaraj et al.   *Journal of Electroanalytical Chemistry 823 (2018) 765–772*

[24] B. Hundhammer, T. Solomon, Determination of standard Gibbs energies of ion partition between water and organic solvents by cyclic voltammetry: part I, J. Electroanal. Chem. 157 (1983) 19–26, http://dx.doi.org/10.1016/S0022-0728(83)80373-8.

[25] T. Wandlowski, V. Mareček, Z. Samec, Galvani potential scales for water-nitrobenzene and water-1,2-dichloroethane interfaces, Electrochim. Acta 35 (1990) 1173–1175, http://dx.doi.org/10.1016/0013-4686(90)80035-M.

[26] M. Blois, Antioxidant determinations by the use of a stable free radical, Nature 181 (1958) 1199–1200, http://dx.doi.org/10.1038/1811199a0.

[27] S.B. Kedare, R.P. Singh, Genesis and development of DPPH method of antioxidant

assay, J. Food Sci. Technol. 48 (2011) 412–422, http://dx.doi.org/10.1007/s13197-011-0251-1.

[28] K. Photinon, Y. Chalermchart, C. Khanongnuch, S.H. Wang, C.C. Liu, A thick-film sensor as a novel device for determination of polyphenols and their antioxidant capacity in white wine, Sensors 10 (2010) 1670–1678, http://dx.doi.org/10.3390/s100301670.

[29] N. Heise, F. Scholz, Assessing the effect of the lipid environment on the redox potentials of the coenzymes Q10 and Q4 using lipid monolayers made of DOPC, DMPC, TMCL, TOCL, and natural cardiolipin (nCL) on mercury, Electrochem. Commun. 81 (2017) 141–144, http://dx.doi.org/10.1016/j.elecom.2017.07.002.

6.2   Publication No. 2

The acid–base and redox properties of menaquinone MK-4, MK-7, and MK-9 (vitamin K_2) in DMPC monolayers on mercury

Karuppasamy Dharmaraj, Javier Ignacio Román Silva, Heike Kahlert, Uwe Lendeckel, Fritz Scholz,

ORIGINAL ARTICLE

The acid–base and redox properties of menaquinone MK-4, MK-7, and MK-9 (vitamin K$_2$) in DMPC monolayers on mercury

Karuppasamy Dharmaraj[1] · Javier Ignacio Román Silva[1] · Heike Kahlert[1] · Uwe Lendeckel[2] · Fritz Scholz[1]

Abstract

The acid–base and redox properties of the menaquinones MK-4, MK-7, and MK-9 (vitamin K$_2$) have been studied in DMPC monolayers on mercury electrodes. The monolayers were prepared by adhesion-spreading of menaquinone-spiked DMPC liposomes on a stationary mercury drop electrode. All three menaquinones possess pK_a constants outside the experimentally accessible range, i.e., they are higher than about 12. The standard potentials of MK-4, MK-7, and MK-9 in the DMPC monolayers are very similar, i.e., 0.351, 0.326, and 0.330 V (corresponding to the biochemical standard potentials − 0.063, − 0.088, and − 0.085 V).

Graphic abstract
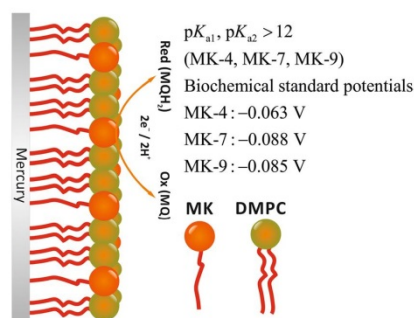
Introduction

A very recent review of the electrochemistry of vitamins highlights the importance of solid thermodynamic data, and it also shows that no reliable data concerning Vitamin K are available (Lovander et al. 2018). Vitamin K, in its hydroquinone state, functions as an exclusive coenzyme of γ-glutamyl carboxylase (GGCX, EC 4.1.1.90), which catalyzes the post-translational γ-carboxylation of a number of vitamin K-dependent proteins (Kleuser 2018). Thereby, important physiological and pathophysiological processes such as blood coagulation, bone metabolism, arterial calcification, oxidative stress, and extrahepatic tissue energy metabolism are regulated (Chatron et al. 2019). Vitamin K is not a single compound but represents a multitude of chemically related molecules with similar biological activity. All K vitamins possess a 2-methyl-1,4-naphthoquinone moiety

✉ Fritz Scholz
fscholz@uni-greifswald.de

[1]   Institute of Biochemistry, University of Greifswald,
      Felix-Hausdorff-Str. 4, 17487 Greifswald, Germany

[2]   Institute of Medical Biochemistry and Molecular Biology,
      University Medicine Greifswald, University of Greifswald,
      Ferdinand-Sauerbruch-Str., 17475 Greifswald, Germany

(menadione, vitamin K_3). In menaquinones (K_2 vitamins), substituents are present in position 3 consisting of different numbers of isoprenyl units (MK-1 to MK-14). GGCX is only activated by vitamin K in its hydromenaquinone state, which in this reaction is converted to the inactive vitamin K epoxide (Oldenburg et al. 2008). Its reactivation is mediated by vitamin K epoxide reductase (VKORC1) (Oldenburg et al. 2008). Studying the interaction of menaquinones, menadione, and phyllochinones with VKORC1, Chatron and co-workers revealed that indeed the length of the isoprenoid substituent determines the affinity of vitamin K derivatives to the VKORC1 (Chatron et al. 2019): binding free energy of the epoxide forms to VKORC1 was highest for MK-7, followed by vitamin K_1 and MK4, whereas that of K_3 (lacking any side chain) was by far lower. This distinguished feature of MK-7 is in accordance with the beneficial effects of this particular derivative in preventing vascular and bone diseases, decreasing the risk of cancer (Nimptsch et al. 2008) and diabetes (Beulens et al. 2010), and decreasing the risk of coronary artery diseases in dialysis patients (Gast et al. 2009). As to how these different biological activities of menaquinones with different isoprenoid chain length is due to their distinct acid–base and redox properties remains to be elucidated.

The compounds studied in this work include the prominent K_2 vitamin family members MK-4, MK-7 as well as a more lipophilic derivate, MK-9. They are listed in Table 1. The biological functions, the biosynthesis and dietary aspects of menaquinones are well covered in the literature (Shearer et al. 2008; Maklashina et al. 2006; Cotrim 2016; Gröber et al. 2014) and do not need to be discussed here.

The menaquinones listed in Table 1 were incorporated in DMPC (1,2-dimyristoyl-sn-glycero-3-phosphocholine) monolayers on the surface of mercury electrodes (stationary hanging drops) to study their redox and acid–base equilibria. The DMPC molecules of the monolayer on mercury form an 'ordered fur' of molecules with the polar

phosphatidylcholine head groups facing the water interface. It is probable, but not yet proven that the menaquinone molecules are arranged between the DMPC molecules with the naphthoquinone head groups also facing the water interface. Whereas MK-4 has a C_{16} chain like the two palmitoyl chains of DMPC, MK-7 has a C_{28} and MK-9 even a C_{36} chain. Clearly, MK-7 and MK-9 have to assume a bended structure, either partly sandwiched between the DMPC monolayer and the mercury surface, or bended between the DMPC molecules.

When the oxidized form is abbreviated by MQ, and the reduced by MQH_2, the following overall equation describes the coupled redox and acid–base equilibria:

$$MQ + 2e^- + 2H_3O^+ \rightleftarrows MQH_2 + 2H_2O$$

(Equilibrium I)

This equilibrium can be split as follows, in the pure redox equilibrium.

$$MQ + 2e^- \rightleftarrows MQ^{2-}$$ (Equilibrium II)

having the standard potential $E_{MQ/MQ^{2-}}^{\ominus}$ and the two acid–base equilibria.

$$MQH_2 + H_2O \rightleftarrows MQH^- + H_3O^+$$ (Equilibrium III)

$$MQH^- + H_2O \rightleftarrows MQ^{2-} + H_3O^+$$ (Equilibrium IV)
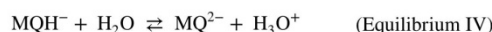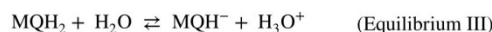
having the two acidity constants K_{a1} and K_{a2} (or pK_{a1}, and pK_{a2}, resp.). The reduction of MQ can proceed in two one-electron steps with a semiquinone radical as intermediate, which may also exist in two protonated forms (see Aguilar-Martínez et al. 2000, where the electrochemistry of 2-phenylamin-1, 4-naphthoquinone in acetonitrile is presented). However, in an aqueous environment, the semiquinones are normally unstable.

The pH dependence of Equilibrium I is described by the following equation (Scholz and Kahlert 2019):
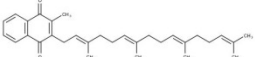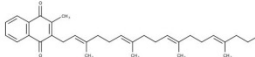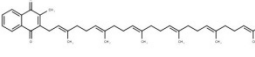
$$E_{MQ/MQ^{2-}} = E_{MQ/MQ^{2-}}^{\ominus} + \frac{RT}{2F} \ln \frac{a_{MQ}}{a_{MQ^{2-}}} + \frac{RT}{2F} \ln \left(\frac{a_{H_3O^+}^2}{K_{a1}K_{a2}} + \frac{a_{H_3O^+}}{K_{a2}} + 1 \right)$$

(1)

Hence, the formal potential $E_{c,\,MQ/MQ^{2-}}^{\ominus'}$, defined for $a_{MQ} = a_{MQ^{2-}}$, is:

$$E_{c,\,MQ/MQ^{2-}}^{\ominus'} = E_{MQ/MQ^{2-}}^{\ominus} + \frac{RT}{2F} \ln \left(\frac{a_{H_3O^+}^2}{K_{a1}K_{a2}} + \frac{a_{H_3O^+}}{K_{a2}} + 1 \right)$$

(2)

The constants $E_{MQ/MQ^{2-}}^{\ominus}$, pK_{a1}, and pK_{a2} can be experimentally determined by plotting the formal potentials versus

Table 1 The three menaquinones used in this study

MK-4	
	Menaquinone-4
MK-7	
	Menaquinone-7
MK-9	
	Menaquinone-9

pH and fitting the plot with Eq. (2), provided there is a pH region in which the formal potentials are independent of pH. The pK_a values can only be determined if they are positioned in the accessible pH range, i.e., between 0 and 14. In case of the menaquinones, the insolubility of these compounds in aqueous solutions is a serious problem for electrochemical measurements. A very early developed strategy to cope with this problem was the preparation of thin films of the insoluble compounds on solid electrodes (Ksenzhek et al. 1977; Petrova et al. 2000). Although, this allowed electrochemical measurements, the state of the molecules in the solid film remains unknown and the meaning of the determined data remains unclear. Later, solid quinoide compounds, esp. ubiquinones, have been incorporated into lipid films on solid electrodes (Gordillo et al. 2000; Marchal et al. 1997) which to a much better extent approaches the situation of these compounds in real membranes. Recently, we have shown that lipid monolayers containing ubiquinones (the coenzymes Q_{10} and Q_4) can be prepared on stationary mercury electrodes (Heise and Scholz 2017), via the adhesion-spreading of quinone-spiked liposomes (Hellberg et al. 2002, 2005; Agmo Hernández et al. 2008, 2013). The same strategy has been followed here to prepare DMPC monolayers spiked with menaquinones in order to allow cyclic voltammetric measurements from which the mid-peak potentials have been taken as the formal potentials (under the provision that the mid-peak potentials do not seriously deviate from the formal potentials) (Scholz 2010).

Standard potentials and acidity constants of compounds dissolved in water are strictly defined for all involved species in the solvated (hydrated) state. Clearly, this is not the case for molecules in a lipid film. Hence, these data should be labelled 'formal acidity constants' and 'formal potentials' in the respective films. They are more akin to similar data of acids and redox species confined to a solid surface. Further, since they are part of a dielectric layer on a metal electrode, effects of the hydrophobic environment have to be considered (White et al. 1998; Pashkovskaya et al. 2018) (see "Results and discussions"). Another complication may also arise from the mobility of the immobilized compounds in the film, i.e., the mobility of the lipid molecules and the menaquinones. The latter may change their position when charged and deprotonated, as it has been discussed for carbonic acids (Creager and Clarke 1994).

Experimental section

Chemicals

The following chemicals were used: citric acid (analytical grade) was from Serva Feinbiochemica GmbH, Germany, trisodium citrate pentahydrate (extra pure) was from Laborchemie, Apolda GmbH, Germany, disodium monohydrogen phosphate dihydrate ($Na_2HPO_4 \cdot 2H_2O$) ($\geq 98\%$), sodium hydroxide (NaOH) ($\geq 99\%$), potassium chloride (KCl) ($\geq 99.5\%$), chloroform (HPLC grade), and methanol ($\geq 99.98\%$, ultra LC–MS grade) were from Carl Roth GmbH, Germany, monosodium dihydrogen phosphate dihydrate ($NaH_2PO_4 \cdot 2H_2O$) (pure pharma grade) was from Applichem GmbH, Germany, disodium carbonate monohydrate ($Na_2CO_3 \cdot H_2O$) ($> 99\%$) was from Fluka Chemika, Germany, sodium bicarbonate ($NaHCO_3$) was from Merck, Germany, DMPC (14:0 PC) (1,2-dimyristoyl-sn-glycero-3-phosphocholine) lipid was from Avanti Polar Lipids, USA, menaquinone 4 (MK-4) and menaquinone 7 (MK-7) were from Sigma Aldrich, Germany; menaquinone 9 (MK-9) was from Caymann Chemical, Germany. The buffer solutions were prepared using citric acid/trisodium citrate pentahydrate for pH 4, $Na_2HPO_4 \cdot 2H_2O/NaH_2PO_4 \cdot 2H_2O$ for pH 6 and 7.4, $Na_2CO_3 \cdot H_2O/NaHCO_3$ for pH 9, $Na_2HPO_4 \cdot 2H_2O/NaOH$ for pH 11 and 11.4 and NaOH for pH 12–14.

Instrumentation

Cyclic voltammograms were recorded with an AUTOLAB PGSTAT 12 (Metrohm, Switzerland) in conjunction with the electrode stand VA 663 (Metrohm, Switzerland). A multimode electrode in the Hanging Mercury Drop Electrode (HMDE) mode (drop size 2, surface area 0.464 mm^2) served as working electrode, a platinum rod and an Ag|AgCl (3 M KCl, $E = 0.207$ V vs. SHE) were used as auxiliary and reference electrodes, respectively. The surface area of the mercury drops has been determined via weighing 6 times 50 mercury drops and calculating the surface area assuming complete sphericity. The standard deviation of the surface area data was 0.0065 mm^2. The redox systems were studied with cyclic voltammetry (staircase) in normal mode using the scan rates 10, 25, 50, 100, 200 mV s^{-1} and a step potential of 0.00412 V. A temperature-controlled bath (Lauda Ecoline 003 E100) was used to ensure that all measurements were performed at 25 °C. All the experiments were repeated at least three times and the mean values were used for the calculations. Chronocoulometry was performed with 10 cycles keeping the electrode in each cycle for 5 s at $E_{ox} = E_{midpeak} + 100$ mV and at $E_{red} = E_{midpeak} - 100$ mV. The interval time was 0.1 s. The pH meter (Qph70, VWR) was calibrated using the buffer solutions pH 2.00 (± 0.02), pH 7.96 (± 0.02) from Carl Roth, Germany, and pH 12.00 (± 0.05) from VWR, Germany. The pH measurements were conducted for all buffer solutions and for pH 14 which was realised by using 1 mol L^{-1} NaOH solution. This solution provides also strong buffering because of its high hydroxide concentration. The number of MK molecules (n_{MK}) was calculated by summing up the surface areas occupied by MK (S_{MK}) and DMPC (S_{DMPC})

molecules and relating the sum to the surface area of the hanging mercury drop ($S_{mercury}$): $S_{mercury} = S_{DMPC} + S_{MK}$, $S_{mercury} = (n_{DMPC} \times S^*_{DMPC}) + (n_{MK} \times S^*_{MK})$, $n_{DMPC} = r \times n_{MK}$, n_{DMPC}: number of DMPC molecules, n_{MK}: number of MK molecules, r: ratio of the numbers of molecules of DMPC to MK, S^*_{DMPC}: surface area of one DMPC molecule, S^*_{MK}: surface area of one MK molecule.

Liposome preparation

Liposomes were prepared according to the modified rapid evaporation method developed by Moscho group (Moscho et al. 1996). The DMPC lipids were dissolved using chloroform, methanol and the desired amounts of menaquinone (for the final concentrations: 2 µmol L^{-1}, 5 µmol L^{-1}, 10 µmol L^{-1} MK) were added from a chloroform stock solution (1 mg mL^{-1}). Final concentrations of 300 µmol L^{-1} DMPC containing menaquinone (2 µmol L^{-1}, or 5 µmol L^{-1}, or 10 µmol L^{-1} of MK-4 or MK-7 or MK-9) were obtained by adding 20 mL of buffer pH 7.4.

Preparation of lipid monolayers on mercury electrode

The liposome suspension was deaerated at least for 30 min with nitrogen. A new mercury drop was formed and then the solution was stirred for 15 min. Then the solution was exchanged with the required buffer for studying the redox properties and the solution was purged with nitrogen for 30 (± 2) minutes. The solution exchange is mandatory to avoid any possible response caused by suspended liposomes.

Results and discussion

The cyclic voltammograms of DMPC films spiked with MK-4, -7 and -9 at pH 7.4 and 12 are shown in Fig. 1.

Table 2 lists the peak separations at the scan rate of 10 mV s^{-1}. The separation of anodic and cathodic peaks is generally small, with an even decreasing tendency at pH values larger than 11. The small peak separation is typical for immobilized redox systems (thin-layer behaviour).

The mid-peak potentials at constant pH are almost constant in the range of 10 to 200 mV s^{-1}, just being scattered within ± 5 mV, and do not differ significantly for all three menaquinones ($p = 0.05$).

Between pH 4 and 12, the mid-peak potentials obey strictly linear dependences (the slopes are given in Table 3), and above pH 12 the curves are bent towards much smaller slopes. This bending can have two reasons: (i) if the two pK_a values are smaller than pH 14, the slope would be about 30 mV in the range $pK_{a1} <$ pH $< pK_{a2}$, and zero for $pK_{a2} <$ pH (cf. Eq. (2)). (ii) Another reason for the bending

could be the interference of another cation, e.g., sodium ions, because pH values above 11 were realised with sodium hydroxide. Then the bending can happen because sodium ions are bond by the anionic species of the hydroquinone forming MQNa$^-$ and MQNa$_2$, respectively. This case would resemble the sodium interference of the glass electrode response. To decide about the reasons of the bending, experiments have been performed by keeping the pH constant and changing the sodium concentration. At sodium concentrations of 0.5 to 2 mol L^{-1} the mid-peak potentials are slightly increasing, but the pH dependence is still almost linear for pH smaller than 11. This suggests that the pK_a values are most probably really above 12, but does not exclude an interference by sodium. At so large sodium concentration (0.5 to 2 mol L^{-1}) activity coefficients deviate so much from unity that a data interpretation is excluded. The least square fitting of the dependences shown in Fig. 2 with Eq. (2) produced in all cases (no significant difference at $p = 0.05$) identical pK_{a1} and pK_{a2} values of 13.7 (± 1.3). The only solid conclusion which can be drawn from the results is that the pK_a values are for sure higher than 12 and a sodium response is, if at all, very weak.

The fitting of the dependences shown in Fig. 2 is based on assuming that the number of electrons is two. To test this assumption, coulometric measurements have been performed. This is not an easy task, because for coulometric measurements, the number of menaquinone molecules on the electrode surface has to be known and was determined as described in the experimental part.

The liposomes have been prepared with varying ratios of DMPC to MK-4 molecules (from 300:1 to 30:1). For the DMPC and MQ molecules rod-like (cylindrical) geometries have been assumed. The base area of the DMPC cylinder was taken as $60.6 \cdot 10^{-20}$ m^2 and that of MK-4 $34.1 \cdot 10^{-20}$ m^2. According to Heppes (Heppes 2003), the maximum surface coverage for two-size disc packing is 0.91. With these data, the results given in Table 4 were obtained. With increasing dilution, the number of electrons approaches 2. This is in remarkable good agreement with the assumption of a $2e^-/2H^+$ process, given the many possibilities of errors (e.g., weighing the compounds, liposome formation, film formation, packing geometry, molecule geometry).

Although the above mentioned identical values of pK_{a1} and pK_{a2}, resulting from the least-square fitting, cannot be taken as strictly proven, this would not be surprising: the phenomenon of identical pK_{a1} and pK_{a2} data of immobilized quinoide compounds is well known (Ksenzhek et al. 1977; Masheter et al. 2007; Lee et al. 2013). Identical $pK_{a,i}$ values have been observed for drop casted films on graphite electrodes, adsorbed quinones, as well as for covalently bond hydroquinones. Anthraquinone modified carbon nanotubes on graphite have also two indistinguishable $pK_{a,i}$ values of 13, and even greater than 14. The authors concluded that
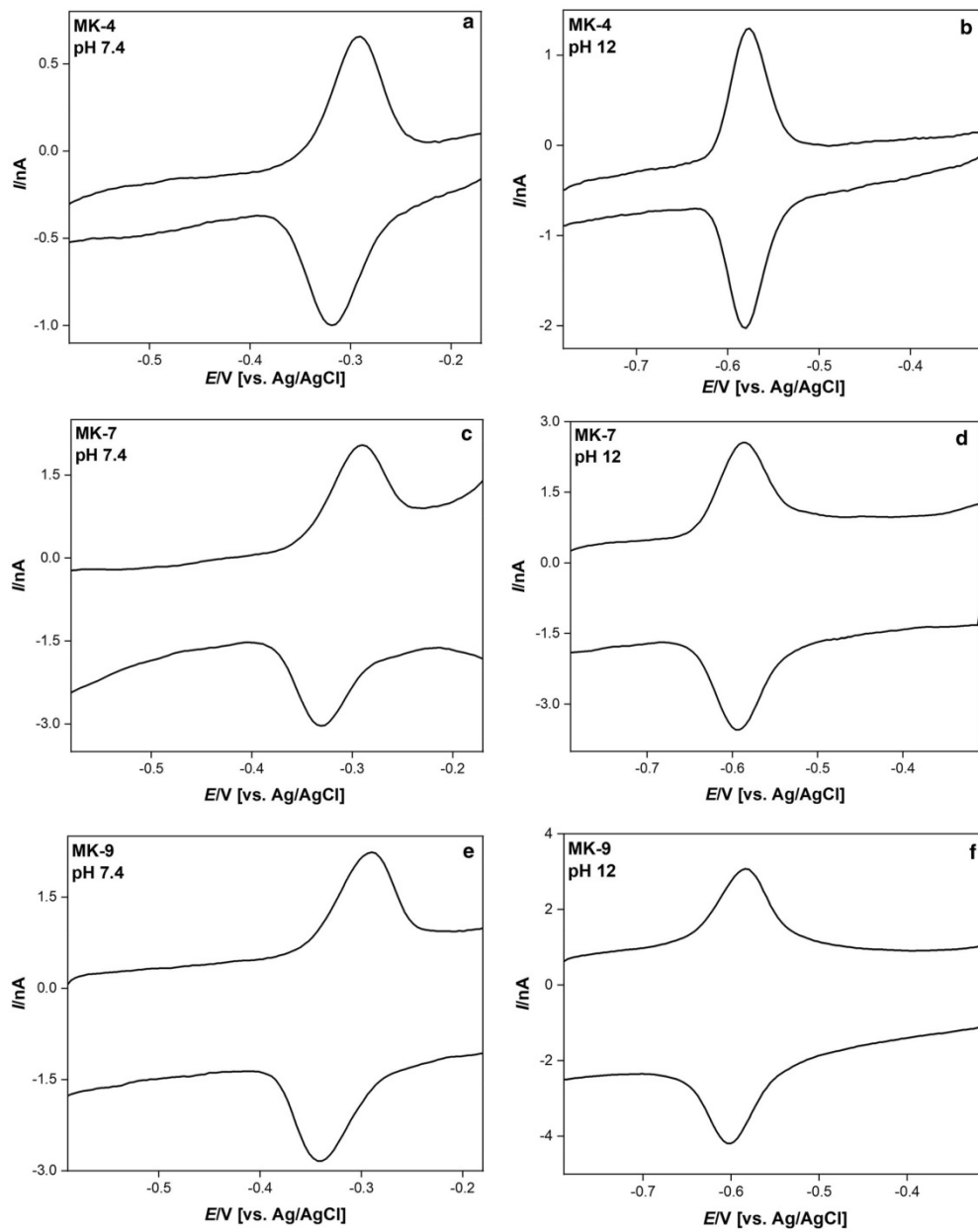
Fig. 1 Cyclic voltommograms of DMPC films spiked with MK-4, -7, and -9 at pH 7.4 and 12. The film composition was 300 μmol DMPC + 2 μmol menaquinones. The scan rate was 25 mV s^{-1}

Table 2 Separation of anodic and cathodic peaks for DMPC films spiked with MK-4, -7, and -9

pH	Peak separation [mV]		
	MK-4	MK-7	MK-9
4.0	8 ($\pm$2)	10 ($\pm$2)	10 ($\pm$2)
6.0	22 ($\pm$11)	22 ($\pm$4)	23 ($\pm$6)
7.4	18 ($\pm$7)	26 ($\pm$2)	33 ($\pm$0)
9.0	15 ($\pm$2)	23 ($\pm$8)	14 ($\pm$2)
11.0	10 ($\pm$2)	6 ($\pm$2)	10 ($\pm$2)
12.0	4 ($\pm$3)	4 ($\pm$0)	8 ($\pm$4)
12.4	8 ($\pm$0)	5 ($\pm$2)	8 ($\pm$0)
13.0	11 ($\pm$2)	3 ($\pm$5)	4 ($\pm$0)
14.0	6 ($\pm$4)	6 ($\pm$4)	8 ($\pm$0)

The film composition was 300 µmol DMPC + 2 µmol menaquinones. The scan rate was 10 mV s^{-1}. In brackets, the standard deviations are given, which are based on at least three measurements

Table 3 Slopes of mid-peak potentials versus pH functions of DMPC films spiked with MK-4, -7, and -9 in the pH range 4 to 11

Menaquinones	Slopes [mV/pH]
MK-4	− 60.63 ($\pm$1.00)
MK-7	− 59.30 ($\pm$1.32)
MK-9	− 59.70 ($\pm$1.29)

The film composition was 300 µmol DMPC + 2 µmol menaquinones. In brackets, the standard deviations are given, which are based on at least 45 measurements

different molecular environments and electronic coupling determine the dissociation constants (Masheter et al. 2007). In addition, adsorbed mercaptohydroquinone on gold has larger $pK_{a,i}$ values than in aqueous buffer solution (Sato et al. 1996). However, when these compounds are dissolved in solution, the two values pK_{a1} and pK_{a2} are well separated. In Table 5 are listed the pK_{a1} and pK_{a2} data of quinoide compounds dissolved in aqueous solutions.

The merging of the two $pK_{a,i}$ values is just one typical feature of immobilized dibasic acids. The other is a remarkable increase of these values compared to the data of acids dissolved in solutions (cf. Table 6). The increase of the $pK_{a,i}$ values of immobilized acids is generally between 2 and 5 units (White et al. 1998; Creager et al. 1994; Chechik et al. 2000), which equals to 11.4 to 29 kJ mol^{-1}.

So far, the increase of $pK_{a,i}$ values has been ascribed to the hydrophobic environment of the acidic groups in the films. However, we think that this is not convincing, as it is well known that the permittivity of the medium and its donor–acceptor properties with respect to protons are most important (Izutsu 1990). Especially for covalently bonded hydroquinones, it is most likely that the acid groups are exposed to the aqueous phase and not housed
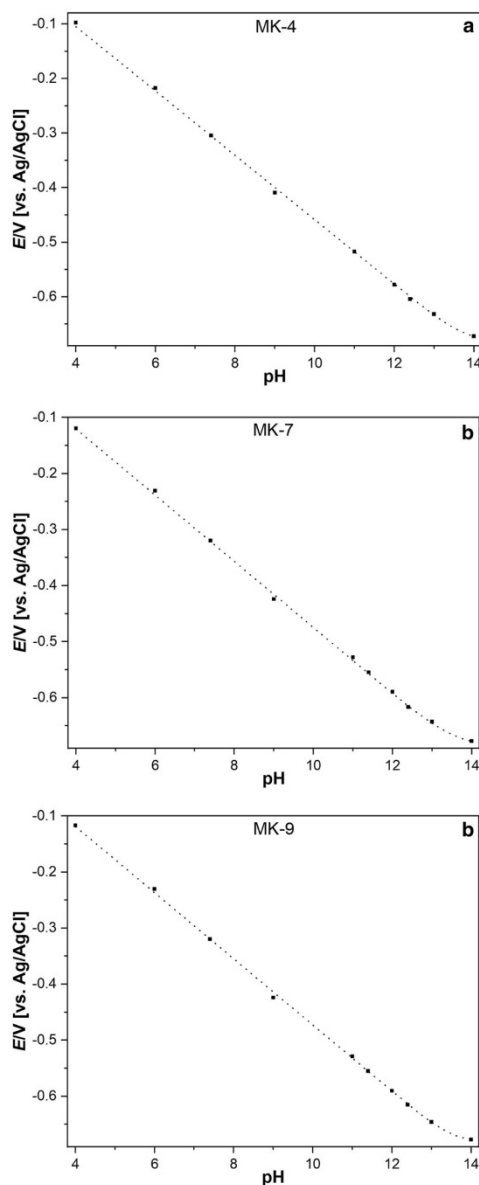
Fig. 2 Dependence of mid-peak potentials of cyclic voltammograms of the menaquinone spiked DMPC films on pH

Table 4 Number of electrons transferred between the reduced and oxidized states of MK-4, as determined in coulometric experiments at different ratios of MK-4: DMPC

MK-4: DMPC	No. of electrons in two separate measurements
1:300	1.96
	2.37
1:200	2.11
	2.13
1:150	1.81
	1.89
1:100	2.11
	1.78
1:60	2.20
	0.98
1:30	1.24
	2.5

At least 2 different monolayers were studied for each ratio. The mean number of electrons for all measurements was 1.92

in a hydrophobic pocket. A "hydrophobic environment" would also be unable to explain the merging of the two $pK_{a,i}$ values, as in organic solvents the $pK_{a,i}$ values are usually well separated. For dissolved dibasic acids with completely independent protonation sides, Adams has shown already in 1916, that the ratio of the two acidity constants cannot be smaller than $K_{a1} : K_{a2} = 4$ (Adams 1916). This ratio was indeed observed in several cases of dissolved acids.

The above-described dependence of mid-peak potentials of cyclic voltammograms of the menaquinone spiked DMPC films on pH is in general agreement with the observations made by other authors in case of immobilized dibasic acids (Masheter et al. 2007; Lee et al. 2013). As discussed before, these authors interpreted their behavior using the common model of two deprotonation steps characterized by the two constants pK_{a1} and pK_{a2}, and finding that these constants are equal, i.e., $pK_{a1} = pK_{a2}$. This, however, allows writing just one acid–base equilibrium:

$$MQH_2 + 2H_2O \rightleftarrows MQ^{2-} + 2H_3O^+ \qquad \text{(Equilibrium V)}$$
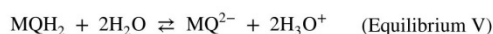
in conjunction with the redox equilibrium.

$$MQ + 2e^- \rightleftarrows MQ^{2-} \qquad \text{(Equilibrium II)}$$

The two-proton acid–base equilibrium has the following equilibrium constant:

$$K_{\bar{a}} = \frac{a_{MQ^{2-}} a_{H_3O^+}^2}{a_{MQH_2}} = K_{a1} K_{a2} \qquad (3)$$

The Nernst equation for Equilibrium II is:

$$E_{MQ/MQ^{2-}} = E_{MQ/MQ^{2-}}^{\ominus} + \frac{RT}{2F} \ln \frac{a_{MQ}}{a_{MQ^{2-}}} \qquad (4)$$

Table 5 pK_{a1} and pK_{a2} data of hydroquinones in aqueous solutions

	pK_{a1}	pK_{a2}	$\Delta pK_{1,2}$	Ref
1,4-Benzohydroquinone	9.9	11.9	2	Bailey and Ritchie (1985)
	9.91	12.04	2.13	Abichandani and Jatkar (1938)
1,4-Naphtohydroquinone	9.3	11.2	1.9	Bailey and Ritchie (1985)
1,4-Anthrahydroquinone	10	12	2	Masheter et al. (2007)
(Aqueous solution containing 5%DMF)	9	12.05	3.05	Revenga et al. (1994)
2-Methyl-naptohydroquinone	10.4	12.55	2.15	Ksenzhek et al. (1977)
2-Methyl-naptohydroquinone	11.5	12.5	1.0	Driebergen et al. (1990)

Table 6 pK_a values of some carboxylic acids, thiophenol and mercaptopyridine immobilized on surfaces and dissolved in solutions

	Surface immobilized acid pK_a	Acid dissolved in solution pK_a	References
4-Mercaptopyridine	4.6	1.4	Bryant and Crooks (1993)
4-Aminothiophenol	6.9	4.3	
$HS(CH_2)_2COOH$	6.5–8.4	4.3	Burris et al. (2008)
$HS(CH_2)_{15}COOH$	8.0, 6.4	4.5	Chechik et al. (2000)
$HS(CH_2)_{10}COOH$	5.5–8.5	4.5	
$HS(CH_2)_7COOH$	8.0	4.5	
$HS(CH_2)_5COOH$	6.0	4.5	
$HS(CH_2)_2COOH$	5.8, 8.0	4.5	

$$E_{MQ/MQ^{2-}} = E^{\ominus}_{MQ/MQ^{2-}} - \frac{RT}{2F} \ln K_{\bar{a}} + \frac{RT}{F} \ln a_{H_3O^+} + \frac{RT}{2F} \ln \frac{a_{MQ}}{a_{MQH_2}}$$
(5)

Since pK_{a1} and pK_{a2} are larger than 11 or 12, and not exactly accessible, only the standard potential $E^{\ominus}_{MQ/MQH_2}$, i.e., the standard potential relating to the couple MQ / MQH$_2$, can be extracted from the experimental dependences shown in Fig. 2. The results are given in Table 7.

We propose the following explanation of the behaviour of immobilized dibasic acids:

i.   From a thermodynamic point of view, an immobilized acid is not anymore an individual molecule, but it is a separate phase with many acidic groups on its surface, possessing a distribution of pK_a values, resulting in one average pK_a value. Because the overall equilibrium involves two electrons and two protons (for aqueous solutions adjacent to the film containing the immobilized acids) it makes sense to define one $pK_{\bar{a}}$ value referring to a two-proton equilibrium. Whether the $pK_{\bar{a}}$ in Eq. (3) is the product $K_{a1}K_{a2}$ or resulting from a distribution of many individual pK_a values cannot be decided now.

ii. The thermodynamics of the protolysis of immobilized acids also fundamentally differs from that of dissolved acids by producing an immobile, i.e., fixed, anion. It is well established that the protolysis of dissolved carbonic acids is mainly driven by the entropy of the formed ions B$^-$ and H$_3$O$^+$ from HB, i.e., by the structuring of the solvent around these ions (Sarmini and Kenndler 1999; Calder and Barton 1971). The enthalpy changes are rather small. The decrease of entropy gain caused by the fixation of the anion must inevitably lead to a higher stability of the protonated form HB, i.e., a lower acidity (larger pK_a value). Clearly, the free energy of protolysis is dominated by the contribution from proton solvation (Liptak and Shields 2001).

The formal potentials of MK-4, -7, -9 at different surface concentrations (2 µmol, 5 µmol, 10 µmol per 300 µmol DMPC) are practically constant. When the concentration is increased above 20 µmol per 300 µmol DMPC, the redox systems behave very differently, possibly because of phase transitions and formation of separate domains of DMPC and menaquinone. This will be studied in near future.

Conclusions

The menaquinones MK-4, MK-7, and MK-9 possess in DMPC monolayers on mercury very similar standard potentials (cf. Table 7). Applying the two $pK_{a,i}$ model, the three

Table 7 Standard redox potentials $E^{\ominus}_{MQ/MQH_2}$ and biochemical standard potentials $E^{\ominus\prime}_{c, MQ/MQH_2}$ of the menaquinones in a DMPC layer, as derived from the plots given in Fig. 2

Menaquinones	Standard redox potential $E^{\ominus}_{MQ/MQ^{2-}}$, (V) vs SHE	Biochemical standard potential $E^{\ominus\prime}_{c, MQ/MQ^{2-}}$, (V) vs SHE
MK-4	0.351	−0.063
MK-7	0.326	−0.088
MK-9	0.330	−0.085

menaquinones have practically identical acidities, and for each menaquinone both $pK_{a,i}$ values are indistinguishable so that the acidity can also be characterized by one $pK_{\bar{a}}$ value for a two-proton step. The experimentally found identity of the two $pK_{a,i}$ values does not mean that they are really identical: $pK_{a,i}$ values between 13 and 14 imply a rather large uncertainty. The acidity constants make clear that under any physiological conditions, only the completely protonated forms exist. Both the $pK_{a,i}$ values and the standard potentials determined in this study make it understandable that these compounds can act as highly efficient molecules to transfer two electrons and two protons in one step.

Compliance with ethical standards

References

Abichandani CT, Jatkar SKK, Abichandani CT, Jatkar SKK (1938) Dissociation constants of ortho-, meta and para-hydroxy benzoic

acids, gallic acid, catechol, resorcinol, hydroquinone, pyrogallol and phloroglucinol. J Indian Inst Sci 21:417–441

Adams EQ (1916) Relations between the constants of dibasic acids and of amphoteric electorolytes. J Am Chem Soc 38:1503–1510. https://doi.org/10.1021/ja02265a008

Agmo Hernández V, Lendeckel U, Scholz F (2013) Electrochemistry of adhesion and spreading of lipid vesicles on electrodes. In: Schlesinger M (ed) Applications of electrochemistry in medicine. Modern aspects of electrochemistry. Springer, Boston, pp 189–24756

Agmo Hernández V, Scholz F (2008) The electrochemistry of liposomes. Isr J Chem 48:169–184. https://doi.org/10.1560/IJC.48.3-4.169

Aguilar-Martínez M, Macías-Ruvalcaba N, González I (2000) Traveling through the square mechanism of the quinone reduction pathways. Influence of the proton donor addition on the reaction intermediaries in a non-aqueous solvent. Rev Soc Quím Méx 44:74–81

Bailey SI, Ritchie IM (1985) A cyclic voltammetric study of the aqueous electrochemistry of some quinones. Electrochim Acta 30:3–12. https://doi.org/10.1016/0013-4686(85)80051-7

Beulens JWJ, van der A DL, Grobbee DE, Sluijs I, Spijkerman AMW, van der Schouw YT (2010) Dietary phylloquinone and menaquinones intakes and risk of type 2 diabetes. Diabetes Care 33:1699–1705. https://doi.org/10.2337/dc09-2302

Bryant MA, Crooks RM (1993) Determination of surface pKa values of surface-confined molecules derivatized with pH-sensitive pendant groups. Langmuir 9:385–387. https://doi.org/10.1021/la00026a005

Burris SC, Zhou Y, Maupin WA, Ebelhar AJ, Daugherty MW (2008) The effect of surface preparation on apparent surface pKa's of ω-mercaptocarboxylic acid self-assembled monolayers on polycrystalline gold. J Phys Chem C 112:6811–6815. https://doi.org/10.1021/jp077052w

Calder GV, Barton TJ (1971) Actual effects controlling the acidity of carboxylic acids. J Chem Educ 48:338–340. https://doi.org/10.1021/ed048p338

Chatron N, Hammed A, Benoit E, Lattard V (2019) Structural insights into phylloquinone (Vitamin K1), menaquinone (MK4, MK7), and menadione (Vitamin K3) binding to VKORC1. Nutrients 11:E67. https://doi.org/10.3390/nu11010067

Chechik V, Crooks RM, Stirling CJ (2000) Reactions and reactivity in self-assembled monolayers. Adv Mater 12:1161–1171. https://doi.org/10.1002/1521-4095(200008)12:16%3c1161::AID-ADMA1161%3e3.0.CO;2-C

Cotrim CA (2016) Biochemical and structural studies on enzymes of menaquinone biosynthesis. Dissertation, Martin-Luther-Universität Halle-Wittenberg, Halle

Creager SE, Clarke J (1994) Contact-angle titrations of mixed.omega.-mercaptoalkanoic acid/alkanethiol monolayers on gold. reactive vs nonreactive spreading, and chain length effects on surface pKa values. Langmuir 10:3675–3683. https://doi.org/10.1021/la00022a048

Driebergen RJ, Den Hartigh J, Holthuis JJM, Hulshoff A, Van Oort WJ, Postma Kelder SJ, Verboom W, Reinhoudt DN, Bos M, Van der Linden WE (1990) Electrochemistry of potentially bioreductive alkylating quinones: Part 1. Electrochemical properties of relatively simple quinones, as model compounds of mitomycin- and aziridinylquinone-type antitumour agents. Anal Chim Acta 233:251–268. https://doi.org/10.1016/S0003-2670(00)83486-8

Gast GC, de Roos NM, Sluijs I, Bots ML, Beulens JW, Geleijnse JM, Witteman JC, Grobbee DE, Peeters PH, van der Schouw YT (2009) A high menaquinone intake reduces the incidence of coronary heart disease. Nutr Metab Cardiovasc Dis 19:504–510. https://doi.org/10.1016/j.numecd.2008.10.004

Gordillo GJ, Schiffrin DJ (2000) The electrochemistry of ubiquinone-10 in a phospholipid model membrane. Faraday Discuss 116:89–107. https://doi.org/10.1039/B004379F

Gröber U, Reichrath J, Holick MF, Kisters K (2014) Vitamin K: an old vitamin in a new perspective. Derm-Endocrinol 6:e968490. https://doi.org/10.4161/19381972.2014.968490

Heise N, Scholz F (2017) Assessing the effect of the lipid environment on the redox potentials of the coenzymes Q10 and Q4 using lipid monolayers made of DOPC, DMPC, TMCL, TOCL, and natural cardiolipin (nCL) on mercury. Electrochem Commun 81:141–144. https://doi.org/10.1016/j.elecom.2017.07.002

Hellberg D, Scholz F, Schauer F, Weitschies W (2002) Bursting and spreading of liposomes on the surface of a static mercury drop electrode. Electrochem Commun 4:305–309. https://doi.org/10.1016/S1388-2481(02)00279-5

Hellberg D, Scholz F, Schubert F, Lovrić M, Omanović D, Agmo Hernández V, Thede R (2005) Kinetics of liposome adhesion on a mercury electrode. J Phys Chem B 109:14715–14726. https://doi.org/10.1021/jp050816s

Heppes A (2003) Some densest two-size disc packings in the plane. Discrete Comput Geom 30:241–262. https://doi.org/10.1007/s00454-003-0007-6

Izutsu K (1990) International Union of Pure and Applied Chemistry Acid-base dissociation constants in dipolar aprotic solvents. Blackwell Scientific Publications; Brookline Village, Mass. : Distributors, USA, Publishers' Business Services, Oxford; Boston

Kleuser B (2018) Vitamin K: Vielseitiger als angenommen. Pharmazeutische Zeitschrift. https://www.pharmazeutische-zeitung.de/ausgabe-092018/vitamin-k-vielseitiger-als-angenommen/. Accessed 27 Feb 2018

Ksenzhek OS, Petrova SA, Kolodyazhny MV, Oleinik SV (1977) Redox properties of K-group vitamins. Bioelectrochem Bioenerg 4:335–345. https://doi.org/10.1016/0302-4598(77)80035-4

Lee PT, Harfield JC, Crossley A, Pilgrim BS, Compton RG (2013) Significant changes in pKa between bulk aqueous solution and surface immobilized species: ortho-hydroquinones. RSC Adv 3:7347–7354. https://doi.org/10.1039/C3RA00164D

Liptak MD, Shields GC (2001) Accurate pKa calculations for carboxylic acids using complete basis set and gaussian-n models combined with CPCM continuum solvation methods. J Am Chem Soc 123:7314–7319. https://doi.org/10.1021/ja010534f

Lovander MD, Lyon JD, Parr DL, Wang J, Parke B, Leddy J (2018) Critical review—electrochemical properties of 13 vitamins: a critical review and assessment. J Electrochem Soc 165:G18–G49. https://doi.org/10.1149/2.1471714jes

Maklashina E, Hellwig P, Rothery RA, Kotlyar V, Sher Y, Weiner JH, Cecchini G (2006) Differences in protonation of ubiquinone and menaquinone in fumarate reductase from Escherichia coli. J Biol Chem 281:26655–26664. https://doi.org/10.1074/jbc.M602938200

Marchal D, Boireau W, Laval JM, Moiroux J, Bourdillon C (1997) An electrochemical approach of the redox behavior of water insoluble ubiquinones or plastoquinones incorporated in supported phospholipid layers. Biophys J 72:2679–2687. https://doi.org/10.1016/S0006-3495(97)78911-2

Masheter AT, Abiman P, Wildgoose GG, Wong E, Xiao L, Rees NV, Taylor R, Attard GA, Baron R, Crossley A, Jones JH, Compton RG (2007) Investigating the reactive sites and the anomalously large changes in surface pKa values of chemically modified carbon nanotubes of different morphologies. J Mater Chem 17:2616–2626. https://doi.org/10.1039/B702492D

Moscho A, Orwar O, Chiu DT, Modi BP, Zare RN (1996) Rapid preparation of giant unilamellar vesicles. Proc Natl Acad Sci USA 93:11443–11447. https://doi.org/10.1073/pnas.93.21.11443

Nimptsch K, Rohrmann S, Linseisen J (2008) Dietary intake of vitamin K and risk of prostate cancer in the Heidelberg cohort of the European Prospective Investigation into Cancer and Nutrition (EPIC-Heidelberg). Am J Clin Nutr 87:985–992. https://doi.org/10.1093/ajcn/87.4.985

Oldenburg J, Marinova M, Müller-Reible C, Watzka M (2008) The vitamin K cycle. Vitam Horm 78:35–62. https://doi.org/10.1016/S0083-6729(07)00003-9

Pashkovskaya AA, Vazdar M, Zimmermann L, Jovanovic O, Pohl P, Pohl EE (2018) Mechanism of long-chain free fatty acid protonation at the membrane-water interface. Biophys J 114:2142–2151. https://doi.org/10.1016/j.bpj.2018.04.011

Petrova SA, Ksenzhek OS, Kolodyazhnyi MV (2000) Redox properties of naturally occurring naphthoquinones: vitamin K2(20) and lapachol. Russ J Electrochem 36:767–772. https://doi.org/10.1007/BF02757678

Revenga J, Rodríguez F, Tijero J (1994) Study of the redox behavior of anthraquinone in aqueous medium. J Electrochem Soc 141:330–333. https://doi.org/10.1149/1.2054725

Sarmini K, Kenndler E (1999) Ionization constants of weak acids and bases in organic solvents. J Biochem Biophys Methods 38:123–137. https://doi.org/10.1016/S0165-022X(98)00033-5

Sato Y, Fujita M, Mizutani F, Uosaki K (1996) Electrochemical properties of the 2-mercaptohydroquinone monolayer on a gold electrode. Effect of solution pH, adsorption time and concentration of the modifying solution1. J Electroanal Chem 409:145–154. https://doi.org/10.1016/0022-0728(95)04421-3

Scholz F (2010) Electroanalytical methods. Springer-Verlag, Berlin Heidelberg

Scholz F, Kahlert H (2019) Chemical equilibria in analytical chemistry. Springer Nature, Switzerland

Shearer MJ, Newman P (2008) Metabolism and cell biology of vitamin K. Thromb Haemost 100:530–547. https://doi.org/10.1160/TH08-03-0147

White HS, Peterson JD, Cui Q, Stevenson KJ (1998) Voltammetric measurement of interfacial acid/base reactions. J Phys Chem B 102:2930–2934. https://doi.org/10.1021/jp980035+

6.3   Publication No. 3

The effects of the chemical environment of menaquinones in lipid monolayers on mercury electrodes on the thermodynamics and kinetics of their electrochemistry

Karuppasamy Dharmaraj, Dirk Dattler, Heike Kahlert, Uwe Lendeckel, Felix Nagel, Mihaela Delcea, Fritz Scholz,

European Biophysics Journal

The effects of the chemical environment of menaquinones in lipid monolayers on mercury electrodes on the thermodynamics and kinetics of their electrochemistry.

--Manuscript Draft--

Manuscript Number:	
Full Title:	The effects of the chemical environment of menaquinones in lipid monolayers on mercury electrodes on the thermodynamics and kinetics of their electrochemistry.
Article Type:	Original Article
Keywords:	Menaquinone, Vitamin K2, electrochemistry, thermodynamics, kinetics, lipid monolayers
Corresponding Author:	Fritz Scholz Universitat Greifswald GERMANY
Corresponding Author Secondary Information:	
Corresponding Author's Institution:	Universitat Greifswald
Corresponding Author's Secondary Institution:	
First Author:	Karuppasamy Dharmaraj, BSc
First Author Secondary Information:	
Order of Authors:	Karuppasamy Dharmaraj, BSc
	Dirk Dattler, Dipl.-Chem.
	Heike Kahlert, PhD, Dr. habil.
	Uwe Lendeckel, PhD
	Felix Nagel, MSc
	Mihaela Delcea, PhD
	Fritz Scholz
Order of Authors Secondary Information:	
Funding Information:	Deutsche Forschungsgemeinschaft (231396381/GRK1947)　　Mr. Karuppasamy Dharmaraj
Abstract:	The effects of the chemical environment of menaquinones (all-trans MK-4, all-trans MK-7) incorporated in lipid monolayers on mercury electrodes have been studied with respect to the thermodynamics and kinetics of their electrochemistry. The chemical environment relates to the composition of lipid films as well as the adjacent aqueous phase. It could be shown that the addition of all-trans MK-4 to TMCL does not change the phase transition temperatures of TMCL. In case of DMPC monolayers, the presence of cholesterol has no effect on the thermodynamics (formal redox potentials) of all-trans MK-7, but the kinetics are affected. Addition of an inert electrolyte (sodium perchlorate; change of ionic strength) to the aqueous phase shifts the redox potentials of all-trans MK-7 only slightly. The formal redox potentials of all-trans MK-4 were determined in TMCL and nCL monolayers and found to be higher in nCL monolayers than in TMCL monolayers. The apparent electron transfer rate constants, transfer coefficients and activation energies of all-trans MK-4 in cardiolipins have been also determined. Most surprisingly, the apparent electron transfer rate constants of all-trans MK-4 exhibit an opposite pH dependence for TMCL and nCL films: the rate constants increase in TMCL films with increasing pH, but in nCL, films they increase with decreasing pH. This study is a contribution to understand environmental effects on the redox properties of membrane bond redox systems.
Suggested Reviewers:	Uwe Schröder, PhD

	Professor, TU Braunschweig: Technische Universitat Braunschweig uwe.schroeder@tu-braunschweig.de bioelectrochemical expertise
	Richard Compton, PhD Professor, Oxford University: University of Oxford richard.compton@chem.ox.ac.uk expertise in physical chemistry
	George Inzelt, PhD Professor, University of Budapest inzeltgy@chem.elte.hu expertise in electrochemistry and physical chemistry
	Peter Pohl, PhD Professor, Johannes Kepler Universität Linz: Johannes Kepler Universitat Linz peter.pohl@jku.at expertise in biophysics
	Gerald Brezesinski, PhD Professor, Max Planck Institute of Colloids and Interfaces: Max-Planck-Institut fur Kolloid und Grenzflachenforschung gerald.brezesinski@mpikg.mpg.de Expertise in membranes and biophysics
	Falk Harnisch, PhD Professor, Universität Leipzig: Universitat Leipzig falk.harnisch@ufz.de expertise in bioelectrochemistry
Opposed Reviewers:	

1   **The effects of the chemical environment of menaquinones in lipid**

2   **monolayers on mercury electrodes on the thermodynamics and kinetics of**

3   **their electrochemistry.**

4   **Karuppasamy Dharmaraj[1], Dirk Dattler[1], Heike Kahlert[1], Uwe Lendeckel[2], Felix Nagel[1],**

5   **Mihaela Delcea[1], Fritz Scholz[1]**

6   E-mail: fscholz@uni-greifswald.de

7   ORCID of the authors:
8   Prof. Dr. Fritz Scholz: 0000-0001-6287-1184
9   Karuppasamy Dharmaraj: 0000-0001-6743-3503
10   PD Dr. Heike Kahlert: 0000-0002-9196-5750
11   Prof. Dr. Mihaela Delcea: 0000-0002-0851-9072
12   Prof. Dr. Uwe Lendeckel: 0000-0002-0684-9959
13   Dirk Dattler: 0000-0002-0139-588X
14   Felix Nagel: 0000-0003-3456-7075
15

16   [1]   Institute of Biochemistry, University of Greifswald, Felix-Hausdorff-Str. 4, 17487

17   Greifswald,   Germany.

18   [2]   Institute of Medical Biochemistry and Molecular Biology, University Medicine

19   Greifswald,   University   of   Greifswald,   Ferdinand-Sauerbruch-Str.,   D-17475

20   Greifswald, Germany.

21   **Abstract:**

22   The effects of the chemical environment of menaquinones (*all-trans* MK-4, *all-trans* MK-7)

23   incorporated in lipid monolayers on mercury electrodes have been studied with respect to the

24   thermodynamics and kinetics of their electrochemistry. The chemical environment relates to

25   the composition of lipid films as well as the adjacent aqueous phase. It could be shown that the

26   addition of *all-trans* MK-4 to TMCL does not change the phase transition temperatures of

27   TMCL. In case of DMPC monolayers, the presence of cholesterol has no effect on the

28   thermodynamics (formal redox potentials) of *all-trans* MK-7, but the kinetics are affected.

29   Addition of an inert electrolyte (sodium perchlorate; change of ionic strength) to the aqueous

30   phase shifts the redox potentials of *all-trans* MK-7 only slightly. The formal redox potentials

31   of *all-trans* MK-4 were determined in TMCL and nCL monolayers and found to be higher in

32   nCL monolayers than in TMCL monolayers. The apparent electron transfer rate constants,

33 transfer coefficients and activation energies of *all-trans* MK-4 in cardiolipins have been also

34 determined. Most surprisingly, the apparent electron transfer rate constants of *all-trans* MK-4

35 exhibit an opposite pH dependence for TMCL and nCL films: the rate constants increase in

36 TMCL films with increasing pH, but in nCL, films they increase with decreasing pH. This

37 study is a contribution to understand environmental effects on the redox properties of

38 membrane bond redox systems.

41 **Declarations**

45 **Conflicts of interest/Competing interests**

46 There are no conflicts of interest or competing interests to be declared.

47 **Availability of data and material**

48 Primary data are stored at the University of Greifswald.

49 **Code availability**

50 Not applicable

51

The effects of the chemical environment of menaquinones in lipid monolayers on mercury electrodes on the thermodynamics and kinetics of their electrochemistry.

Karuppasamy Dharmaraj[1], Dirk Dattler[1], Heike Kahlert[1], Uwe Lendeckel[2], Felix Nagel[1], Mihaela Delcea[1], Fritz Scholz[1]

E-mail: fscholz@uni-greifswald.de

ORCID of the authors:
Prof. Dr. Fritz Scholz: 0000-0001-6287-1184
Karuppasamy Dharmaraj: 0000-0001-6743-3503
PD Dr. Heike Kahlert: 0000-0002-9196-5750
Prof. Dr. Mihaela Delcea: 0000-0002-0851-9072
Prof. Dr. Uwe Lendeckel: 0000-0002-0684-9959
Dirk Dattler: 0000-0002-0139-588X
Felix Nagel: 0000-0003-3456-7075

[1]   Institute of Biochemistry, University of Greifswald, Felix-Hausdorff-Str. 4, 17487 Greifswald, Germany.

[2]   Institute of Medical Biochemistry and Molecular Biology, University Medicine Greifswald, University of Greifswald, Ferdinand-Sauerbruch-Str., D-17475 Greifswald, Germany.

Abstract:

The effects of the chemical environment of menaquinones (*all-trans* MK-4, *all-trans* MK-7) incorporated in lipid monolayers on mercury electrodes have been studied with respect to the thermodynamics and kinetics of their electrochemistry. The chemical environment relates to the composition of lipid films as well as the adjacent aqueous phase. It could be shown that the addition of *all-trans* MK-4 to TMCL does not change the phase transition temperatures of TMCL. In case of DMPC monolayers, the presence of cholesterol has no effect on the thermodynamics (formal redox potentials) of *all-trans* MK-7, but the kinetics are affected. Addition of an inert electrolyte (sodium perchlorate; change of ionic strength) to the aqueous

83   phase shifts the redox potentials of *all-trans* MK-7 only slightly. The formal redox potentials

84   of *all-trans* MK-4 were determined in TMCL and nCL monolayers and found to be higher in

85   nCL monolayers than in TMCL monolayers. The apparent electron transfer rate constants,

86   transfer coefficients and activation energies of *all-trans* MK-4 in cardiolipins have been also

87   determined. Most surprisingly, the apparent electron transfer rate constants of *all-trans* MK-4

88   exhibit an opposite pH dependence for TMCL and nCL films: the rate constants increase in

89   TMCL films with increasing pH, but in nCL, films they increase with decreasing pH. This

90   study is a contribution to understand environmental effects on the redox properties of

91   membrane bond redox systems.

92

93   **Keywords:** Menaquinone, Vitamin K_2, electrochemistry, thermodynamics, kinetics, lipid

94   monolayers

95

96   **Graphical Abstract:**
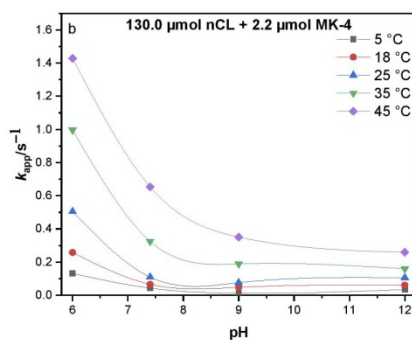
97

98   **Introduction**

99   Menaquinones (MK-*n*), the vitamin K_2 class of compounds with a 2-methyl-1,4-

100   naphthoquinone moiety connected with *n* isoprenyl units, are crucially involved in diverse

101   biological functions and insufficient levels of vitamin K result in diseases (2002). Indeed, only

102   the *all-trans* form of MK-7 is biological active (Lal et al. 2020). Recently, the acid-base and

103   the redox properties of *all-trans* MK-4, -7, and -9 in 1, 2-dimyristoyl-sn-glycero-3-

4

104 phosphocholine (DMPC) monolayers on mercury electrodes have been studied (Dharmaraj et

105 al. 2020). This has been done because only very limited electrochemical data were available

106 (Lovander et al. 2018), particularly for vitamins K in biological membranes. Composition

107 effects, including the nature of lipid phases, cholesterol content, and inert salt addition to the

108 aqueous phase, and also temperature effects on the redox properties of menaquinones in

109 membranes are of interest to understand the complex membrane machineries. For instance,

110 phase transitions of the lipids in membranes are known to have a strong effect on the

111 permeation of H^+ / OH^- ions (Elamrani et al. 1983). Model systems, such as lipid monolayers

112 and liposomes, can be used to understand the thermodynamics and kinetics of the redox

113 reactions. Lipid monolayers on mercury electrodes are excellent model systems because the

114 measurements are highly reproducible, among others, because the formation and structure of

115 the monolayers on mercury are highly reproducible. Important questions to be addressed are:

116 (i) How does the nature of lipids affect the redox potential of quinoid membrane constituents

117 (e.g. of ubiquinone (Heise et al. 2017), menaquinones, etc.)? (ii) How does the cholesterol

118 content of the membranes affect the redox properties of quinoid membrane constituents

119 (Schroeder et al. 1991), and how it affects the membrane fluidity, ion transport, signal

120 transduction, etc. (Simons et al. 2004; Levitan et al. 2010; Bastiaanse et al. 1983; Fielding et

121 al. 2004; Lange et al. 2016; Madden et al.1980; Cornelius 2001)? (iii) How does the addition

122 of an inert salt affect the redox properties of the quinoid membrane constituents? Inert salts

123 change not only the ionic strength, but also the water activity, which is known to have an effect

124 on the intramolecular properties at catalytic sites (Disalvo 2015; George et al. 1970). Here we

125 report attempts to partially answer these questions by experiments in which menaquinones have

126 been incorporated in lipid monolayers on a stationary mercury drop electrode. This approach

127 allows analysing both the thermodynamics as well as the kinetics of electrochemistry of the

128 naphthoquinone/naphthohydroquinone redox couple. The results may allow drawing

129 conclusions with respect to the chemical redox switching when the menaquinones operate in

130 the respiration chain.

131

132 **Experimental section**

133 **Chemicals**

134 The following chemicals were used: trisodium citrate pentahydrate (extra pure) and sodium

135 perchlorate (NaClO$_4$) (extra pure) were from Laborchemie, Apolda GmbH, Germany,

136 Disodium monohydrogen phosphate dihydrate ($Na_2HPO_4 \cdot 2H_2O$) (≥98%), sodium hydroxide

137 (NaOH) (≥99%), potassium chloride (KCl) (≥99.5%), chloroform ($CHCl_3$) (HPLC grade) and

138 methanol (CH_3OH) (≥99.98%, ultra LC–MS grade) were from Carl Roth GmbH, Germany,

139 monosodium dihydrogen phosphate dihydrate ($NaH_2PO_4 \cdot 2H_2O$) (pure pharma grade) was from

140 Applichem GmbH, Germany, disodium carbonate monohydrate ($Na_2CO_3 \cdot H_2O$) (>99%) was

141 from Fluka Chemika, Germany, mercury (99.9999 Suprapur), hydrochloric acid (HCl) ((32%)

142 for analysis), sodium bicarbonate ($NaHCO_3$) and citric acid monohydrate (analytical grade)

143 were from Merck, Germany, DMPC (14:0 PC) (1,2-dimyristoyl-sn-glycero3-phosphocholine)

144 (>99%), TMCL (1,1',2,2' Tetramyristoyl Cardiolipin) (14:0 Cardiolipin (sodium salt)) (1',3'-

145 bis[1,2-dimyristoyl-sn-glycero-3-phospho]-glycerol   (sodium   salt))   (>99%)   and   nCL

146 (Cardiolipin (Heart, Bovine) (sodium salt)) (>99%) lipids were from Avanti Polar Lipids, USA,

147 *all-trans* menaquinone 4 (*all-trans* MK-4) (analytical standard), *all-trans* menaquinone 7 (*all-*

148 *trans* MK-7) (United States Pharmacopeia (USP) Reference Standard) and cholesterol (Sigma

149 Grade ≥99%) were from Sigma-Aldrich, Germany. The buffer solutions were prepared using

150 citric   acid   monohydrate/trisodium   citrate   pentahydrate   for   pH   4.0,

151 $Na_2HPO_4 \cdot 2H_2O / NaH_2PO_4 \cdot 2H_2O$ for pH 6.0 and 7.4, $Na_2CO_3 \cdot H_2O / NaHCO_3$ for pH around 9.0,

152 and NaOH for pH 12.0 (Dawson et al. 1986). For adjusting the buffer pH, HCl and NaOH were

153 used.

154

Instrumentation

156 The electrochemical measurements were performed with the AUTOLAB PGSTAT 12, in

157 conjunction with the electrode stand VA 663 (Metrohm, Switzerland). A multimode electrode

158 in which the hanging mercury drop electrode (HMDE) mode (drop size 2, surface area 0.464

159 mm^2) served as working electrode, a platinum rod and an Ag | AgCl (3 M KCl, E=0.207 V vs.

160 SHE (standard hydrogen electrode)) (connected to the cell via a saturated KCl salt bridge)

161 electrode were used as auxiliary and reference electrodes, respectively. The redox systems were

162 studied with cyclic voltammetry (staircase) in normal mode applying different scan rates with

163 step potential of 0.00045 V. A temperature-controlled bath (Lauda Ecoline 003 E100) was used

164 for all measurements. The calorimetric measurements were recorded with a MicroCal VP-DSC

165 by Malvern Panalytical at the scan rate of 90 K/h.

166

167   **Liposome preparation**

168   The liposomes were prepared according to Moscho's rapid evaporation technique (Moscho et

169   al. 1996). The lipids (DMPC, TMCL and nCL), cholesterol, and the MK were dissolved

170   separately in chloroform to prepare stock solution. The lipids from the stock solution were

171   diluted with chloroform and methanol (ratio 3:1) and the desired amount of menaquinone was

172   added from the chloroform stock solution (1 mg mL^{-1}), so that the desired molar ratio

173   lipid:menaquinone (60:1) was reached. This was followed by adding 20 mL of aqueous buffer

174   (pH 7.4). The organic solvents were removed using the rotation evaporator Laborota 4000

175   (Heidolph, Germany) and the Rotavac control pump (Heidolph, Germany) at 50 °C, 60 rpm

176   and a final pressure of 100 mbar. For the liposomes containing cholesterol (Hernández et al.

177   2008), the desired amount of lipids, cholesterol and *all-trans* MK-7 were diluted with

178   chloroform and methanol (ratio 3:1) in a round bottomed flask and the solvents were removed

179   at 45 °C and a final pressure of 100 mbar. After the solvent evaporation, the lipid-cholesterol-

180   *all-trans* MK-7 film was dried again with a stream of nitrogen for 30 minutes. The aqueous

181   buffer pH 7.4 (30 mL) was added into the round bottomed flask with glass pearls containing

182   the dried films on the inner side of the glass vessel and kept in the water bath (45 °C) at 180

183   rpm for 10 min. The hydrated liposome suspension was extruded at 45 °C with a total of 10

184   passes through a 400 nm filter using the Avanti Mini Extruder (Avanti Polar Lipids, Inc., USA).

185   The total amount of DMPC or DMPC/Chol composition was 300 µmol.

186

187   **Electrochemical measurements**

188   The melting point (T_m) of DMPC is 23.9 °C (Mabrey S et al. 1976). Three phase transition

189   regions have been found in the DMPC – cholesterol system: existence of gel (G) or fluid

190   lamellar disordered phases (L$_\alpha$(d)) at low cholesterol (~<6 mol %) content, fluid lamellar

191   ordered (L$_\alpha$(o)) phases at high cholesterol content (~>30 mol %) and between these, the

192   existence of G + L$_\alpha$(o) or L$_\alpha$(d) + L$_\alpha$(o) phases (Almeida et al. 1992; Hernández et al. 2008).

193   Therefore, three DMPC/Chol compositions 95/5 mol %, 80/20 mol % and 65/35 mol % at 20

194   °C and 28 °C temperatures were chosen for the electrochemical investigations. 5 µmol *all-*

195   *trans* MK-7 was used for the studies of cholesterol and water activity on *all-trans* MK-7

196   measurements. Sodium perchlorate was used to interrogate the effect of an inert salt, and thus

197   also for the effect of water activity at 25 °C in aqueous buffer pH 7.4. The TMCL (1′,3′-bis[1,2-

198   dimyristoyl-sn-glycero-3-phospho]-glycerol (sodium salt)) exhibits the lamellar gel (L$_\beta$) to

7

lamellar liquid crystalline (L$_\alpha$) and subgel (L$_c$) to lamellar gel (L$_\beta$) transitions at 40.3 °C and 24.2 °C respectively. Addition of 2.2 µmol *all-trans* MK-4 to 130 µmol TMCL has practically no effect on transition temperatures (40.7 °C and 23.8 °C) (Fig. S1). Natural cardiolipins (nCL) and nCL containing *all-trans* MK-4 liposomes do not exhibit any phase transitions in the temperature range 7 to 90 °C. The voltammetric measurements to study the behavior of *all-trans* MK-4 in different cardiolipin phases were performed at 5 °C, 18 °C, 25 °C, 35 °C, and 45 °C. A non-isothermal electrochemical cell configuration was used by keeping the reference electrode at ambient temperature. The liposome suspension was deaerated for at least 30 min. A mercury drop was formed and the solution was stirred for 15 min to form a monolayer. The liposome solution was replaced with aqueous buffer, and the buffer solution was purged with nitrogen to remove the dissolved oxygen. Then the monolayer was characterized by electrochemical measurements.

Abbreviations and symbols:

α	– electron transfer coefficient
E_{act}	– activation energy
$E_c^{\ominus}{}'$	– formal potential
E_{mp}	– midpeak potential
E_{pa}	– anodic peak potential
E_{pc}	– cathodic peak potential
$E_{pc(pa)}$	– cathodic peak potential or anodic peak potential
$\Delta E' = E_{mp,\,exp} - E_{mp,\,theoretical\ at\ given\ pH}$	
$\Delta E_{pa/pc}$	– peak separation between anodic and cathodic peaks
F	– Faraday constant (96485.3 C mol^{-1})
k_{app}	– apparent electron transfer rate constant
R	– gas constant (8.3145 J mol^{-1} K^{-1})
υ_a	– critical anodic scan rate
υ_c	– critical cathodic scan rate
$\Delta G^{\ominus}$	– standard free energy change
ΔG	– free energy change
$\Delta H^{\ominus}$	– standard enthalpy change
ΔH	– enthalpy change
$\Delta S^{\ominus}$	– standard entropy change
ΔS	– entropy change
Chol	– cholesterol
CL	– cardiolipin

8

235 DMPC – (14:0 PC) 1,2-dimyristoyl-sn-glycero-3-phosphocholine
236 DMPC/Chol – DMPC lipids films containing Chol at different mol %
237 DMPC/Chol/*all-trans* MK-7 – *all-trans* menaquinone-7 in DMPC/Chol films
238 G   – gel phase of DMPC/Chol mixtures
239 *I*   – ionic strength of the solution
240 L$_\alpha$ – lamellar liquid crystalline phase of TMCL
241 L$_\beta$ – lamellar gel phase of TMCL
242 L$_c$ – subgel phase of TMCL
243 L$_\alpha$ (d) – fluid lamellar disordered phase of DMPC/Chol mixtures
244 L$_\alpha$ (o) – fluid lamellar ordered phase of DMPC/Chol mixtures
245 nCL   – natural cardiolipin (Heart, Bovine) (sodium salt)
246 TMCL – (14:0 cardiolipin (sodium salt)) 1',3'-bis[1,2-dimyristoyl-sn-glycero-3-phospho]-
247 glycerol (sodium salt)
248 $T_{m, DMPC}$ – phase transition temperature of DMPC
249 TMCL/*all-trans* MK-4 – *all-trans* menaquinone-4 in TMCL films
250 nCL/*all-trans* MK-4 – *all-trans* menaquinone-4 in nCL films
251

252 **Results and discussion**

253 ***Thermodynamics of the electrochemistry of menaquinones in DMPC/cholesterol***
254 ***monolayers on mercury***

255 In DMPC/Chol monolayers, *all-trans* MK-7 exhibits in cyclic voltammetry a reversible redox
256 system (Fig. 1). The mid-peak potentials of *all-trans* MK-7 are higher in the fluid phase, i.e.,
257 above the $T_{m, DMPC}$, for pH 7.4 and pH 9. Since the pK_a values of menaquinones are above 12
258 (Dharmaraj et al. 2020) this observation cannot be caused by the acidity of menaquinone, but
259 it is obviously associated with the nature of the lipid phase. Measured in electrolytes of pH
260 4.0 to 12.0, the mid-peak potentials do not depend on the cholesterol content (0 to 35%).
261 They are scattered within a 7 mV range (

262 Table 1). This indicates that the thermodynamics of the redox system is not affected by
263 cholesterol. However, the kinetics is affected (Table 2), as indicated by an increased peak
264 separation at high cholesterol content. With the exception of pH 12.0, the high cholesterol
265 content (35 mol %) in the DMPC films causes a slowdown of the kinetics of the *all-trans* MK-
266 7 redox system. At that cholesterol content DMPC is present as fluid lamellar ordered phase
267 (L$_\alpha$ (o)). The peak separations are small when the DMPC exists as gel phase (G), G + L$_\alpha$ (o)
268 and fluid lamellar disordered phase (L$_\alpha$ (d)) + L$_\alpha$ (o). There the peak separation is only a few
269 mV, as typical for surface confined redox systems. The presence of cholesterol does not
270 substantially affect the redox potentials of *all-trans* MK-7 system in DMPC/Chol films.
271 Previously, a similar result has been reported by Becucci et al. (Becucci et al. 2011), who found

9

272   that the thermodynamic redox potential of ubiquinone is not affected by the presence of

273   cholesterol in dioleoylphosphatidylcholine-palmitoylsphingomyelin mixtures.

274
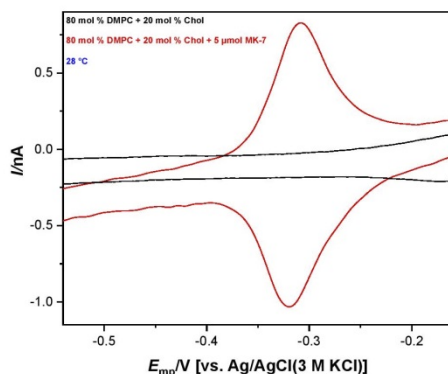
Fig. 1 Cyclic voltammograms of DMPC/Chol and DMPC/Chol/*all-trans* MK-7 films in pH 7.4 at 28 °C. Scan rate: 10 mV s^{-1}

Table 1 Mid-peak potentials E_{mp} (versus Ag/AgCl(3 M KCl)) for DMPC/Chol films spiked with *all-trans* MK-7 for pH 4.0, 7.4, 9.0, and 12.0 at 20 °C and 28 °C. At least 3 different monolayers were studied for each mid-peak potentials determination. Scan rate: 10 mV s^{-1}

	E_{mp} [V vs. Ag/AgCl(3 M KCl)]							
	20 °C	28 °C	20 °C	28 °C	20 °C	28 °C	20 °C	28 °C
pH								
	0 mol % Chol		5 mol % Chol		20 mol % Chol		35 mol % Chol	
4.0	−0.109	−0.107	−0.099	−0.104	−0.104	−0.109	−0.094	−0.109
7.4	−0.307	−0.314	−0.299	−0.313	−0.303	−0.313	−0.304	−0.319
9.0	−0.409	−0.419	−0.398	−0.419	−0.401	−0.413	−0.407	−0.416
12.0	−0.580	−0.579	−0.575	−0.570	−0.576	−0.578	−0.577	−0.582

281

Table 2 Separation of anodic and cathodic peaks for DMPC/Chol films spiked with *all-trans* MK-7. Scan rate: 10 mV s^{-1}. At least 3 different monolayers were studied for each $\Delta E_{pa/pc}$ determination. In brackets, the standard deviations are given

	$\Delta E_{pa/pc}$ [mV]							
pH	20 °C	28 °C	20 °C	28 °C	20 °C	28 °C	20 °C	28 °C

10

	0 mol % Chol		5 mol % Chol		20 mol % Chol		35 mol % Chol	
4.0	8 (±2)	10 (±4)	8 (±2)	1 (±0)	18 (±4)	13 (±2)	65 (±25)	55 (±11)
7.4	3 (±1)	7 (±1)	5 (±2)	8 (±2)	5 (±1)	8 (±2)	43 (±3)	44 (±23)
9.0	6 (±4)	3 (±2)	3 (±3)	9 (±2)	5 (±2)	3 (±1)	89 (±32)	13 (±4)
12.0	2 (±1)	0 (±0)	2 (±1)	3 (±1)	1 (±1)	3 (±0)	5 (±1)	3 (±0)

285

286

Kinetics of the electrochemical redox reactions of menaquinones in DMPC/cholesterol monolayers

A commonly used method to access the electron transfer rate constants of adsorbed redox systems is the Laviron formalism (Laviron 1979; Laviron 1982). The apparent rate constants (k_{app}) for peak separations, $\Delta E_{pa/pc} < 200$ mV/n and $\Delta E_{pa/pc} > 200$ mV/n are determined according to the Laviron formalism. For the non-reversible case, where $\Delta E_{pa/pc} > 200$ mV/n, the following equations have to be used:

$$E_{pc} = E_c^{\ominus}{}' - \left(\frac{2.3RT}{\alpha nF}\right)\log\left[\frac{\alpha nF \upsilon_c}{RTk_{app}}\right] \tag{1}$$

$$E_{pa} = E_c^{\ominus}{}' - \left(\frac{2.3RT}{(1-\alpha)nF}\right)\log\left[\frac{(1-\alpha)nF \upsilon_a}{RTk_{app}}\right] \tag{2}$$

$$k_{app} = \frac{\alpha nF \upsilon_c}{RT} = \frac{(1-\alpha)nF \upsilon_a}{RT} \tag{3}$$

The critical scan rates υ_a and υ_c are obtained by plotting $E_{pc(pa)} - E_c^{\ominus}{}'$ vs. log υ, and extrapolating the slopes to $E_{pc(pa)} - E_c^{\ominus}{}' = 0$, i.e. the x-intercept, where $E_{pc(pa)}$ are the cathodic and anodic peak potentials, respectively, and $E_c^{\ominus}{}'$ is the formal (or mid-peak) potential. The values of αn and $(1-\alpha)n$ are calculated from the slopes of $E_{pc(pa)} - E_c^{\ominus}{}'$ vs. log υ where the slope is $-2.3\dfrac{RT}{\alpha nF}$ for the cathodic branch and $2.3\dfrac{RT}{(1-\alpha)nF}$ for the anodic branch respectively. The rate constants are calculated for both critical scan rates and the mean values are given here. For the reversible and quasi-reversible cases, where $\Delta E_{pa/pc} < 200$ mV/n, the value of α for

11

304   different temperatures was found by relating the ratio $y = \left| \dfrac{E_{pc} - E_c^{\ominus'}}{E_{pa} - E_c^{\ominus'}} \right|$ to $\Delta E_{pa/pc}$. Since y was

305   equal to 1, α is 0.5, independent of the peak separations. The rate constants for different

306   temperatures are determined from the plot of $\Delta E_{pa/pc}$ < 200 mV/n vs 1/m for $\alpha = 0.5$, where

307   $\dfrac{1}{m} = \dfrac{nF\upsilon}{RTk_{app}}$. For different scan rates, k_{app} is calculated and the mean values are reported.

308   There might be small errors in k_{app} values because the Laviron method is available only for 25

309   °C.

310   Using the Laviron formalism, the electron transfer rate constants of *all-trans* MK-7 in

311   DMPC/Chol films were calculated at above and below the $T_{m,DMPC}$ (Fig. 2, Table S1). The k_{app}

312   data do not follow any specific dependence; rather several cases are observed:

313   i.   The k_{app} of *all-trans* MK-7 in L$_\alpha$ (d) + L$_\alpha$ (o) phase (above the $T_{m,\,DMPC}$) is higher than

314   in the G + L$_\alpha$ (o) phase for all pH.

315   ii.   In the G phase, the k_{app} of *all-trans* MK-7 increases with increasing pH, but in the (L$_\alpha$

316   (d)) phase, the k_{app} of *all-trans* MK-7 is almost constant at pH 7.4 and 9.0 which is also

317   lower than the value at pH 4.0.

318   iii. Even in the (L$_\alpha$ (o)) phase, two different cases are observed at 20 °C and 28 °C: At 28

319   °C, k_{app} increases with decreasing in proton activity, and at 20 °C, the rate constants

320   decline with decreasing proton activity (with the exception of pH 12.0).

321   iv.   Generally in all phases, k_{app} is larger in the alkaline solution (pH 12.0).

322   The reason for the complex dependence of the k_{app} of *all-trans* MK-7 on cholesterol content

323   might be the presence of different structural phases. The presence of cholesterol disturbs the

324   order of the lipids, fluidity of the monolayer, reduces the surface area per lipid and causes a

325   phase separation (domains or rafts) (Hernández et al. 2008). The presence of domains and the

326   changes in the organization of the lipids can affect the *all-trans* MK-7 molecules for the

327   electron transfer and accessibility of the protons. Fig. 2 clearly indicates that large cholesterol

328   concentrations decrease the rate constant.

12
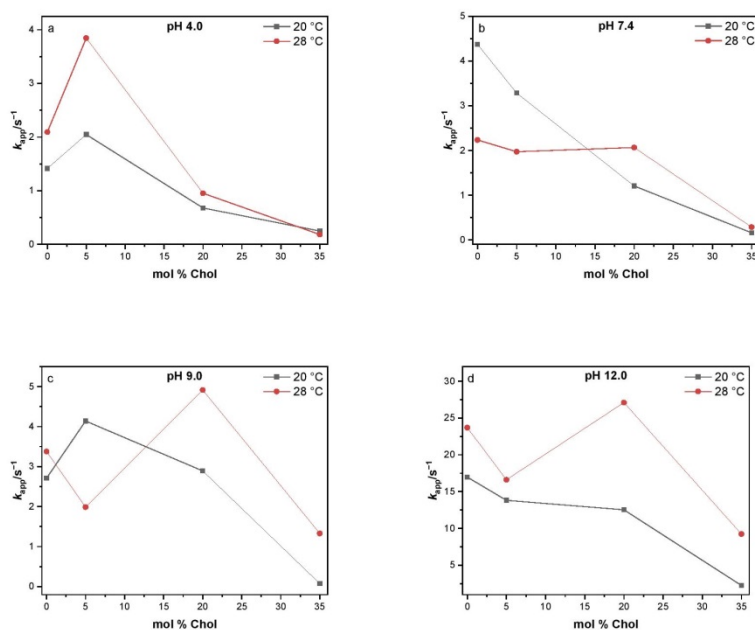
Fig. 2 Dependence of apparent electron transfer rate constants of *all-trans* MK-7 on cholesterol content in DMPC films at 20 °C and 28 °C for (a) pH 4.0, (b) pH 7.4, (c) pH 9.0, and (d) pH 12.0

In Fig. S2, the apparent electron transfer rate constants of MK-7 in DMPC/Chol monolayers is given as function of pH at temperatures above and below the phase transition temperature of DMPC. In all cases, the rate constants increase considerably in the alkaline range, i.e., in a clearly non-physiological range. See further down a completely different pH behaviour in case of monolayers of natural cardiolipins.

Effects of an inert salt (sodium perchlorate) addition to the aqueous phase on the thermodynamics and kinetics of the electrochemistry of all-trans MK-7 in DMPC monolayers

The inner of cells and mitochondria is by far no diluted aqueous solution, but a rather concentrated, quasi crystalline solution of proteins and salts. Therefore it is desirable to study not only the effects of membrane composition on the electrochemistry of menaquinones, but also the effects of composition of the aqueous phase. Hence, experiments have been performed in which an inert salt (sodium perchlorate) has been added to the aqueous buffer

phase. The addition of this salt results at least in the following three alterations: (i) it changes the ionic strength (see

Table 3). (ii) It changes the water activity. In 6 m (molal) solutions of $NaClO_4$ water activity decreases to about 0.8 (Toner et al. 2016). (iii) The salt addition also diminishes the diffusion coefficient of protons (Roberts et al. 1974), which may affect the kinetics of the $2e^-/2H^+$ redox reaction of the naphthoquinone unit. The inert salt also affects the pH of the buffer solutions, but that effect has been taken into consideration as follows: the pH of the solutions with salt additions has been measured and the midpeak potential of the *all-trans* MK-7 of these solutions has been compared with that of $NaClO_4$-free solutions of the respective pH values. To study the salt effect, the concentration of sodium perchlorate has been varied from 0 up to 5 mol kg^{-1}, in addition to the used buffers (see experimental part). The measured potential differences $\Delta E' = E_{mp, exp} - E_{mp, theoretical\ at\ given\ pH}$ are given in

Table 3. Clearly, the effect of sodium perchlorate addition to the aqueous phase on the mid-peak potentials, i.e., on thermodynamics, is not negligible but small (1 to 29 mV). The effect on kinetics (anodic-cathodic peak separation) is, if at all, also very small (cf.

Table 3).

Table 3 DMPC films spiked with *all-trans* MK-7: $\Delta E' = E_{mp, exp} - E_{mp, theoretical\ at\ given\ pH}$: Difference between experimentally measured mid-peak potentials and those at the measured pH, but without sodium perchlorate. $\Delta E_{pa/pc}$ is the peak separation between anodic and cathodic peaks. The film composition was 300 µmol DMPC + 5 µmol MK-7

NaClO$_4$ [m]	pH	I [mol kg^{-1}]	$\Delta E'$ [V]	$\Delta E_{pa/pc}$ [V]
0.0	7.36	0.259	0	0.008 (±0.003)
0.1	7.22	0.359	0.001	0.015 (±0.001)
1.0	6.82	1.259	0.013	0.013 (±0.001)
3.0	6.41	3.259	0.029	0.015 (±0.005)
5.0	6.23	5.259	0.022	0.013 (±0.003)

Thermodynamics of the electrochemistry of menaquinones in cardiolipin monolayers on mercury

14

373 Since cardiolipins are major constituents of mitochondrial membranes, the electrochemistry of

374 menaquinones has been interrogated in monolayers of an artificial cardiolipin (TMCL) and in

375 monolayers of natural cardiolipin (nCL).

376
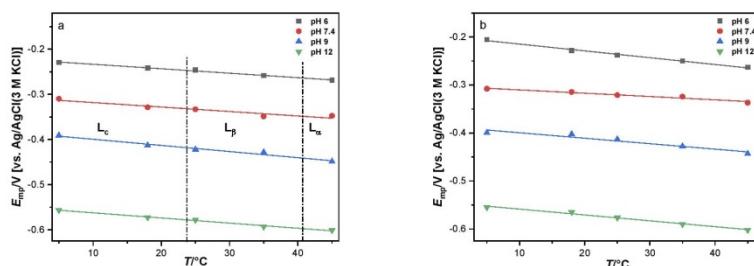
Fig. 3 Dependence of mid-peak potentials of *all-trans* MK-4 spiked in (a) TMCL and (b) nCL films on temperature. Scan rate: 10 mV s^{-1}. The dash dotted lines in TMCL/*all-trans* MK-4 film represent the phase transition temperatures. The ratio of *all-trans* MK-4 to TMCL was 2.2 μmol to 130.0 μmol TMCL (nCL, respectively)

381

382 The mid-peak potentials of *all-trans* MK-4 in TMCL and nCL monolayers continuously shift

383 in the negative direction with increasing temperature (5 °C to 45 °C). There is no indication

384 that the phase transitions of TMCL affect the potential shift (cf. Fig. 3). The temperature

385 dependence of the mid-peak potentials allows calculating the reaction entropy ΔS given by:

$$\Delta S = nF\left(\frac{dE_{midpeak}}{dT}\right) = S_{MQH_2} - S_{MQ} \tag{4}$$

387 where $\left(\dfrac{dE_{midpeak}}{dT}\right)$ is the slope in the plot of $E_{midpeak}$ vs T.

388 Table 4 shows the reaction entropies of *all-trans* MK-4 in TMCL and nCL films.

389

390 **Table 4** Reaction entropies of *all-trans* MK-4 in TMCL and nCL films. The ratio of *all-trans* MK-4 to TMCL
391 was 2.2 μmol to 130.0 μmol TMCL (nCL, respectively)

pH	$\Delta S_{TMCL/MK-4}$ [J K^{-1}mol^{-1}]	$\Delta S_{nCL/MK-4}$ [J K^{-1}mol^{-1}]
6.0	−191 (±8)	−274 (±14)
7.4	−191 (±33)	−133 (±16)

15

9.0	−262 (±24)	−220 (±37)
12.0	−220 (±11)	−235 (±16)

392

393 Since these entropies refer to the reduction of the naphtoquinone to the naphtohydroquinone

394 moiety

395 $R - NQ + 2\,e^- + 2H^+ \rightarrow R - NQH_2$
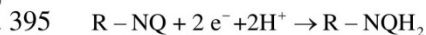
396 it involves the dehydration of the protons, which is known to *increase* the entropy by +131 J

397 K^{-1} mol^{-1} (Marcus Y 2015). For the reduction of tetrafluoroquinone (TFQ) dissolved in

398 aqueous solution, Yousoufian (Yousofian-Varzaneh et al. 2015) determined a *loss* of entropy

399 of −3.665 kJ K^{-1} mol^{-1}, and they assumed as reason the decrease of number of particles during

400 the reduction $TFQ + 2\,e^- + 2H^+ \rightarrow TFQH_2$. Wass et al. (Johnsson Wass et al. 2006) performed

401 a quantum chemical modelling of the reduction of some quinones, including p-naphtoquinone

402 to *cis*- and *trans*-naphtohydroquinone. They have found the following data for the reduction of

403 p-naphtoquinone to the more stable *cis*- naphtohydroquinone: $\Delta G^\circ = -50.0$ kJ mol^{-1},

404 $\Delta H^\circ = -86.0$ kJ mol^{-1} and $\Delta S^\circ = -121$ J K^{-1} mol^{-1}. These data are not in contradiction to the

405 experimental data, which we report here for *all-trans* MK-4 in TMCL and nCL films (Table 5-

406 7). However, it is interesting that the entropy loss is in case of the immobilized menaquinones

407 much larger than in case of dissolved naphthoquinone. This may indicate a strong ordering of

408 the menaquinone environment in the monolayer upon reduction.

409

410 **Table 5** Thermodynamic parameters for the *all-trans* MK-4 redox couple MQ/MQH$_2$ in TMCL and nCL films at
411 pH=0

$\Delta S_{pH=0}$		T [K]	$\Delta G_{pH=0} = -nFE_{mp}$ *		$\Delta H_{pH=0} = \Delta G_{pH=0} + T\Delta S$	
[J K^{-1}mol^{-1}]			[kJ mol^{-1}]		[kJ mol^{-1}]	
TMCL+MK-4	nCL+MK-4		TMCL+MK-4	nCL+MK-4	TMCL+MK-4	nCL+MK-4
−161.60	−208.41	278.15	−58.22	−64.31	−103.17	−122.28
		291.15	−55.51	−59.58	−102.56	−120.26
		298.15	−54.87	−58.72	−103.05	−120.85
		308.15	−52.77	−57.86	−102.57	−122.08
		318.15	−51.80	−55.22	−103.22	−121.53

412 * E_{mp} vs SHE

413

414 **Table 6** Thermodynamic parameters for the *all-trans* MK-4 redox couple MQ/MQH$_2$ in TMCL films

TMCL/MK-4											
$\Delta G=-nFE_{mp}$* [kJ mol^{-1}]				$T\Delta S$ [kJ mol^{-1}]				$\Delta H=\Delta G+T\Delta S$ [kJ mol^{-1}]			
T [K]	pH 6.0	pH 7.4	pH 9.0	pH 12.0	pH 6.0	pH 7.4	pH 9.0	pH 12.0	pH 6.0	pH 7.4	pH 9.0	pH 12.0
278.15	4.27	19.86	35.52	67.39	−53.13	−53.20	−73.00	−61.19	−48.86	−33.34	−37.48	6.20
291.15	6.74	23.49	39.73	70.51	−55.61	−55.68	−76.41	−64.05	−48.87	−32.19	−36.68	6.46
298.15	7.59	24.39	41.53	71.62	−56.95	−57.02	−78.25	−65.59	−49.35	−32.64	−36.71	6.03
308.15	9.91	27.39	42.75	74.49	−58.86	−58.94	−80.87	−67.79	−48.94	−31.54	−38.12	6.70
318.15	11.93	27.11	46.68	76.04	−60.77	−60.85	−83.50	−69.99	−48.84	−33.74	−36.81	6.05

415 * E_{mp} vs SHE

416

417 **Table 7** Thermodynamic parameters for the *all-trans* MK-4 redox couple MQ/MQH$_2$ in nCL films

nCL/MK-4											
$\Delta G=-nFE_{mp}$* [kJ mol^{-1}]				$T\Delta S$ [kJ mol^{-1}]				$\Delta H=\Delta G+T\Delta S$ [kJ mol^{-1}]			
T [K]	pH 6.0	pH 7.4	pH 9.0	pH 12.0	pH 6.0	pH 7.4	pH 9.0	pH 12.0	pH 6.0	pH 7.4	pH 9.0	pH 12.0
278.15	−0.30	19.50	37.22	67.13	−76.22	−37.06	−61.19	−65.48	−76.52	−17.56	−23.97	1.65
291.15	4.12	20.79	37.71	69.07	−79.78	−38.79	−64.05	−68.54	−75.66	−18.00	−26.34	0.53
298.15	5.92	22.03	39.80	71.30	−81.70	−39.72	−65.59	−70.19	−75.78	−17.69	−25.79	1.11
308.15	8.34	22.64	42.61	73.89	−84.44	−41.06	−67.79	−72.55	−76.10	−18.42	−25.18	1.34
318.15	10.82	25.07	45.61	76.24	−87.18	−42.39	−69.99	−74.90	−76.36	−17.32	−24.38	1.34

418 * E_{mp} vs SHE

419 Since the addition of 2.2 µmole *all-trans* MK-4 to TMCL has practically no effect on the phase

420 transition temperatures of TMCL (40.7 °C and 23.8 °C) (Fig. S1) determined previously in a

421 chronoamperometry study (Zander et al. 2012), it can be assumed that the two components do

422 not form specific phases, and further, that the menaquinone does not alter the TMCL phases.

423 Natural cardiolipins (nCL) and nCL containing *all-trans* MK-4 liposomes do not exhibit any

424 phase transitions in the temperature range 7 to 90 °C. Because *all-trans* MK-4 has no effect on

425 the TMCL phases, it is reasonable to assume that *all-trans* MK-4 forms also in nCL just a

426 diluted solution.

427 The TMCL/*all-trans* MK-4 and nCL/*all-trans* MK-4 exhibit slow electron transfer kinetics and

428 the quantitative evaluation was performed using the Laviron formalism (see below). The

429 separation of anodic and cathodic peak potentials decreases considerably with increasing

430 temperature (Figs. S3 to S6). In case of TMCL the different phases exhibit different slopes of

peak separation and peak potentials versus temperature. This clearly indicates, that the nature

of the phases affects the kinetics. The formal potential ($E_{MQ/MQH_2}^{\ominus'}$) of the MQ/MQH$_2$ couple for

different temperatures are easily obtained from the dependence of E_{mp} on pH by extrapolating

to the unitary proton activity (pH=0) and the slopes obey linear dependences (Fig. S7, Table

S2) between pH 6.0 and 12.0. *All-trans* MK-4 shows in nCL films higher redox potentials than

in TMCL films (cf. Fig. 4). Thus, the nature of the lipids housing the *all-trans* MK-4 determines

the redox potential, which is highly important to understand the biochemical reactions, notably

in biological membranes.
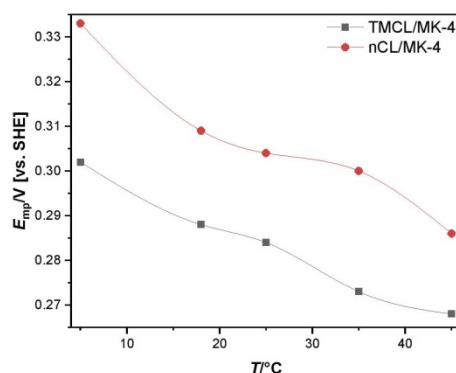
Fig. 4 Redox potentials of *all-trans* MK-4 in TMCL ($E_{TMCL/MK-4}^{\rightleftarrows'}$) and in nCL ($E_{nCL/MK-4}^{\rightleftarrows'}$) films at different temperatures. Scan rate: 10 mV s^{-1}. The ratio of *all-trans* MK-4 to TMCL was 2.2 μmol to 130.0 μmol TMCL (nCL, respectively)

Kinetics of the electrochemistry of menaquinones in cardiolipin monolayers on mercury

The apparent electron transfer coefficient, α of *all-trans* MK-4 in TMCL and nCL films was

determined (Table S3). For $\Delta E_p > 200/n$ mV, the mean value of anodic and cathodic α is

around 0.5 which agrees with $n = 2$. For the quasi- and completely reversible system, where

$\Delta E_{pa/pc} < 200/n$ mV, α is 0.5 (Laviron formalism). The k_{app} of *all-trans* MK-4 in TMCL and

nCL was estimated using the Laviron method (see rate constants determination section). For

18

452 nCL/*all-trans* MK-4 films, k_{app} is always highest at pH 6.0, given that only the pH range of 6.0

453 to 12.0 has been studied. Most interestingly, in contrast to these results, *all-trans* MK-4 in

454 TMCL exhibits highest k_{app} values at pH 12.0 (Fig. 5, Fig. 6, and Table S4).

455
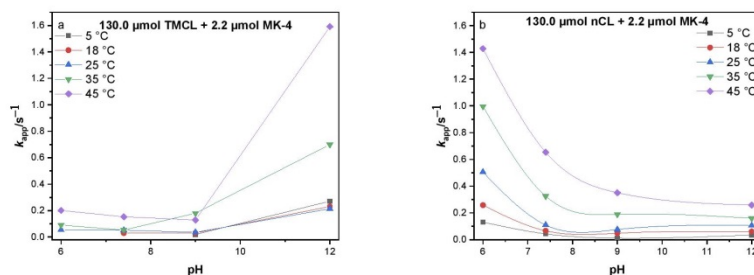
Fig. 5 Apparent electron transfer rate constants of MK-4 in (a) TMCL and (b) nCL films dependence on pH. The ratio of *all-trans* MK-4 to TMCL was 2.2 µmol to 130.0 µmol TMCL (nCL, respectively)

458 Looking at the dependence of k_{app} on the concentration of *all-trans* MK-4 in the films, in

459 TMCL as well as in nCL, decreasing amounts of *all-trans* MK-4 give larger rate constants (cf.

460 Fig. 7). Indeed, also in case of ubiquinone-10 monolayers, the maximum electron transfer rate

461 constants have been found at lowest surface concentration (Sek et al. 1999). The rate constants

462 k_{app} generally increase with increasing temperature for each concentration of *all-trans* MK-4

463 in TMCL and nCL films (Fig. 7). In TMCL films, the k_{app} of 4.4 µmol *all-trans* MK-4 slightly

464 decreases in L_c and L_β phases, and increased in L_α phase. There is also an abruptly high k_{app}

465 for the lowest *all-trans* MK-4 content (0.88 µmol) in the L_β phase. The correctness of this result

466 is support by 3 independent film preparations and measurements.
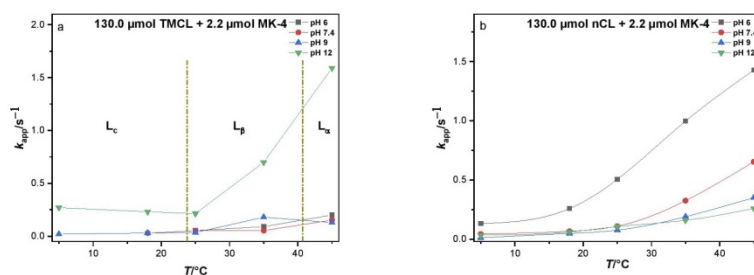
Fig. 6 Dependence of rate constants k_{app} of *all-trans* MK-4 in (a) TMCL and (b) nCL films on temperatures. The ratio of *all-trans* MK-4 to TMCL was 2.2 µmol to 130.0 µmol TMCL (nCL, respectively)
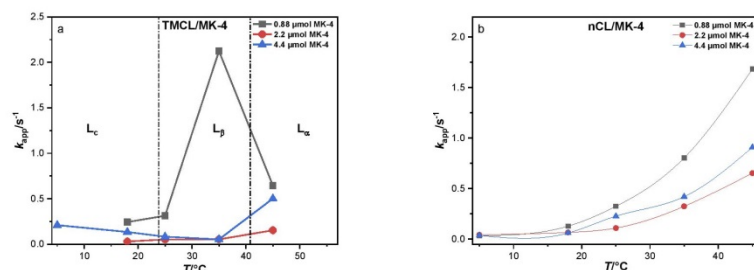
Fig. 7 Dependence of rate constants of *all-trans* MK-4 concentrations (0.88 µmol, 2.2 µmol, 4.4 µmol per 130.0 µmol TMCL (nCL, respectively) in (a) TMCL and (b) nCL films on temperatures for pH 7.4

Using the apparent electron transfer constants at different temperatures, the apparent activation energies are obtained using the Arrhenius equation (5) for TMCL/MK-4 and nCL/MK-4 films (

Table 8).

$$\ln k_{app} = \frac{-E_{act}}{R}\left(\frac{1}{T}\right) + \ln A \tag{5}$$

where E_{act} is the apparent activation energy, A the Arrhenius constant, k_{app} the apparent electron transfer rate constant, R the gas constant, and T the temperature in Kelvin.

482

Table 8 Apparent activation energies of *all-trans* MK-4 spiked in TMCL and nCL films for pH=6.0, pH=7.4, pH=9.0, and pH=12.0. The ratio of all-trans MK-4 to TMCL was 2.2 µmol to 130.0 µmol TMCL (nCL, respectively)

pH	E_{act}, TMCL/MK-4 [eV]	E_{act}, nCL/MK-4 [eV]
6.0	0.53 (±0.08)	0.48 (±0.03)
7.4	0.43 (±0.12)	0.54 (±0.08)
9.0	0.43 (±0.12)	0.64 (±0.02)
12.0	0.82 (±0.07) [$T \geq 298.15$ K] −0.08 (±0.00) [$T \leq 298.15$ K]	0.39 (±0.02)

486

487 For films of hydroquinone covalently bond to PEDOT Sterby et al. (Sterby et al. 2019) found
488 an activation energy of 0.3 eV for the electrochemical redox reaction. Samuelson and Sharp
489 (Samuelsson et al. 1978) determined the activation energies for 1,4-benzoquinone, 1,4-
490 naphthoquinione and for 9,10-anthraquinone in acetonitrile solutions at Pt, Au and graphite
491 electrodes to be all around 0.23 eV. The higher, but still very similar, values found for *all-trans*
492 MK-4 can be easily explained with the long chain of the menaquinone-4 (4 isoprenoyl units,
493 i.e., 16 carbon atoms in the chain, and 4 double bonds interconnected by 2 sp^3 hybridized
494 carbons). These chains are rather long and because of the sp^3 hybridized carbons they are
495 obviously rather bad conductors for electrons, which explains the slower redox kinetics.

496

Conclusion

498 The thermodynamics and kinetics of electrochemistry of menaquinones have been studied
499 using lipid monolayers on mercury. These are the conclusions:

i. 500 There is no significant effect of cholesterol when added to the films on the
501 thermodynamics of *all-trans* MK-7 in DMPC films, but the kinetics of the
502 electrochemistry of *all-trans* MK-7 is affected at high cholesterol content. The electron
503 transfer rate constants depend on the DMPC phases and the pH. The fact that the
504 thermodynamics of the electrochemistry of *all-trans* MK-7 in DMPC films is not
505 affected by the presence of cholesterol indicates that the latter does not interact directly
506 with the menaquinone in the film. The effect of cholesterol on the kinetics may result
507 from a changed double layer structure at the solution|film interface.

21

508   ii.   There is a slight increase of the thermodynamic mid-peak potentials of *all-trans* MK-7
509   in DMPC films on lowering the water activity by increasing inert salt concentration
510   (ionic strength) in the aqueous phase. The effect is small, but not negligible. The water
511   activity (ionic strength) has practically no effect on the kinetics of the electrochemistry
512   of *all-trans* MK-7.
513   iii.   The addition of *all-trans* MK-4 to TMCL does not change the phase transitions of
514   TMCL. The changes in reaction entropy, enthalpy and free energy, and activation
515   energies were determined for *all-trans* MK-4 in TMCL and nCL films. The nature of
516   the lipids affects the redox potential of *all-trans* MK-4. The electron transfer rate
517   constant of *all-trans* MK-4 is affected by the type of lipids, the nature of lipid phases,
518   the temperature, and the amount of *all-trans* MK-4.
519   iv.   The pH dependence of rate constants of *all-trans* MK-4 in TMCL and nCL films are
520   completely opposite. This is most interesting and indicates that natural cardiolipins
521   have obviously very special properties for redox reactions of incorporated redox
522   species. It may not be accidental that natural cardiolipins provide high rate constants of
523   redox cycling at physiological pH and temperature.

524   The investigations reported in this work emphasise that the environment of redox systems in
525   membranes is important for their thermodynamics and kinetics. Therefore, elucidating the
526   quantitative function of electron shuttling molecules in membranes needs model systems which
527   include all constituents of membranes. Unfortunately, here we could not include membrane
528   bound proteins, which have to be included in future studies.

529

Acknowledgement
530

533

References
534

535   Almeida PF, Vaz WL, Thompson TE (1992) Lateral diffusion in the liquid phases of
536   dimyristoylphosphatidylcholine/cholesterol lipid bilayers: a free volume analysis.
537   Biochemistry 31:6739-6747. https://doi.org/10.1021/bi00144a013

538   Bastiaanse EL, Höld KM, Van der Laarse A (1997) The effect of membrane cholesterol content
539   on ion transport processes in plasma membranes. Cardiovasc Res 33:272-283.
540   https://doi.org/10.1016/S0008-6363(96)00193-9

541   Becucci L, Scaletti F, Guidelli R (2011) Gel-phase microdomains and lipid rafts in monolayers
542   affect the redox properties of ubiquinone-10. Biophys J 101:134-143.
543   https://doi.org/10.1016/j.bpj.2011.05.051

544   Cornelius F (2001) Modulation of Na, K-ATPase and Na-ATPase activity by phospholipids
545   and cholesterol. I. Steady-state kinetics. Biochemistry 40:8842-8851.
546   https://doi.org/10.1021/bi010541g

547   Dawson RMC, Elliott DC, Elliott WH, Jones KM (1986) Data for biochemical research. 3rd
548   edition, Oxford Science Publications, OUP, Oxford.

549   Dharmaraj K, Silva JIR, Kahlert H, et al (2020) The acid–base and redox properties of
550   menaquinone MK-4, MK-7, and MK-9 (vitamin K2) in DMPC monolayers on mercury. Eur
551   Biophys J 49:279-288. https://doi.org/10.1007/s00249-020-01433-0

552   Disalvo EA (2015) Membrane Hydration: The Role of Water in the Structure and Function of
553   Biological Membranes. In Subcellular Biochemistry. Vol 71, Springer International
554   Publishing, Switzerland. https://doi.org/10.1007/978-3-319-19060-0

555   Elamrani K, Blume A (1983) Effect of the lipid phase transition on the kinetics of H+/OH−
556   diffusion across phosphatidic acid bilayers. Biochim Biophys Acta Biomembr 727:22-30.
557   https://doi.org/10.1016/0005-2736(83)90364-4

558   Farhadi Moghadam B, Fereidoni M (2020) Neuroprotective effect of menaquinone-4 (MK-4)
559   on transient global cerebral ischemia/reperfusion injury in rat. Plos one 15:e0229769.
560   https://doi.org/10.1371/journal.pone.0229769

561   Fielding CJ, Fielding PE (2004) Membrane cholesterol and the regulation of signal
562   transduction. Biochem Soc Trans 32:65-69. https://doi.org/10.1042/bst0320065

563   George P, Witonsky RJ, Trachtman M, et al (1970) "Squiggle-H2O". An enquiry into the
564   importance of solvation effects in phosphate ester and anhydride reactions. Biochim Biophys
565   Acta Bioenerg 223:1-15. https://doi.org/10.1016/0005-2728(70)90126-X

23

566   Halder M, Petsophonsakul P, Akbulut AC, et al (2019) Vitamin K: double bonds beyond
567   coagulation insights into differences between vitamin K1 and K2 in health and disease. Int J
568   Mol Sci 20:896. https://doi.org/10.3390/ijms20040896

569   Heise N, Scholz F (2017) Assessing the effect of the lipid environment on the redox potentials
570   of the coenzymes Q10 and Q4 using lipid monolayers made of DOPC, DMPC, TMCL, TOCL,
571   and   natural   cardiolipin   (nCL)   on   mercury.   Electrochem   Commun   81:141-144.
572   https://doi.org/10.1016/j.elecom.2017.07.002

573   Hernández VA, Scholz F (2008) The electrochemistry of liposomes. Isr J Chem 48:169-184.
574   https://doi.org/10.1560/IJC.48.3-4.169

575   Hernández VA, Scholz F (2008) The lipid composition determines the kinetics of adhesion and
576   spreading   of   liposomes   on   mercury   electrodes.   Bioelectrochemistry   74:149-156.
577   https://doi.org/10.1016/j.bioelechem.2008.06.007

578   Johnsson Wass JT, Ahlberg E, Panas I, Schiffrin DJ (2006) Quantum chemical modeling of
579   the reduction of quinones. J Phys Chem A 110:2005-2020. https://doi.org/10.1021/jp055414z

580   Lal N, Berenjian A (2020) Cis and trans isomers of the vitamin menaquinone-7: which one is
581   biologically   significant?.   Appl   Microbiol   Biotechnol   104:2765–2776.
582   https://doi.org/10.1007/s00253-020-10409-1

583   Lange Y, Steck TL (2016) Active membrane cholesterol as a physiological effector. Chem
584   Phys Lipids 199:74-93. https://doi.org/10.1016/j.chemphyslip.2016.02.003

585   Laviron E (1979) General expression of the linear potential sweep voltammogram in the case
586   of diffusionless electrochemical systems. J Electroanal Chem Interfacial Electrochem 101:19-
587   28. https://doi.org/10.1016/S0022-0728(79)80075-3

588   Laviron E (1982) Voltammetric methods for the study of adsorbed species. In: Bard A J (ed)
589   ELECTROANALYTICAL CHEMISTRY A SERIES OF ADVANCES, Vol 12, Marcel
590   Dekker Inc., New York and Basel, pp. 53 – 157.

591   Levitan I, Fang Y, Rosenhouse-Dantsker A, Romanenko V (2010) Cholesterol and Ion
592   Channels. In: Harris J (eds) Cholesterol Binding and Cholesterol Transport Proteins:.
593   Subcellular Biochemistry, vol 51. Springer, Dordrecht. https://doi.org/10.1007/978-90-481-
594   8622-8_19

595   Lovander MD, Lyon JD, Parr IV DL, et al (2018) Critical review—electrochemical properties
596   of 13 vitamins: a critical review and assessment. J Electrochem Soc 165:G18-G49.
597   https://doi.org/10.1149/2.1471714jes

598   Mabrey S, Sturtevant JM (1976) Investigation of phase transitions of lipids and lipid mixtures
599   by sensitivity differential scanning calorimetry. Proc Natl Acad Sci U S A 73:3862-3866.
600   https://doi.org/10.1073/pnas.73.11.3862

601   Madden TD, Vigo C, Bruckdorfer KR, Chapman D (1980) The incorporation of cholesterol
602   into inner mitochondrial membranes and its effect on lipid phase transition. Biochim Biophys
603   Acta Biomembr 599:528-537. https://doi.org/10.1016/0005-2736(80)90197-2

604   Marcus Y (2015) Ion Solvation in Neat Solvents In: Ions in Solution and their Solvation, John
605   Wiley & Sons, Inc., U S A, pp. 107-155. https://doi.org/10.1002/9781118892336

606   Moscho A, Orwar O, Chiu DT, et al (1996) Rapid preparation of giant unilamellar vesicles.
607   Proc Natl Acad Sci U S A 93:11443-11447. https://doi.org/10.1073/pnas.93.21.11443

608   Roberts NK, Northey HL (1974) Proton and deuteron mobility in normal and heavy water
609   solutions   of   electrolytes.   J   Chem   Soc   Faraday   Trans   1   70:253-262.
610   https://doi.org/10.1039/F19747000253

611   Samuelsson R, Sharp M (1978) The effect of electrode material on redox reactions of quinones
612   in acetonitrile. Electrochim Acta 23:315-317. https://doi.org/10.1016/0013-4686(78)80067-X

613   Sato T, Inaba N, Yamashita T (2020) MK-7 and Its Effects on Bone Quality and Strength.
614   Nutrients 12:965. https://doi.org/10.3390/nu12040965

615   Schroeder F, Jefferson JR, Kier AB, et al (1991) Membrane cholesterol dynamics: cholesterol
616   domains   and   kinetic   pools.   Proc   Soc   Exp   Biol   Med   196:235-252.
617   https://doi.org/10.3181/00379727-196-43185

618   Schurgers LJ, Vermeer C (2002) Differential lipoprotein transport pathways of K-vitamins in
619   healthy subjects. Biochim Biophys Acta Gen Subj 1570:27-32. https://doi.org/10.1016/S0304-
620   4165(02)00147-2

621   Sek S, Bilewicz R (1999) Voltammetric Probing of Molecular Assemblies of Ubiquinone-10
622   at   the   Air–Water   Interfaces.   Journal   of   Inclusion   Phenomena   35:55-62.
623   https://doi.org/10.1023/A:1008194314304

25

624   Simons K, Vaz WL (2004) Model systems, lipid rafts, and cell membranes. Annu Rev Biophys

625   Biomol Struct 33:269-295. https://doi.org/10.1146/annurev.biophys.32.110601.141803

626   Sterby M, Emanuelsson R, Mamedov F, Strømme M, Sjödin M (2019) Investigating electron

627   transport in a PEDOT/Quinone conducting redox polymer with in situ methods. Electrochim

628   Acta 308:277-284. https://doi.org/10.1016/j.electacta.2019.03.207

629   Toner JD, Catling DC (2016) Water activities of $NaClO_4$, $Ca(ClO_4)_2$, and $Mg(ClO_4)_2$ brines

630   from experimental heat capacities: water activity >0.6 below 200 K. Geochim Cosmochim

631   Acta 181:164-174. https://doi.org/10.1016/j.gca.2016.03.005

632   Yousofian-Varzaneh H, Zare HR, Namazian M (2015) Thermodynamic parameters and

633   electrochemical behavior of tetrafluoro-p-quinone in aqueous solution. J Electrochem Soc

634   162:G63. https://doi.org/10.1149/2.0931508jes

635   Zander S, Hermes M, Scholz F, et al (2012) Membrane fluidity of tetramyristoyl cardiolipin

636   (TMCL) liposomes studied by chronoamperometric monitoring of their adhesion and spreading

637   at the surface of a mercury electrode. J Solid State Electrochem 16:2391-2397.

638   https://doi.org/10.1007/s10008-012-1758-8

639

26

640
641   **Supporting information**

The effects of the chemical environment of menaquinones in lipid monolayers on mercury electrodes on the thermodynamics and kinetics of their electrochemistry.

Karuppasamy Dharmaraj[1], Dirk Dattler[1], Heike Kahlert[1], Uwe Lendeckel[2], Felix Nagel[1], Mihaela Delcea[1], Fritz Scholz[1]

E-mail: fscholz@uni-greifswald.de

ORCID of the authors:
Prof. Dr. Fritz Scholz: 0000-0001-6287-1184
Karuppasamy Dharmaraj: 0000-0001-6743-3503
PD Dr. Heike Kahlert: 0000-0002-9196-5750
Prof. Dr. Mihaela Delcea: 0000-0002-0851-9072
Prof. Dr. Uwe Lendeckel: 0000-0002-0684-9959
Dirk Dattler: 0000-0002-0139-588X
Felix Nagel: 0000-0003-3456-7075

1   Institute of Biochemistry, University of Greifswald, Felix-Hausdorff-Str. 4, 17487 Greifswald,   Germany.

2   Institute of Medical Biochemistry and Molecular Biology, University Medicine Greifswald, University   of Greifswald, Ferdinand-Sauerbruch-Str.,   D-17475 Greifswald, Germany.

663

664 **Fig. S1** Differential scanning calorimetry (DSC) heating thermograms of (a) TMCL and TMCL/ *all-trans* MK-4
665 and (b) nCL and nCL/ *all-trans* MK-4 liposomes in pH 7.4 buffer. The ratio of *all-trans* MK-4 to TMCL was 2.2
666 μmol to 130.0 μmol TMCL (nCL, respectively)

667

668

669

670
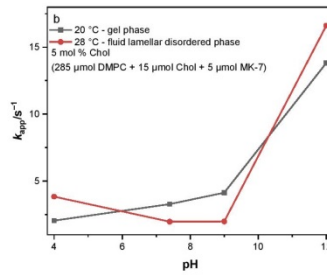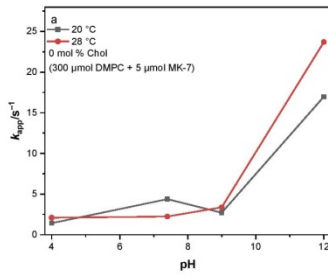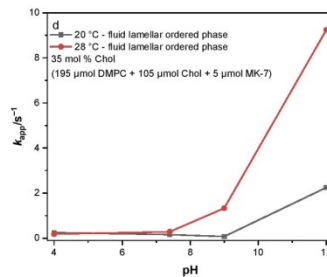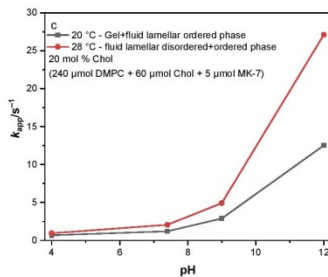
671
1 672
2 673

Fig. S2 Apparent electron transfer rate constants of MK-7 in DMPC/Chol monolayers as function of pH at above and below the phase transition temperature of DMPC. (a) 0 mol % Chol, (b) 5 mol % Chol, (c) 20 mol % Chol, and (d) 35 mol % Chol

674

675

676
677
678
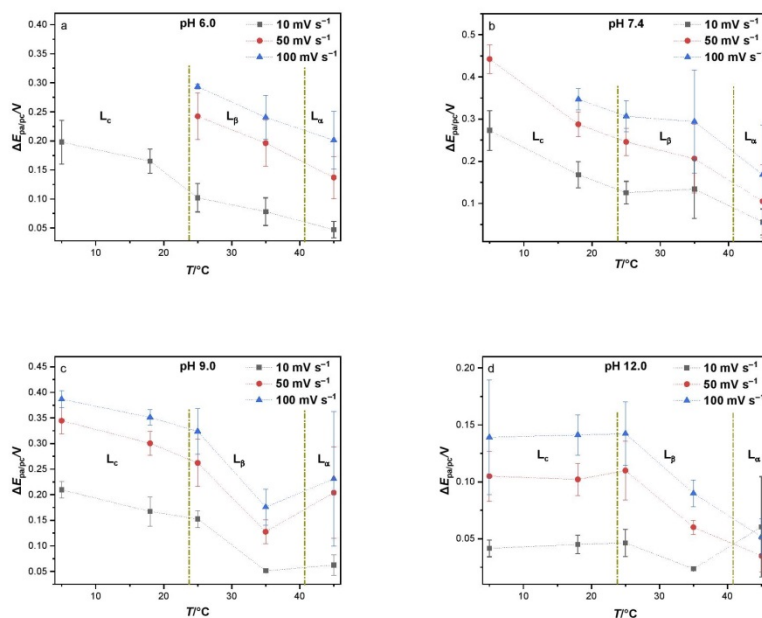
Fig. S3 Peak separations between anodic and cathodic peaks dependence on temperatures of TMCL films spiked with MK-4 for (a) pH 6.0, (b) pH 7.4, (c) pH 9.0, and (d) pH 12.0. The dash dotted lines represent the phase transition temperatures. The film composition was 130.0 μmol TMCL + 2.2 μmol MK-4

679

680
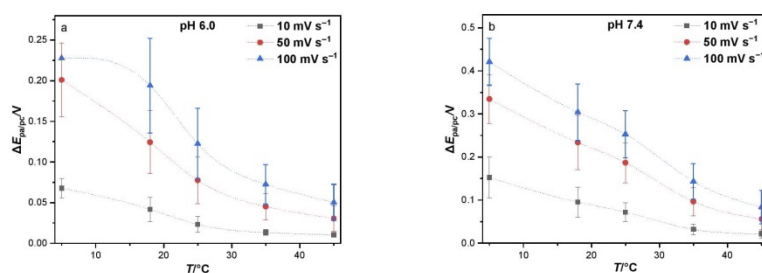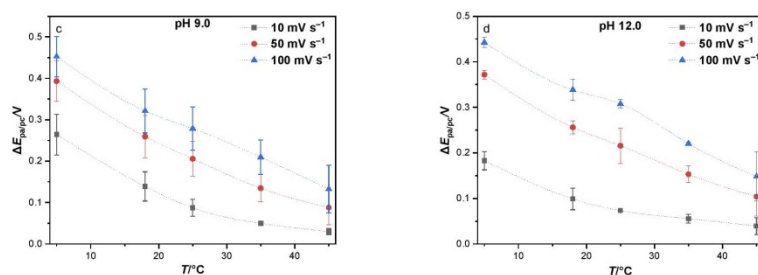
Fig. S4 Peak separations between anodic and cathodic peaks dependence on temperatures of nCL films spiked with MK-4 for (a) pH 6.0, (b) pH 7.4, (c) pH 9.0, and (d) pH 12.0. The film composition was 130.0 μmol nCL + 2.2 μmol MK-4
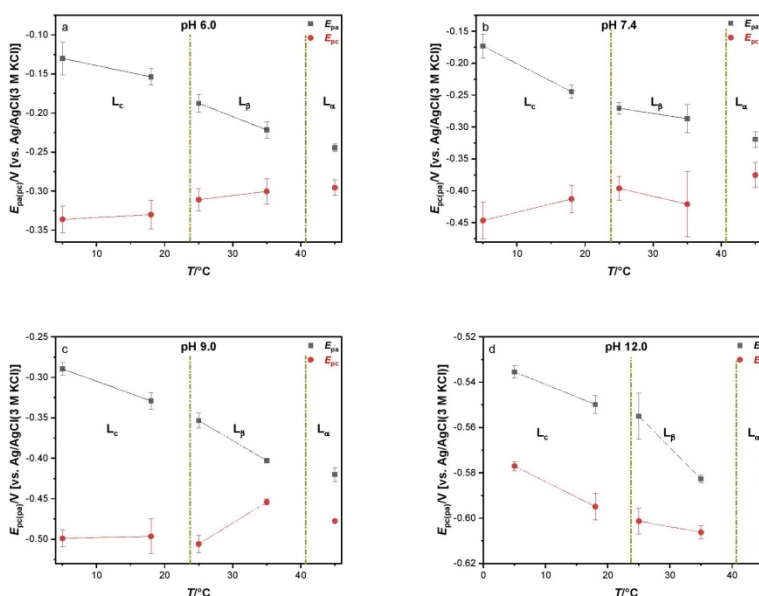
Fig. S5 Anodic peak potentials and cathodic peak potentials dependence on temperatures of TMCL films spiked with MK-4 for (a) pH 6.0, (b) pH 7.4, (c) pH 9.0, and (d) pH 12.0. The dash dotted lines represent the phase transition temperatures. Scan rate: 10 mV s⁻¹. The film composition was 130.0 μmol TMCL + 2.2 μmol MK-4
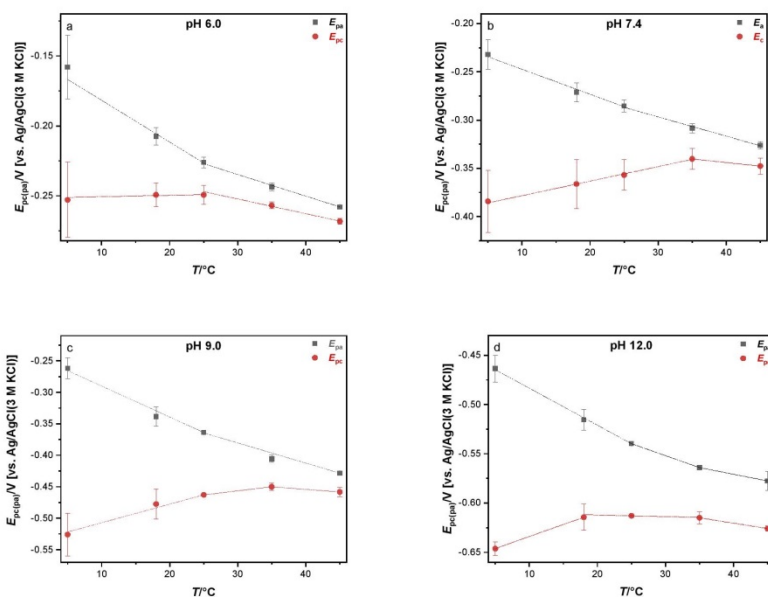
Fig. S6 Anodic peak potentials and cathodic peak potentials dependence on temperatures of nCL films spiked with MK-4 for (a) pH 6.0, (b) pH 7.4, (c) pH 9.0, and (d) pH 12.0. Scan rate: 10 mV s^{-1}. The film composition was 130.0 µmol nCL + 2.2 µmol MK-4
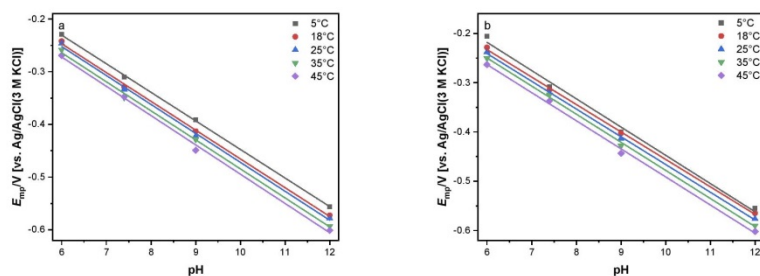
Fig. S7 Dependence of mid-peak potentials of MK-4 in (a) TMCL and (b) nCL films on pH. Scan rate: 10 mV s^{-1}. The ratio of all-trans MK-4 to TMCL was 2.2 µmol to 130.0 µmol TMCL (nCL, respectively)

Table S1 Apparent electron transfer rate constants of MK-7 in DMPC/Chol films above and below $T_{m, DMPC}$ for pH 4.0, 7.4, 9.0, and 12.0

pH 4.0	20 °C	28 °C
mol % Chol	k_{app} [s^{-1}]	k_{app} [s^{-1}]

0	1.42	2.09
5	2.05	3.84
20	0.68	0.95
35	0.25	0.18

704

pH 7.4	20 °C	28 °C
mol % Chol	k_{app} [s^{-1}]	k_{app} [s^{-1}]
0	4.37	2.24
5	3.28	1.97
20	1.21	2.07
35	0.16	0.28

705

pH 9.0	20 °C	28 °C
mol % Chol	k_{app} [s^{-1}]	k_{app} [s^{-1}]
0	2.71	3.38
5	4.14	1.99
20	2.89	4.91
35	0.08	1.33

706

pH 12.0	20 °C	28 °C
mole % Chol	k_{app} [s^{-1}]	k_{app} [s^{-1}]
0	16.97	23.69
5	13.82	16.61
20	12.53	27.10
35	2.25	9.24

707
708
709
710

Table S2 Slopes of mid-peak potentials vs pH of TMCL and nCL films spiked with MK-4 in the pH range 6.0 to 12.0. The ratio of all-trans MK-4 to TMCL was 2.2 µmol to 130.0 µmol TMCL (nCL, respectively)

711

T [°C]	TMCL/MK-4	nCL/MK-4
	Slopes [mV/pH]	Slopes [mV/pH]
5	−0.054 (± 0.001)	−0.057 (± 0.003)
18	−0.055 (± 0.001)	−0.056 (± 0.001)
25	−0.055 (± 0.002)	−0.056 (± 0.001)
35	−0.055 (± 0.002)	−0.057 (± 0.001)
45	−0.056 (± 0.002)	−0.057 (± 0.002)

712
713
714
715

Table S3 Apparent electron transfer coefficients of MK-4 in TMCL and nCL films. The ratio of *all-trans* MK-4 to TMCL was 2.2 µmol to 130.0 µmol TMCL (nCL, respectively)

716

TMCL/MK-4					nCL/ MK-4				
pH	T [°C]	$(1-\alpha)n$	αn	mean α (n=2)	pH	T [°C]	$(1-\alpha)n$	αn	mean α (n=2)
6.0	25	0.68	0.66	0.49	7.4	5	0.60	0.32	0.43

32

7.4	18	0.65	0.65	0.50	9.0	5	0.57	0.48	0.48
	25	0.66	0.66	0.50		18	0.56	0.62	0.51
	35	0.77	0.91	0.54					
9.0	5	0.59	0.54	0.49	12.0	5	0.42	0.42	0.50
	18	0.62	0.61	0.50					
	25	0.64	0.77	0.53					

Table S4 Apparent electron transfer rate constants of MK-4 in TMCL and nCL films at different temperatures for pH 6.0, pH 7.4, pH 9.0, and pH 12.0. The ratio of *all-trans* MK-4 to TMCL was 2.2 µmol to 130.0 µmol TMCL (nCL, respectively)

pH 6.0

T [°C]	TMCL/MK-4, k_{app} [s^{-1}]	nCL/MK-4, k_{app} [s^{-1}]
5		0.13
18		0.26
25	0.05	0.51
35	0.09	1.00
45	0.20	1.43

pH 7.4

T [°C]	TMCL/MK-4, k_{app} [s^{-1}]	nCL/MK-4, k_{app} [s^{-1}]
5		0.04
18	0.03	0.07
25	0.05	0.11
35	0.05	0.33
45	0.15	0.65

pH 9.0

T [°C]	TMCL/MK-4, k_{app} [s^{-1}]	nCL/MK-4, k_{app} [s^{-1}]
5	0.02	0.01
18	0.03	0.05
25	0.04	0.08
35	0.18	0.19
45	0.13	0.35

pH 12.0

T [°C]	TMCL/MK-4, k_{app} [s^{-1}]	nCL/MK-4, k_{app} [s^{-1}]
5	0.27	0.03
18	0.23	0.06
25	0.21	0.11

| | 35 | 0.70 | 0.16 |
| | 45 | 1.59 | 0.26 |

726

727

34

7 Appendix

7.1 Eigenständigkeitserklärung

Hiermit erkläre ich, dass diese Arbeit bisher von mir weder an der Mathematisch-Naturwissenschaftlichen Fakultät der Universität Greifswald noch einer anderen wissenschaftlichen Einrichtung zum Zwecke der Promotion eingereicht wurde.

Ferner erkläre ich, dass ich diese Arbeit selbstständig verfasst und keine anderen als die darin angegebenen Hilfsmittel und Hilfen benutzt und keine Textabschnitte eines Dritten ohne Kennzeichnung übernommen habe.

Karuppasamy Dharmaraj

7.2   Curriculum vitae

Personal details

First and last name: Karuppasamy Dharmaraj

Date of birth: May 22, 1996

Place of birth: Sivakasi, India

Nationality: Indian

Education

11/2017 – present   PhD, University of Greifswald, Germany

08/2013 – 04/2017   Bachelor of Technology in Chemical and Electrochemical
                       Engineering, CSIR – CECRI, India

Contributions to the conferences during PhD study

11/2018   Oral: "The electrochemistry of DPPH for ion transfer in three phase
                       electrode system", 7th Baltic Electrochemistry Conference: Finding
                       New Inspiration, Estonia

01/2019   Poster: "Redox properties of menaquinone-4 in a DMPC monolayer on
                       mercury : preliminary results",   Twelfth International Symposium
                       on Advances in Electrochemical Science and Technology (iSAEST-
                       12), India

06/2019   Poster: "The Acidity Constants (pK_{a1} and pK_{a2}) of Menaquinones
                       (MK-4) in a DMPC Monolayer on Mercury : preliminary results",
                       International Workshop on Electrochemistry of Electroactive Materials
                       WEEM-2019, Bulgaria

& internal RTG seminars and workshops

Karuppasamy Dharmaraj

7.3   Acknowledgements